ELECTRIC POTENTIAL RESPONSE OF THE QUARTZ BEARING ROCKS UNDER UNIAXIAL LOADING

A THESIS SUBMITTED TO
THE GRADUATE SCHOOL OF NATURAL AND APPLIED SCIENCES
OF
MIDDLE EAST TECHNICAL UNIVERSITY

BY

HİKMET SİNAN İNAL

IN PARTIAL FULFILLMENT OF THE REQUIREMENTS
FOR
THE DEGREE OF MASTER OF SCIENCE
IN

MINING ENGINEERING

SEPTEMBER 2004

Approval of the Graduate School of Natural and Applied Sciences.

Prof. Dr. Canan ÖZGEN
Director

I certify that this thesis satisfies all the requirements as a thesis for the degree of Master of Science.

Prof. Dr. M. Ümit ATALAY
Head of the Department

This is to certify that we have read this thesis and that in our opinion it is fully adequate, in scope and quality, as a thesis for the degree of Master of Science.

Assoc. Prof. Dr. H. Aydın BİLGİN
Supervisor

Examining Committee Members

Prof. Dr. Naci Bölükbaşı	(METU, MINE)	
Assoc. Prof. Dr. H. Aydın Bilgin	(METU, MINE)	
Prof. Dr. Tevfik Güyagüler	(METU, MINE)	
Assoc. Prof. Dr. Levent Tutluoğlu	(METU, MINE)	
Assist. Prof. Dr. M. Ali Hindistan	(Hacettepe Univ., MINE)	

I hereby declare that all information in this document has been obtained and presented in accordance with academic rules and ethical conduct. I also declare that, as required by these rules and conduct, I have fully cited and referenced all material and results that are not original to this work.

Name, Last name: Hikmet Sinan İnal

Signature :

ABSTRACT

ELECTRIC POTENTIAL RESPONSE OF THE QUARTZ BEARING ROCKS UNDER UNIAXIAL LOADING

İnal, Hikmet Sinan

M.Sc., Department of Mining Engineering

Supervisor: Assoc. Prof. Dr. H. Aydın Bilgin

September 2004, 114 Pages

The electric potential changes under uniaxial loading in some minerals and rocks have long been recognized. To daylight the electrical response of some minerals and rocks against applied stress, both theoretical studies and laboratory experiments are conducted. Some theories are also proposed by different researchers, in order to explain the electric potential variations. However, the mechanisms leading to electrical potential generation have not been fully explained yet.

In the explanation of electric potential changes observed in rocks, type of the observed rock and the rock forming minerals in the rock fabric play an important role. One theory is based on the fundamentals of piezoelectricity only. However the relation between the stress state and the electric generation is not fully understood. This thesis aims to make a further contribution to the studies on understanding the electric potential change in

rocks, containing quartz, which is a common piezoelectric mineral, under uniaxial loading conditions.

Three types of rocks, namely quartz-sandstone, granite and granodiorite, are tested, and the stress and electric potential (EP) variations are recorded during the uniaxial loading experiments in a continuous manner. The experiments are conducted at three different loading rates, in order to investigate the effect of loading rate on the electrification mechanism. Also step loading experiments are conducted.

Results indicated that, application of uniaxial stress creates a clear change in the EP responses of three quartz bearing rock types. The possible relationships between the EP generation and the level of applied stress are investigated based on the initial and final potential values ($EP_{initial}$, EP_{final}), the potential just before the time of failure (EP_{UCS}), the spike-like potential jump at the time of failure (ΔV), which are derived from the recorded data of the experiments.

Keywords: Quartz bearing rocks, piezoelectricity, electric potential change, uniaxial compression tests.

ÖZ

KUVARZ İÇEREN KAYALARIN TEK EKSENLİ YÜKLEME SIRASINDAKİ ELEKTRİK POTANSİYEL DAVRANIŞLARI

İnal, Hikmet Sinan
Yüksek Lisans, Maden Mühendisliği Bölümü
Tez yöneticisi: Doç. Dr. H. Aydın Bilgin

Eylül 2004, 114 Sayfa

Bazı kaya ve mineral oluşumlarında elektriksel potansiyel değişimlerinin varlığı uzun süredir bilinmektedir. Bu kaya ve mineral oluşumlarındaki elektriksel değişimleri açıklamak amacıyla, hem bazı teorik çalışmalar hem de laboratuvar deneyleri gerçekleştirilmiştir. Bu değişimleri açıklamak amacıyla, bazı araştırmacılar tarafından değişik teoriler de ortaya atılmış bulunmaktadır. Fakat kayalardaki elektriksel değişimlere sebep olan mekanizmalar henüz tam anlamıyla açıklanabilmiş değildir.

Kayalarda oluşan elektriksel değişimleri açıklamada, gözlem yapılan kayanın cinsi ve yapısında bulunan minerallerin türleri büyük önem taşımaktadır. Önerilen teorilerden birisi piezoelektrik temellere dayanmaktadır. Fakat basınç değişimleri ve elektrik potansiyel oluşumu arasındaki ilişkiler tam olarak anlaşılabilmiş değildir. Bu tez, yaygın bir piezoelektrik mineral olan kuvarz içeren kayalarda, tek eksenli basınç deneyleri sırasında oluşan elektrik potansiyel değişimlerin açıklanması çalışmalarına bir katkı sağlamayı amaçlamaktadır.

Kuvarz-kumtaşı, granit ve granodiorit olmak üzere üç farklı kaya türü üzerinde gerçekleştirilen deneylerde, tek eksenli yükleme sırasında, kayalarda meydana gelen elektrik potansiyel ve basınç değişimleri gözlemlenmiş ve sürekli olarak kaydedilmiştir. Deneyler, yükleme hızının oluşan potansiyel değişimler üzerindeki etkisini de incelemek amacıyla üç farklı yükleme hızında gerçekleştirilmiştir. Ayrıca kademeli yükleme deneyleri de, bu çalışma kapsamında gerçekleştirilmiştir.

Sonuçlar, kuvarz içeren üç kaya türünde de, üzerlerine uygulanan basınçla ilişkili olarak elektriksel potansiyel (EP) değişimler oluştuğunu açık şekilde göstermiştir. Uygulanan basınç ve oluşan potansiyel değişim arasındaki muhtemel ilişkiler, yükleme öncesi ve sonrası durağan halde gözlenen potansiyeller ($EP_{initial}$, EP_{final}), kırılmadan hemen önce ulaşılan potansiyel değeri (EP_{UCS}), kırılma anında keskin zıplama şeklinde oluşan potansiyel (V_{jump}) gibi, kaydedilen deney sonuçlarından tesbit edilen olgular incelenerek ortaya çıkarılmaya çalışılmıştır.

Anahtar kelimeler: Kuvarz içeren kayalar, piezoelektrik, elektrik potansiyel değişimi, tek eksenli yükleme deneyleri.

TO MY LOVELY WIFE

ACKNOWLEDGEMENTS

I would like to express my deepest appreciation to my advisor Assoc. Prof. Dr. H. Aydın BİLGİN for his kind supervision. Without his understanding, support, and guidance this thesis would not have been completed.

Special thanks are presented to the members of the examining committee: Prof. Dr. Naci BÖLÜKBAŞI, Prof. Dr. Tevfik GÜYAGÜLER, Assoc. Prof. Dr. Levent TUTLUOĞLU and Assist. Prof. Dr. M. Ali HİNDİSTAN for their valuable comments on this study.

Muharrem KILIÇ is gratefully acknowledged for his help in sample preparation, experiment conduction and his critics about the study.

I also wish to express my sincere appreciations to M. Esenay HACIOSMANOĞLU for her unique friendship and endless support.

Special thanks are gratefully extended to Ahmet KARAKAŞ, Sinem ŞENER and Koray ÖNAL for valuable friendship and sharing their knowledge on the instrumentation.

To my family, I would like to express my great pleasure for their support.

TABLE OF CONTENTS

LIST OF TABLES

LIST OF FIGURES

LIST OF SYMBOLS

σ: Stress

ε: Strain

E: Electric field

P: Polarization

T: Temperature

c: Elastic stiffness

s: Elastic compliance

η'': Dielectric susceptibility (constant strain)

η': Dielectric susceptibility (constant stress)

β: Dielectric impermeability

d: Piezoelectric strain coefficient

e: Piezoelectric stress coefficient

a: Coefficient of expansion

p: Pyroelectric coefficient

q: Coefficient of Thermal stress

R: Resistivity

ρ: Relative resistivity

VAN: Varotsos Alexopoulos Network

SES: Seismic electric signal

ΔV: Maximum observed potential value of SES

M: Magnitude of the earthquake

r: Distance between epicenter and observing point

J: Current density

E_d: Dynamic Young's modulus

ν: Poisson's ratio

V_p: P-wave velocity

V_s: S-wave velocity

L: Length

W: Weight

D: Diameter

ϕ: Unit weight

G_d: Dynamic Shear modulus

V_{up}, V_{down}: Electric potential jump

V_{jump}: Total electric potential jump

EP: Electric potential

LR: Loading rate

UCS: Uniaxial compressive strength

CHAPTER 1

INTRODUCTION

First attempts for discovering the electrification mechanisms of earth materials were performed for the earthquake prediction purposes. The frame of the innovative studies on the topic, were based on the search for an anomalous change in the Electric Potential (EP) of earth, which occurs within a certain time before the earthquake. Fedotov et al. (1970) and Sobolev (1975) were the first researchers, who have conducted field studies on the earth current measurement. Within this frame, continuous observations and the theory stated by Varotsos and Alexopoulos (1984) are still on the way of being tested.

With the improving technology, more sophisticated instrumentation become available for measurement of different variables. In the following years, it could be possible to reveal the relationship between EP changes and applied stress for certain rock types. Outcomes of such a discovery, may find application areas in mining engineering discipline, also.

In the recent years some promising theoretical and laboratory studies were performed by some researchers. Especially, the studies performed by Aydan et al. (2001, 2003) on both piezoelectric and non-piezoelectric geomaterials, Freund (2002) on igneous rocks, Yoshida et al. (1997) on stick-slip of granite and Bishop (1981) on quartz-rich rocks, can be listed among the important contributions to the topic.

Although several promising studies have been conducted as referred above, none of them have studies the effect of the loading rate on the development and variation of electric potential (EP). Therefore this study aims to investigate the effect of loading rate on EP generation under uniaxial loading conditions.

After the introductory chapter of this thesis, the theory of piezoelectricity, basics of crystallography of quartz and the summary of previous studies conducted on the subject are reviewed in Chapter 2. Chapter 3 and Chapter 4 are devoted to the experimental set-up used in the study and experimental procedure and materials tested in the study, respectively. The results and the discussions of the results are given in Chapter 5. Chapter 6 includes the main conclusions drawn from this study and the recommendations for future work.

CHAPTER 2

LITERATURE SURVEY

2.1 PIEZOELECTRICITY

The existence of pyroelectricity was well known long before the discovery of piezoelectric effect. The people of Ceylon and India have been aware of the tourmaline crystals which become electrically polarized when heated. After the scientific origins of pyroelectric effect are recognized by scientists, some other questions are brought to mind about occurrence of electrical phenomena on different minerals and crystals when they are exposed to different conditions. One of such questions was the reaction of crystals when they are subjected to some loading conditions.

The first possibility of electricity production in the crystals when they are subjected to pressure was pronounced by Charles Augustine de Coulomb (Ballato, 1996). Following his conjecture, different scientists like René-Just Haüy and Antoine-César Becquerel conducted experiments and sought for the traces and relations between the pressure and electricity (Ballato, 1996). However the experiments did not lead to a conclusive result; any charges produced might have been caused by friction or contact electricity.

The first “true” evidence of piezoelectricity was discovered by Pierre Curie and Paul-Jacques Curie brothers in 1880 (Ikeda, 1996). The invention of Curie brothers was not limited only with the existence of electricity; two brothers also stated that, when some crystals are compressed in particular directions they show positive and negative charges on certain portions of their surfaces. These charges are proportional with the applied pressure and disappear when the pressure is drawn back.

The discovery of piezoelectricity in 1880 by Pierre and Paul-Jacques Curie brothers is followed by the Lippmann's prediction of the converse effect in 1881 (Ballato, 1996). Lipmann, on thermodynamic grounds, predicted that the converse effect should also exist, that is the imposition of surface charges induces mechanical deformation. In the same year the Curie brothers verified the converse effect and showed that the coefficients for both the direct and the converse effects were identical (Ballato, 1996). The name of the converse effect is "electrostriction".

The word piezoelectricity means "pressure electricity", it is the combination of piezo which is derived from Greek word "piezein" meaning "to press" and electricity. The word has been generally defined by Cady (1964) as follows: "Piezoelectricity is electric polarization produced by mechanical strain in crystals belonging to certain classes, the polarization being proportional to the strain and changing direction with it". A piezoelectric crystal is defined as; the crystal in which electricity or electric polarity produced when squeezed or stretched. In addition, when the direction (sign) of the applied pressure is changed the sign of the polarity or the direction of the produced current is also changed, that is the piezoelectric crystals have certain one-wayness in its internal structure. Applied pressure or stress need not to be only compression or tension, other stress types such as shear, bending or torsion producing strain, may also lead to production of piezoelectric polarization on certain crystals (Trainer, 2003).

The piezoelectricity in a crystal can not be treated as an isolated phenomenon which is solely an interaction of mechanical and electrical processes. Actual conditions and the reversibility property of the piezoelectricity, requires the thermal conditions to be also considered. In Figure 2.1, the relationship between elastic, dielectric and thermal processes are schematically shown. Here σ, E and δQ corresponds to stress, electric field and electrocaloric effect (change of heat due to application of an electric field E) respectively. In the same manner ε, P and ϑ stands for strain, polarization and temperature respectively. The arrows indicate the directions in which the various effects usually takes place in relation with coefficients b, p, s, n, c, a and k according to the theory of Voldemar Voight (Cady, 1964). For example an electric field of strength E causes a piezoelectric stress σ = k E, similarly ε and σ are related by an equation ε = s σ. Nine straight lines given on the graph indicates the direct way of respective processes. On the other hand one process can occur with an indirect path through or as a result of other phenomena.

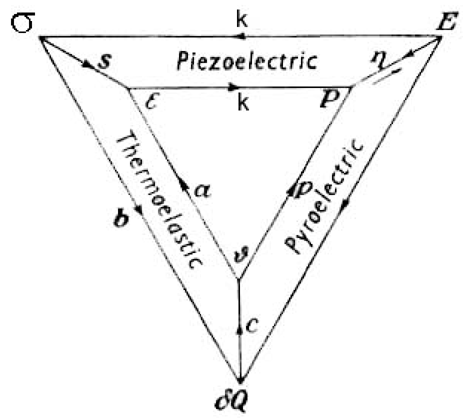

Figure 2.1 Heckmann diagram (Cady, 1964)

It was definite expressions of thermodynamical principals stated by Lord Kelvin that builds-up the phenomenological theory of piezoelectricity (Ikeda, 1996). In the treatment of the problems in elasticity, Green (1837) (in Ikeda, 1996) introduced the “strain-energy function”. This function, when applied to a reversible system, is commonly called the free energy of the system and has been extended to include thermal and electrical as well as elastic effects. The term “thermodynamic potential” was used by Lord Kelvin and Gibbs and applied to crystals by Duhem and by Voight (Cady, 1964).

When the free energy is expressed in terms of strains, it is known as the first thermodynamic potential and is denoted by the symbol ξ (Cady, 1964). The free energy is also expressed in terms of stresses. It is then called the second thermodynamic potential and denoted by the symbol ζ (Cady, 1964). Assuming that a crystal plate is subjected simultaneously to an arbitrary uniform mechanical stress, a uniform electric field in any orientation and to be at a temperature differing from a standard temperature T by the amount υ= ΔT, the two thermodynamic potentials can be written in terms of mechanical, electrical and thermal effects as follows (Cady, 1964);

$$\xi = -\frac{1}{2}\sum_{h}^{6}\sum_{i}^{6} c_{hi}\varepsilon_h\varepsilon_i + \frac{1}{2}\sum_{k}^{3}\sum_{m}^{3}\eta''_{km}E_kE_m + \sum_{m}^{3}\sum_{h}^{6} e_{mh}E_m\varepsilon_h + \frac{1}{2}\frac{c\upsilon^2}{T} + \upsilon\sum_{h}^{6} q_h\varepsilon_h + \upsilon\sum_{m}^{3} p_mE_m \tag{2.1}$$

$$\zeta = \frac{1}{2}\sum_{h}^{6}\sum_{i}^{6} s_{hi}\sigma_h\sigma_i + \frac{1}{2}\sum_{k}^{3}\sum_{m}^{3}\eta'_{km}E_kE_m + \sum_{m}^{3}\sum_{h}^{6} d_{mh}E_m\sigma_h + \frac{1}{2}\frac{c\upsilon^2}{T} - \upsilon\sum_{h}^{6} a_h\sigma_h + \upsilon\sum_{m}^{3} p_mE_m \tag{2.2}$$

The frame of reference has its X, Y and Z axes parallel to the principal orthogonal axes of the crystal. The six terms in each equation represents the energy in terms of the elastic, dielectric, piezoelectric, thermal, thermoelastic, and pyroelectric properties of the material respectively. These terms correspond to the three radial and the three peripheral relations represented in Figure 2.1.

In these equations the ε_h and ε_i denote components of the total strain due to all causes, while σ_h and σ_i are components of externally applied mechanical stress; c_{hi} and s_{hi} are coefficients of elastic stiffness and compliance, respectively (their values are assumed to be those which would observed at constant electric field and at the temperature T); η''_{km} and η'_{km} are dielectric susceptibilities at constant strain and stress respectively. E_k and E_m are components of the field strength in the crystal maintained constant by potentials applied to the suitable electrodes; d_{mh} and e_{mh} are piezoelectric strain and stress coefficients. C is the specific heat in calories g^{-1} deg^{-1}; q_h is coefficient of thermal stress (Cady, 1964 therein Voigt, V., Lehrbuch der Kristalphysik) in erg $cm^{-1}deg^{-1}$; a_h is coefficient of expansion in deg^{-1}; and p_m is pyroelectric constant in statcoulomb cm^{-2} deg^{-1}. The constants $s_{hi} = s_{ih}$, $c_{hi} = c_{ih}$ and $\eta_{km} = \eta_{mk}$ have commutative subscripts; such commutation is not permissible with the piezoelectric coefficients (Cady, 1964).

For the Equations 2.1 and 2.2 the number of elastic compliance and stiffness coefficient are 32 for each. Whereas the number of coefficients are reduced with the increasing symmetry of the crystals. The crystal with the lowest symmetry has all the 21 constants different from zero (not 36 since; $s_{hi} = s_{ih}$, $c_{hi} = c_{ih}$).

Another important factor about the problems concerning piezoelectricity is the conditions under which the process is taking place, since the conditions affect the coefficient to be used. In the static cases the isothermal, that is constant temperature conditions are assumed, whereas in the dynamic cases the adiabatic, that is constant entropy conditions are accepted (Cady, 1964).

Since 6 independent components (σ_x, σ_y, σ_z,...) of a stress and 3 electric polarization components exist, there are 18 possible relations between the mechanical and the electrical states of the crystal. Thus, theoretical number of e_{mh} and d_{mh}, the piezoelectric strain and stress coefficients, are 18 separately. If all of the 18 piezoelectric strain and 18 piezoelectric stress coefficients of a crystal are different from zero, any random stress producing a strain in any particular direction will cause a piezoelectric polarization proportional with the stress applied. However, this is not the case with most of the crystal classes. Only the asymmetric triclinic class, with the lowest degree of symmetry, has all the coefficients different from zero. With the increasing symmetry the number of individual coefficients decreases, reducing down to one for some classes of high symmetry (Cady, 1964).

Due to the nature and the long time span of the earthquake phenomenon, it would be more suitable to handle the problems within the static constraints, as far as piezoelectricity is concerned. As a result, isothermal conditions are considered throughout the derivation of the rest of the piezoelectric formulations.

In the derivation of the fundamental piezoelectric equations, the Equations 2.1 and 2.2 are utilized. Assuming isothermal conditions, the last 3 terms in the equations are automatically cancelled out. The coordinate system of the equations is parallel to the orthogonal crystallographic axes. Then derivation of remaining terms of the equations (2.1) and (2.2), with respect to strain and electrical field leads to the fundamental piezoelectric equations, that is Equations (2.3a), (2.3b), (2.4a) and (2.4b), which are given below (Cady, 1964):

From Eq.(2.1):

$$\frac{\partial \xi}{\partial \varepsilon_h} = \sum_i^6 c_{hi}^E \varepsilon_i - \sum_m^3 e_{mh} E_m = \sigma_h \qquad \text{(converse effect)} \qquad (2.3a)$$

$$\frac{\partial \xi}{\partial E_h} = \sum_k^3 \eta''_{km} E_k - \sum_h^6 e_{mh} \varepsilon_h = P_m \qquad \text{(direct effect)} \qquad (2.3b)$$

From Eq.(2.2):

$$\frac{\partial \zeta}{\partial \sigma_h} = \sum_i^6 s_{hi}^E \sigma_i - \sum_m^3 d_{mh} E_m = \sigma_h \qquad \text{(converse effect)} \qquad (2.4a)$$

$$\frac{\partial \zeta}{\partial E_h} = \sum_k^3 \eta'_{km} E_k - \sum_h^6 d_{mh} \sigma_h = P_m \qquad \text{(direct effect)} \qquad (2.4b)$$

More brief and simplified forms of the theory of piezoelectricity can be found in the papers by Trainer, (2003) and Ballato, (1995, 1996).

According to Trainer (2003), applying a stress σ_j to a crystal with no center of symmetry results in a production of electric polarization of P_i according to equation:

$$P_i = d_{ij}\,\sigma_j \qquad (i= 1,2,3;\ j=1,2,...,6) \qquad (2.5)$$

Where $\{d_{ij}\}$ is the (3 x 6) piezoelectric coefficients matrix and tabulated as:

$$\begin{bmatrix} d_{11} & d_{12} & d_{13} & d_{14} & d_{15} & d_{16} \\ d_{21} & d_{22} & d_{23} & d_{24} & d_{25} & d_{26} \\ d_{31} & d_{32} & d_{33} & d_{34} & d_{35} & d_{36} \end{bmatrix}$$

According to the symmetry class of the crystal some of the coefficients have value 0 and some have identical numerical values. As an example the coefficient matrix of quartz of trigonal class is as follows:

$$\begin{bmatrix} d_{11} & d_{-11} & 0 & d_{14} & 0 & 0 \\ 0 & 0 & 0 & 0 & d_{14} & -2d_{11} \\ 0 & 0 & 0 & 0 & 0 & 0 \end{bmatrix}$$

The values of d_{11} and d_{14} for quartz are -2.3 x 10^{-12} C N^{-1} and -0.67 x 10^{-12} C N^{-1} respectively. Applying a compressive stress of 1 kg / cm^2 (σ_1 = 9.81 x

10^4 N / m^2) parallel to the electric axis of the quartz crystal results in a polarization of (Trainer, 2003):

$P_1 = d_{11}\ \sigma_1$ = (-2.3 x 10^{-12} C N^{-1}) x (9.81 x 10^4 N / m^2) = 2.3 x 10^{-7} C / m^2

Kelvin had calculated the value of d_{11} for quartz as 2.14 x 10^{-12} C N^{-1} by applying a tensile stress of 1 kg / cm^2 (Trainer, 2003 therein Suda et al., 1985).

In the electrostriction (converse effect), the application of electric field E_i deforms the piezoelectric material with an amount of the strain tensor $\{x_j\}$.

$x_j = d_{ij}\ E_i$ (i= 1,2,3; j=1,2,...,6) (2.6)

The unit of the d_{ij} coefficient is m V^{-1} for the converse effect. The change of shape may be contraction or expansion depending upon the direction of the applied electric field.

The relationship between polarization and strain where $\{e_{ij}\}$ is the third rank piezoelectric tensor. Unit of the e_{ij}'s is C m^{-2}:

$P_i = e_{ij}\ x_j$ (i= 1,2,3; j=1,2,...,6) (2.7)

And at constant strain, the electric field and stress are interrelated with the equation. In this equation the unit of the coefficient e_{ij} is N V^{-1} m^{-1}.

$\sigma_j = e_{ij}\ E_i$ (i= 1,2,3; j=1,2,...,6) (2.8)

Ballato (1995), interprets the formulations of piezoelectricity in a more compact form, by using compressed matrix notation. Formulas include the couplings between mechanical stress (σ), strain (ε), electric (field) intensity (E), and displacement (polarity) (P) as follows:

$$[\sigma]=\left[c^{E}\right][\varepsilon]-[e]^{'}[E] \tag{2.9a}$$

$$[P]=[e][\varepsilon]+\left[\eta^{''}\right][E] \tag{2.9b}$$

$$[\sigma]=\left[c^{D}\right][\varepsilon]-[h]^{'}[P] \tag{2.10a}$$

$$[E]=-[h][\varepsilon]+\left[\beta^{S}\right][P] \tag{2.10b}$$

$$[\varepsilon]=\left[s^{E}\right][\sigma]+[d]^{'}[E] \tag{2.11a}$$

$$[P]=[d][\sigma]+\left[\eta^{'}\right][E] \tag{2.11b}$$

$$[\varepsilon]=\left[s^{D}\right][\sigma]+[g]^{'}[P] \tag{2.12a}$$

$$[E]=-[g][\sigma]+\left[\beta^{T}\right][P] \tag{2.12b}$$

In these equations $[E]$ and $[P]$ are first order tensors, whereas $[\sigma]$ and $[\varepsilon]$ are second rank tensors. Elastic stiffness and compliance coefficients $\left[c^{E}\right]$, $\left[c^{P}\right]$ and $\left[s^{E}\right]$, $\left[s^{P}\right]$ are (6 x 6) symmetric matrices at constant E and P. $\left[\eta^{''}\right]$, $\left[\eta^{'}\right]$ and $\left[\beta^{S}\right]$, $\left[\beta^{T}\right]$ are (3 x 3) dielectric permittivity (susceptibility) and impermeability matrices at constant ε and σ. A prime indicates the transpose. These matrices, with equations (1a) to (4b), are used as follows:

The application of electric field E_i along the X_i axis, results in a stress:

$$\sigma_{\lambda}=-e_{i\lambda}E_{i} \tag{2.13}$$

Index i takes values 1, 2, 3 which corresponds to orthogonal X, Y and Z axis. The subscript λ changes from 1 to 6 and these numbers represent the tensor indexes according to scheme: 1→11; 2→22; 3→33; 4→23 or 32; 5→31 or 13; 6→21 or 12. Each line of matrix $[e]$ is affected or multiplied by a different component of electric field vector to produce a stress tensor of rank two.

Ballato (1995) also lists the units of the tensors, coefficients and constants, which are tabulated in the units of the various quantities as given by Ballato.

Field Tensors:

Mechanical stress, σ:	Pascal, Pa = Newton / meter^2 = N /m^2
Mechanical strain, ε:	meter / meter = m / m (dimensionless)
Electric intensity, E:	volt / meter = V / m
Displacement, P:	coulomb / meter^2 = C / m^2

Matter tensors:

Permittivity, $\eta^{'}$, $\eta^{''}$:	farad / meter = F / m = C / (m-V)
Impermeability, β^T, β^S:	meter / farad = m / F = (m-V) / C

Piezo constants:

e:	C/ m^2 = N / (m-V)
d:	m / V = C / N
h:	V / m = N / C
g:	m^2 / C = (m-V) / N
Elastic stiffness, c^E, c^D:	Pa = N / m^2 = J / m^3
Elastic compliance, s^E, s^D:	(Pa)$^{-1}$ = m^2 / N = m^3 / J

2.2 CRYSTALLOGRAPHY OF QUARTZ

For a better understanding of piezoelectricity, basics of crystallography should also be revised and understood, since piezoelectricity is strongly linked to crystallography. All the conventions about the positive directions location of the axes are defined by crystallography. In this section, only the crystallography of quartz will be given, since this study is concerned with the piezoelectricity of quartz.

Classification of the possible crystal structures is the first thing to be emphasized in crystallography. It is shown that, the number of possible crystalline structures, that will completely fill the 3 dimensional space, are limited to 7 (Bravais, 1850). The names of the seven classes are as listed below:

- Triclinic
- Monoclinic
- Orthorhombic
- Tetragonal
- Cubic
- Trigonal
- Hexagonal

The 7 “crystal classes” are divided into sub groups named as “point groups” according to the possible combinations of points of the lattices. Total number of the three dimensional point groups is 32 and it was first listed by Hessel in 1930 (Giacovazzo, 1992).

Quartz belongs to the trigonal holoaxial class domain and the point group D_3 (or 32) (Cady, 1964). D_3 means that there exist three principle axes with three secondary axes normal to it, according to threefold symmetry. Quartz is also an enantiomorphous crystal, that is, it can be found both in left and right quartz forms (Ikeda, 1996), which is better illustrated in the Figure 2.2 (Bottom, 1982).

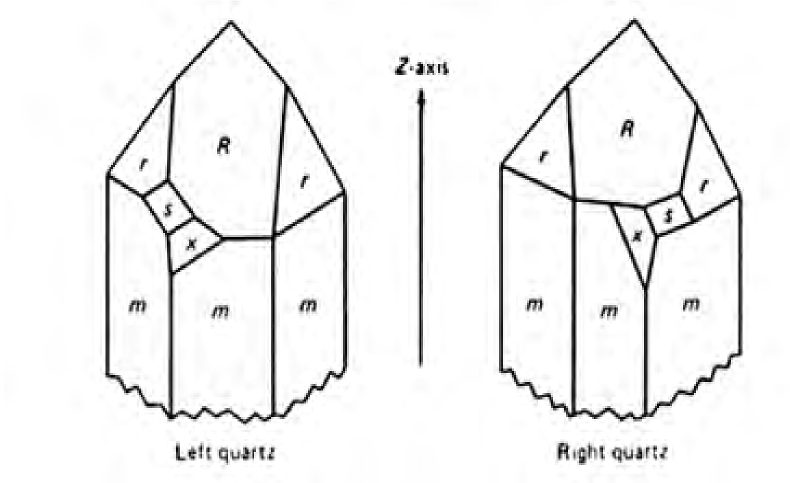

Figure 2.2 Left and Right quartz forms (Bottom, 1982)

In crystallography, two different systems for locating the coordinate axes are used: Bravais-Miller axial system and the conventional orthogonal coordinate system. Bravais-Miller system is more suitable for specifying the natural faces and planes in quartz, whereas orthogonal system is more useful for the computational purposes as far as mechanical and piezoelectrical properties and computations are concerned (Bottom, 1982). It is also customary to use the a, b and c letters respectively instead of X, Y and Z axes of orthogonal coordinate system in crystallography.

First rule of thumb in locating the crystallographical axes; if an axis is unique i.e. possession of trigonal symmetry, it is made the c axis and if the c axis is a non-polar axis than the location of positive direction is arbitrary. When all the axes (X, Y and Z) are considered in terms of polarity, following the IEEE standards, the sense of positive direction is conventionally defined as the direction of the axis in which a positive strain produces a positive charge.

The positive strain in crystallography is defined as extension resulting due to tensional stress (Bottom, 1982), which is completely the reverse order accepted and used in rock mechanics. The location of both the Bravais-Miller axes and the orthogonal coordinate axes for the quartz crystal are shown in Figure 2.3 (Bottom, 1982).

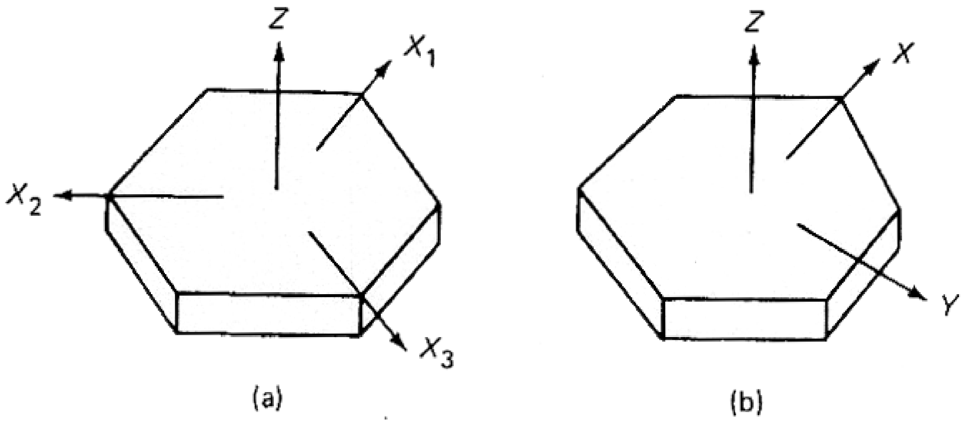

Figure 2.3 Location of the axes according to two systems, (a) Bravais-Miller (b) orthogonal (Bottom, 1982)

The enantiomorphic property of quartz dictates that, a right hand coordinate system should be used for a right quartz crystal, whereas a left hand coordinate is more appropriate for a left quartz crystal, as shown in Figure 2.4 (Cady, 1964). This convention is standardized by IEEE (Bottom, 1982). By this standardization all the properties and the constants for left and right quartz crystals became identical. In addition, as indicated in the Figure 2.2 and Figure 2.4, certain faces of the crystal are denoted by certain letters also.

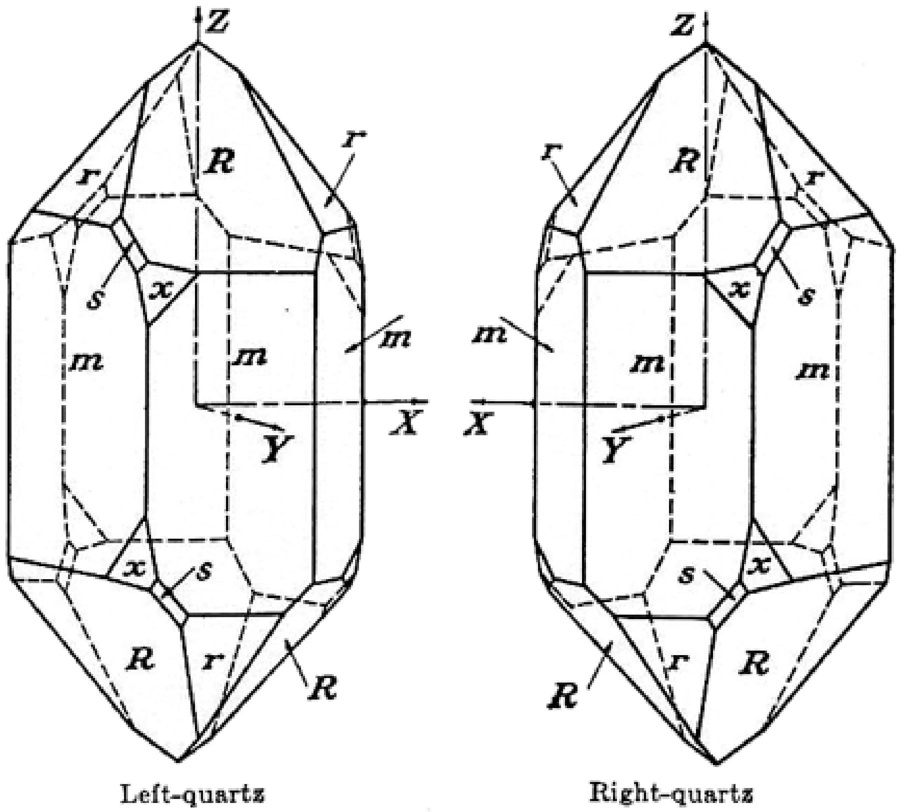

Figure 2.4 The full face appearance of left and right quartz forms (Cady, 1964)

The elastic coefficient matrices have 36 terms (6x6 square matrix) theoretically, however due to the symmetry properties of the crystals some of the terms become zero, with the increasing symmetry. In the lowest symmetry class the number of elastic stiffness and compliance coefficients is 21 for each separately. Material property matrices of elastic stiffness and elastic compliance coefficients and piezoelectric stress and strain coefficients, are also affected by the trigonal symmetry of the quartz. In the quartz, the number of terms in the matrices is 18 for compliance and 18 for stiffness, owing to the trigonal symmetry of the crystal. These 18 terms are the repetitions of 7 different values of coefficients according to the symmetry and the rule "$s_{hi} = s_{ih}$, $c_{hi} = c_{ih}$". The rest of the coefficients are equal to 0. The matrix notations of the elastic compliance and stiffness coefficients are as given below. Also the numerical values of the coefficients are also given in Table 2.1.

Table 2.1 The Elastic Coefficients of alpha quartz (Bottom, 1982)

	Stiffness (N/m^2)			Compliance (m^2/N)	
	Bechmann	Mason		Bechmann	Mason
c_{11}	86,74	86,05 x 10^9	s_{11}	12,77	12,79 x 10^{-12}
c_{12}	6,99	5,05	s_{12}	-1,79	-1,535
c_{13}	11,91	10,45	s_{13}	-1,22	-1,10
c_{14}	-17,91	18,25*	s_{14}	4,50	-4,46
c_{33}	107,2	107,1	s_{33}	9,60	9,56
c_{44}	57,94	58,65	s_{44}	20,04	19,78
c_{66}	39,88	40,5	s_{66}	29,12	28,65

* It is more convenient to assign a positive sign to the c_{14}, since the rotational equations about X-axis require the sign of the c_{14} to be positive (Bottom, 1982).

$$\begin{bmatrix} c_{11} & c_{12} & c_{13} & c_{14} & 0 & 0 \\ c_{12} & c_{11} & c_{13} & -c_{14} & 0 & 0 \\ c_{13} & c_{13} & c_{33} & 0 & 0 & 0 \\ c_{14} & -c_{14} & 0 & c_{44} & 0 & 0 \\ 0 & 0 & 0 & 0 & c_{44} & c_{14} \\ 0 & 0 & 0 & 0 & c_{14} & \tfrac{1}{2}(c_{11}-c_{12}) \end{bmatrix} \quad \text{and} \quad \begin{bmatrix} s_{11} & s_{12} & s_{13} & s_{14} & 0 & 0 \\ s_{12} & s_{11} & s_{13} & -s_{14} & 0 & 0 \\ s_{13} & s_{13} & s_{33} & 0 & 0 & 0 \\ s_{14} & -s_{14} & 0 & s_{44} & 0 & 0 \\ 0 & 0 & 0 & 0 & s_{44} & 2s_{14} \\ 0 & 0 & 0 & 0 & 2s_{14} & 2(s_{11}-s_{12}) \end{bmatrix}$$

In the same manner, the piezoelectric stress (d) and strain (e) coefficients are also affected by the symmetry of quartz and some of the 18 terms in piezoelectric stress and strain coefficient matrices (6x3) take the value of zero. That is, some applied stress in a certain direction results in an electrical change in some direction but has no electrical effect in some other directions or vice versa. The matrix notation of piezoelectric stress and strain coefficients respectively, are as follows. Also the numerical values of the coefficients are given in the Table 2.2.

Table 2.2 Piezoelectric stress and strain coefficients of alpha quartz. (Bottom, 1982)

Stress coefficients (m/V)		Strain Coefficients (C/m^2)	
d_{11}	2,27 x 10^{-12}	e_{11}	0,173
d_{14}	-0,67	e_{14}	0,040

$$\begin{bmatrix} d_{11} & 0 & 0 \\ -d_{11} & 0 & 0 \\ 0 & 0 & 0 \\ d_{14} & 0 & 0 \\ 0 & -d_{14} & 0 \\ 0 & -2d_{11} & 0 \end{bmatrix} \quad \text{and} \quad \begin{bmatrix} e_{11} & 0 & 0 \\ -e_{11} & 0 & 0 \\ 0 & 0 & 0 \\ e_{14} & 0 & 0 \\ 0 & -e_{14} & 0 \\ 0 & -2e_{11} & 0 \end{bmatrix}$$

2.3. BRIEF HISTORY OF EARTHQUAKE PREDICTION SCIENCE

In many countries, which are seismologically highly active, the desire for earthquake prediction has always been so intense that, from the ancient times people searched and relied on many techniques and persons for the early recognition of the earthquakes. The results of the earthquakes were usually so destructive that the techniques used varied from superstitious fortune-telling techniques to scientific methods in the latest times.

Since predicting the earthquakes used to be the job of fortune-tellers, it was away from being scientific and it was not treated as a serious topic to be dealed with scientifically until the establishment of the earthquake prediction science (Rikitake, 1976). Wyss (2000), stated that: “Many good and outstanding scientists fear damaging their reputations if they should get involved in a project like earthquake-prediction research, which appears tainted because incompetent individuals debate on it…”

Because of the fact that, it is a highly active country in terms of earthquakes, Japan used to be the leading country in the earthquake science. After the large and destructive Nobi Earthquake (28 October 1891), Japanese Government decided to set up the Imperial Earthquake Investigation Committee. In the following years the effect of 1 September 1923 Kanto Earthquake was so severe that, the intense public demand on the earthquake research lead to the establishment of Earthquake Research Institute, which was attached to the Tokyo Imperial University (now University of Tokyo), in year 1925. 30 years of knowledge and experience gathering resulted in some debates about the predictability of the earthquakes. As a result a group of scientists formed the “Earthquake Prediction Group” and published the report “Prediction of Earthquakes - Progress to Date and Plans for Further Development” (Rikitake, 1976, therein Tsuboi et al., 1962). This report is today known as famous “BLUE PRINT” of earthquake prediction research. In the Blue Print, the methods, necessary preparations and the variables to be observed for the earthquake prediction are explained and listed (Rikitake, 1976).

Turkey, as a seismically highly active country, has two projects about earthquake prediction, which are still being conducted along the famous North Anatolian Fault Zone. One of the projects is a Turkish-German joint-venture project conducted between Abant and Akyazı with the collaboration of the Earthquake Research Department of the General Directorate of

Disaster Affairs of Turkish Government and GeoForschungs Zentrum-Postdam. The other project is conducted by the KOERI and Japan Scientists on the same fault zone and to the west of the other project (Yılmaz, 2001).

According to Wyss (2000), our understanding degree of a physical phenomenon is measured by our ability to predict it. In addition to this, Wyss (2000) gives the general definition of prediction, which is also valid for the earthquake prediction, as follows: Specify the location, size and time of the occurrence, all within the error windows, and the probability that this event will occur (Table 2.3).

Table 2.3. Elements necessary for a valid earthquake prediction (Wyss, 2000)

1	Location ± uncertainty
2	Size ± uncertainty
3	Occurrence time ± uncertainty
4	Probability

Considering the occurrence time of an earthquake, the prediction is divided into 4 categories (Yılmaz, 2001):

- I- Long-term prediction (a few years – a few decades)
- II- Mid-term prediction (a few months – a few years)
- III- Short-term prediction (a few weeks – a few months)
- IV- Imminent or warning (a few hours – a few days)

The detailed investigation of pre-occurred earthquake catalogue of any region is always used for the determination of seismicity laws and regularities of continuous seismic processes of that region. Long-term prediction studies are usually based on these data and probability calculations.

On the other hand, as the time period of prediction is shortened, that is as we go towards Short-term prediction (III) or Imminent / Warning (IV), prediction required to be more dynamic. Real time monitoring of some physical, geophysical or seismological properties of the ground is performed for determining the earthquake related anomalies in the observed variables. According to Rikitake (1976), 15 variables to be observed as possible precursors of earthquake are listed and explained as follows:

2.3.1 Land Deformation (l)

According to plate tectonics and regional movement of large rock masses, there exists a continuous movement on the earth's surface. There are a number of instances in which some land deformations are detected by repeated leveling surveys and geodetic work prior to an earthquake (Rikitake, 1976).

2.3.2 Tilt and Strain (t)

Repetition of geodetic surveys is certainly useful for detecting precursory and coseismic land deformations, but it is impossible to monitor the land deformation continuously only by geodetic studies. Thus, using arrays of tiltmeters or strainmeters is more suitable for the purpose of continuous observation of crustal movement.

2.3.3 Foreshock (f)

The small shocks prior to the main large earthquake are often reported (Rikitake, 1976).

2.3.4 b-value (b)

It is well known that the smaller the earthquake magnitude is, the larger is the number of occurrences (Rikitake, 1976 therein Gutenberg and Richter, 1944). Decreases in the value of the constant b in the Gutenberg-Richter formula are sometimes reported (Rikitake, 1976).

2.3.5 Microseismicity (m)

The microfracture formation, as stated in the rock engineering, occurs in the plastic zone of the rock failure. However according to the wet dilatancy model, in the later phases of load increase, the developing pore pressure results in the strain-hardening and prevents the further development of the microcracks to some extent, which indicates the process is approaching the final stage of failure. In accordance with this theory, some cases are reported, in which a decrease in the microearthquake prior to a main shock are observed (Rikitake, 1976).

2.3.6 Source Mechanism (s):

In some earthquakes the direction of compression has showed a rotation between small earthquakes prior to main shock and the larger earthquake (Rikitake, 1976).

2.3.7 Fault Creep Anomaly (c)

The creep rate along the fault zones are observed for an unusual rate of displacement. Some anomalous cases are reported, along the San Andreas Fault and the North Anatolian Fault (Rikitake, 1976).

2.3.8 V_p/V_s Ratio (v)

The decrease and recovery of V_p/V_s ratio has been observed prior to an earthquake in some countries (Rikitake, 1976). The change of V_p/V_s is also explained by the theory of wet dilatancy (Scholz et all., 1973)

2.3.9 V_p and V_s (w)

When a high-quality observation is available, it is possible to determine V_p and V_s separately by means of the ordinary techniques of seismometry. It is known that rocks indicate a velocity anisotropy under nonhydrostatic stresses giving rise to the splitting of S-waves into SV and SH waves. Particle motions for these waves are in the vertical and horizontal planes, respectively. The SH-phase usually arrives slightly earlier than the SV-phase. There are cases, in which the $V_{sh} - V_{sv}$ increased 2.3 to 2.5 %, 10 to 38 days prior to large earthquakes.

2.3.10 Geomagnetic Change (g)

According to Rikitake (1976) very few and reliable examples of geomagnetic anomalous cases have been reported.

2.3.11 Oil Flow (o)

The oil level in some wells is also observed, which is thought to show some anomalous changes due to underground fracturing. Anomalous cases are also reported (Rikitake, 1976 therein, Arieh and Merzer, 1974)

2.3.12 Resistivity (r)

Anomalous electrical resistivity changes prior to earthquakes, was first observed by the Sobolev, (1975) in the Kamchatka region of former U.S.S.R. and used for the prediction of earthquakes.

2.3.13 Radon Emission (i)

Radon, due to its short half life period (3.5 days) and abundancy in underground waters, observed for the purpose of earthquake prediction studies. Some anomalies have been also observed in the radon content of underground waters, e.g. Tashkent earthquake, April, 1966 (Rikitake, 1976).

2.3.14 Underground Water (u)

The water levels (heights) of underground reservoirs are also monitored for the purpose of earthquake prediction. With the idea that, as the stress level increases, the underground crack formation should affect the underground water amount of reservoirs and water level should show some fluctuations prior to earthquakes.

2.3.15 Earth Currents (e)

Electrical potential or current variations prior to some earthquakes have also been reported (Fedotov et all. 1970, 1972, Sobolev, 1975). Since the subject of this thesis is concentrated on potential variations on rock samples with the applied stress, detailed information about the studies on Earth Current precursors will be given in the following section.

2.4 REVIEW OF PREVIOUS STUDIES

2.4.1 Field Studies

One of the first studies on the earth current is performed in Russia (former U.S.S.R.) by Fedotov et al. (1970) in the Kamchatka region. In this study, Fedotov and colleagues performed a three branched study, in which they investigated the Kamchatka-Komandorskiye Islands seismicity laws and proposed some long-term predictions, searched for the connection between earthquakes and the electric anomalies and observed the amplitudes, velocities and other features of P-waves in the Pacific Seismic focal zone near Kamchatka.
The electric potential observations are conducted in the parallel directions from 3 different stations namely N1, N2 and N3, which are 100 km apart from each other. After the observations during the September 1967 – February 1968 period, Fedotov and colleagues concluded that, electric potential variations do occur before and after the earthquakes, generally in the range of 10 hours before and 16 hours after the earthquake. Table 2.4, shows the distribution of electric potential anomaly times, relative to the earthquake occurrence instant. They also added that anomalous disturbances seemed to occur with the intensity of 50 kV/km.

The earth potential on December 19, 1968 Kamchatka earthquake, has showed a sharp decrease for the 6 days period before the earthquake with a rate of 60 mV/km per day and a 300 mV/km peak value (Figure 2.5). These sharp and distinct changes in electrical potential values, followed by earthquakes, are due variation of tension in some part of the focal zone (creep etc.), which are caused by the electrification (mechano-electrical effect) of mountain rocks (piezoelectric origin), Fedotov et al. (1970).

Table 2.4. Distribution of electrotelluric field anomalies in time, relative to the moments of earthquakes (Fedotov et al.,1970)

	Before the moment of shock (h)			**After the moment of shock (h)**		
	24-16	16-8	8-0	0-8	8-16	16-24
Number of Electric Anomalies	2	5	21	9	5	-

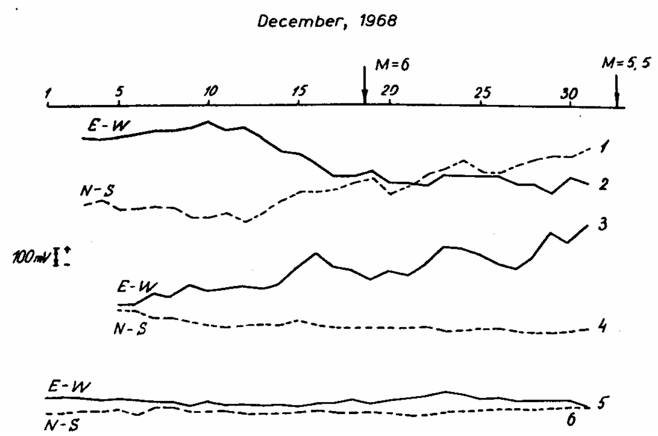

Figure 2.5 Earth potential variations before December 19, 1968 Kamchatka (Fedotov et al., 1970)

On the same region of Kamchatka, Sobolev, (1975), continued the earth potential precursor studies. He was also one of the co-workers of Fedotov et al. (1970). His studies might be devoted as the first work, concentrated on the earth potential measurements. The field studies by Sobolev (1975), are conducted by a network of stations spaced at a distance of 100-200 km apart and measurements are taken in the north-south and east-west directions. The distance between the lead electrodes was set as 200 m.

Sobolev (1975), reported that, in the majority of the cases, the changes in the electrotelluric field before an earthquake do not exceed the background noise. This makes it impossible to distinguish precursors through the recording of one measuring line. As a result, recordings of several stations are processed by a computer algorithm in order to filter the high frequency noise. By using this method, Sobolev (1975), claims that during the period of February, 1972 – December, 1973, 8 earthquakes out of 12 are predicted successfully with a precursory time interval of 5-20 days.

After the probability calculations, considering the alarm time, area of alarm region etc., Sobolev (1975), concluded that conducting a continuous forecast program on Kamchatka, is of scientific interest only. The efficiency of forecast is too low for practical purposes.

Le Mouel and Morat (1987), observed the resistivity changes in the pillars of an old room and pillar mine, located in a limestone reserve, while the surface of the mine was loaded with large land fill (200 000 m^3). The porosity of the rock was 28-46 % and saturation amount of these pores were about 60-70 % in pillars. The measurements were conducted by using a set of electrodes located in a 20X20 mesh pattern, on one rectangular face of certain pillars. The injection current was provided by thin graphite stripes spread on the edges of the related rectangular pillar faces. The two scientists, considered the relative resistivity change ($\rho(t) = \left[R(t) - R(t_0)\right] / R(t_0)$). After continuous observations and weekly data gathering during the period of December 5, 1984 to July, 1985, Le Mouel and Morat (1987), concluded that resistivity variations do occur in the pillars and there are three reasons determined as the possible cause of these fluctuations:

1. An annual wave with an amplitude of a few percent that attributed to an annual variation of temperature and water saturation.

2. The second phenomenon is about 3 percent change in resistivity, attributed to the primary compression phase due to loading of landfill.
3. Finally variations of resistivity between the electrodes of closer grid point of the mesh, caused by the reversible changes of the mechanical state of the rock, in the elastic range.

About the first reason stated, Le Mouel and Morat (1987), also criticized that any decrease in permeability resulted in an increase of resistivity. This behavior is also supported by the explanation of resistivity changes by wet dilatancy model (Scholz et al. 1973).

Most recent examples of field studies, related with earth current, can be attributed to Varotsos and Alexopoulos (1984a, 1984b). Although studies of the Varotsos and Alexopoulos, dates back to 1984, they are treated as recent, since the outcomes of the field studies are still on the course of being tested. Although some researchers reject the validity of the proposed method (Geller et al., 1997), the claimed success rate of the proposed method also increases the importance of the studies (Varotsos and Lazaridou, 1991, Varotsos et al. 1993).

The field studies of Varotsos and Alexopoulos (1984a, 1984b,), includes observation and recording of the electric potential changes of the earths crust in a network of 18 stations across Greece. The 18 observatories of the network were used for continuous monitoring of the electric potential changes in two perpendicular directions (N-S - E-W) and reporting the data to a center, through a phone line network. The recorded electric anomalies were named as, so called, seismic electric signals (SES), and the method used for the analysis of the datum, is named as “VAN” (Varotsos Alexopoulos Network) Method.

The basis of the VAN method is constructed on empirical analysis of the SES (ΔV), magnitude of the expected/related earthquake (M) and distance (r) from the epicenter of the expected/related earthquake to the observatory. According to Varotsos and Alexopoulos when log(ΔV) are calculated and drawn versus M values, the resulting graph always gives a slope between 0.3-0.4 (Figure 2.6). On the other hand, empirical formulation offered by Varotsos and Alexopoulos, offer no relationship between the duration and lead time of the electric signal and the M of the earthquake.

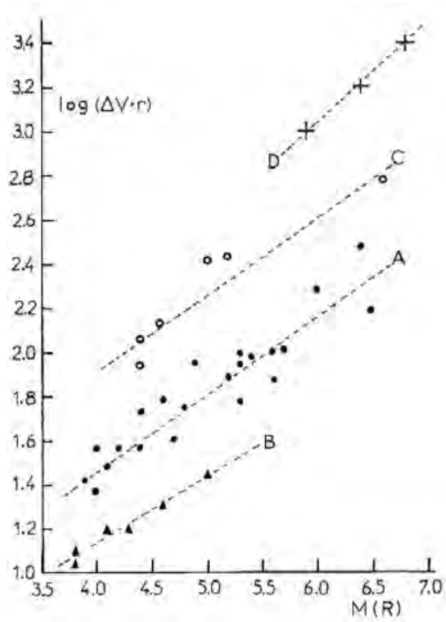

Figure 2.6 M vs. ΔV plot of observed earthquakes (Varotsos and Alexopoulos, 1984a)

The lead times of SES (transient variation of the telluric current) are mainly classified in two groups;

- group I : lead time between 6-13½ h with a maximum around 7h
- group II : lead times between 43-60 h with a flat maximum interval 45-54 h

According to VAN Method, the current density (j) of any detected SES is calculated with the formula:

$$J_{rel} = \left(\left.\frac{\Delta V/L}{\rho_{rel}}\right|_{E-W}^{2} + \left.\frac{\Delta V/L}{\rho_{rel}}\right|_{N-S}^{2} \right)^{1/2} \tag{2.14}$$

Where L denotes the distance between measuring electrodes, ρ_{rel} stands for relative resistivity of the region with respect to other measuring stations, accounting for nonhomogeneities and structural differences. When the calculated $\log(J_{rel} \times r)$ are plotted versus M, a linear relationship is obtained which always has a slope between 0.3 to 0.4, (Figure 2.7, Varotsos and Alexopoulos,1984a).

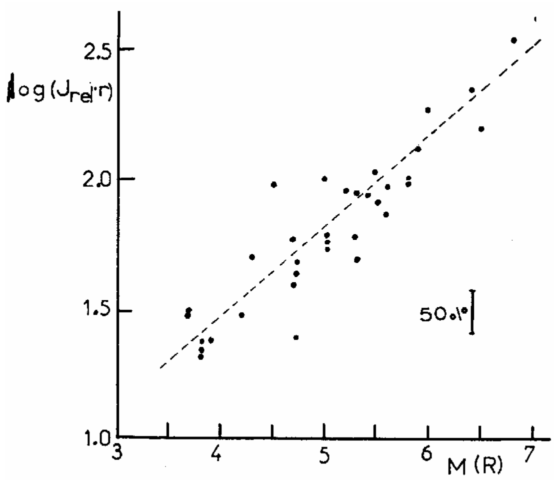

Figure 2.7 Relative current density vs. EQ magnitude
(Varotsos and Alexopoulos,1984a)

If the SES of a certain earthquake is recorded by more than one measuring station, the J_{rel} values of different measuring stations are used for drawing the Apollonian circles and locating the epicenter of related earthquake (Varotsos and Alexopoulos, 1984b).

2.4.2 Laboratory Studies

Bishop (1981), conducted a study about the piezoelectric effects in quartz rich rocks, claiming that; aggregates of piezoelectric grains are themselves piezoelectric, if the grains are suitably aligned (piezoelectric fabric). In the experiments, Bishop used cubic specimens, cut from various quartz rich rock types, in order to record the electrical changes of samples in three orthogonal directions. After the experiments, Bishop concluded that, all quartz rich rocks (quartzites, granites, gneisses, and mylonites) exhibit piezoelectric responses when stressed. According to Bishop, these responses were in two categories:

- Effects due to piezoelectric fabrics, called true piezoelectric effect.
- Effects due to random distributions of the piezoelectric vectors, called statistical effects (Figure 2.8)

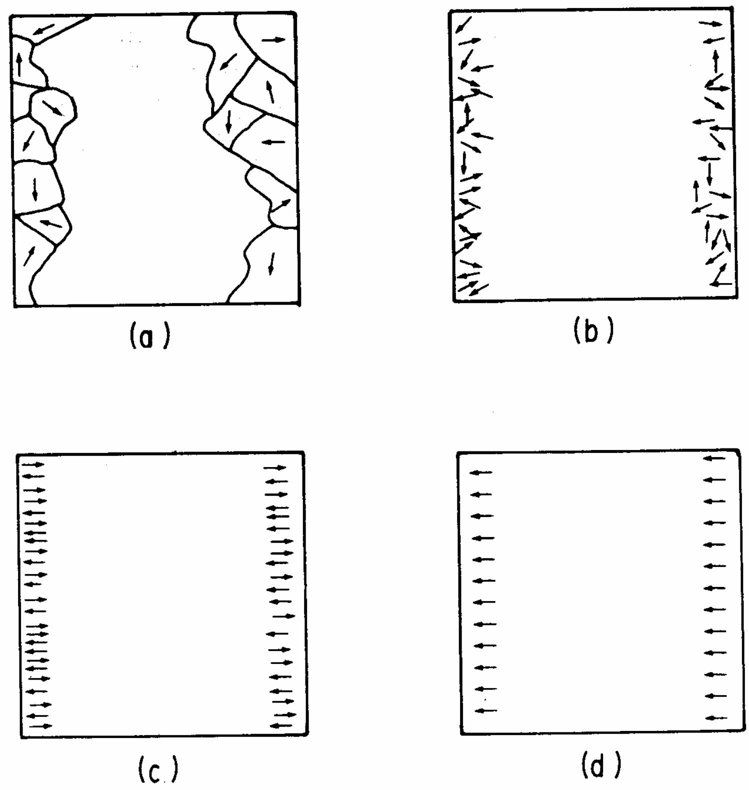

Figure 2.8 Statistical and true piezoelectric effects. (a) Large random grains, large statistical effect. (b) Small random grains, small statistical effect. (c) Spatially aligned but random polarity, a statistical effect. (d) polar aligned, true piezoelectric effect (Bishop, 1981).

The true piezoelectric effect and the statistical piezoelectric effect are distinguished by Bishop (1981) using three criteria:

1. A comparison between the observed results and the values expected from an aggregate with randomly aligned grains of the same size. Piezoelectric results, that are significantly larger than the magnitudes predicted for a specimen with a random crystallographic distribution pattern, would assist the argument that the effects are non-random.

2. Agreements between results of a number of specimens cut from one sample; all specimens having the same orientation. A statistically strong correlation between such specimens would also indicate non-random effects. It would then be likely that these results were associated with the specimen's fabric.
3. Agreement between calculated crystallographic axis orientations and optically observed patterns.

One of the remarkable studies on uniaxial rock breaking experiments is conducted by Hadjicontis and Mavromatou (1994). In their experiments, Hadjicontis and Mavromatou used a hand operated hydraulic pump for loading the samples, in order to eliminate the risk of any electrical noise produced by a motor. The complete experimental setup, used for breaking quartz, granite and limestone samples gathered from different places of Greece, is illustrated in Figure 2.9.

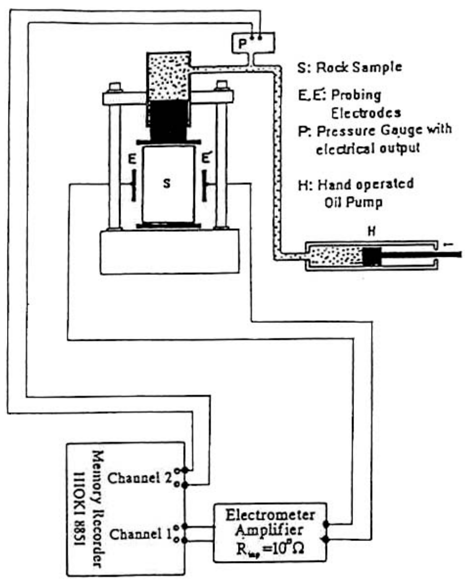

Figure 2.9 Experimental apparatus used by Hadjicontis and Mavromatou (1994)

The combined graphics of stress (σ), stress rate and electric potential of compression of mineral quartz is given in Figure 2.10. According to these graphics besides the existence of transient electric signals, two scientists also proposed a theory about the explanation of these transient signals. The graphical representation of the theoretical response suggested by Hadjicontis and Mavromatou (1994) is given in Figure 2.11. According to this theory, electric signal caused by the effect of applied stress on sample (thus electric dipoles), seem to follow in form, the first derivative of the stress.

According to Hadjicontis and Mavromatou (1994), the formerly existing linear defects in the rock, namely charged edge dislocations, and the Debye-Hückel charge clouds formed by point defects and impurities around the dislocations, consists a system which can be characterized by a relaxation time τ.

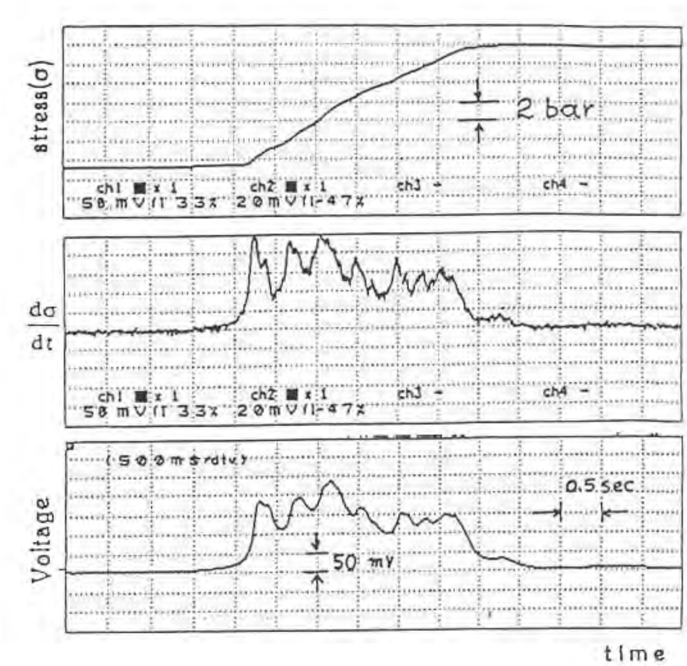

Figure 2.10 Compression of quartz mineral
(Hadjicontis and Mavromatou, 1994)

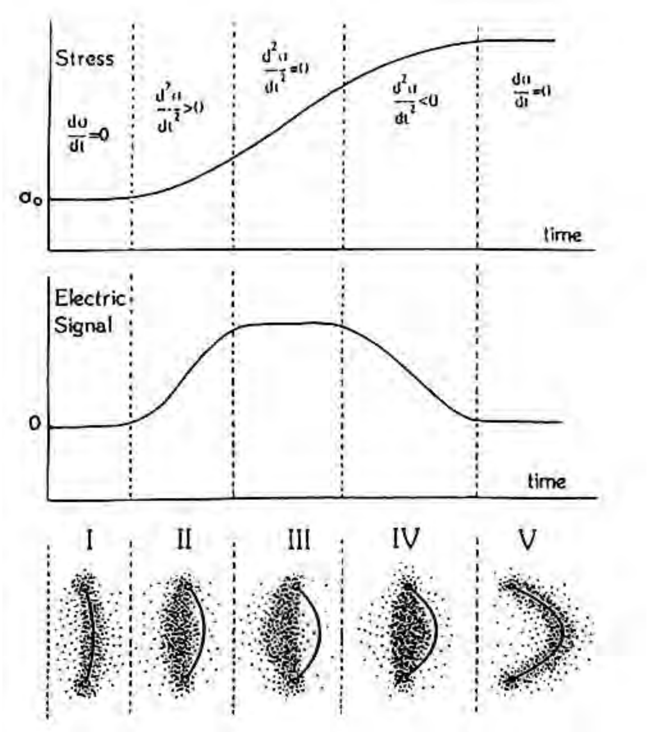

Figure 2.11 The behavior of charge cloud and dislocation (Hadjicontis and Mavromatou, 1994)

From Figure 2.11 Hadjicontis and Mavromatou (1994), distinguishes the following cases:

i) When the stress increases with a variable rate (i.e. $d\sigma/dt > 0$ and $d^2\sigma/dt^2 \neq 0$) the dislocation responds faster than its charge cloud to the abrupt changes of the externally applied stress. This results in the separation of the two opposite charges which form an electric dipole. There are two possibilities:
   - $d^2\sigma/dt^2 > 0$: the dislocation accelerates and moves forward relative to its charge cloud and their distance increases which means that the polarization increases as well (Figure 2.11, stage II).

- $d^2\sigma/dt^2 < 0$: the dislocation slows down, the cloud approaches to it and their distance decreases and hence the polarization decreases (Figure 2.11, stage IV).

ii) When an external constant stress has already been applied, (i.e. $d\sigma/dt = 0$) no dislocation movement is observed and a steady state of equilibrium is established; therefore no polarization arises, (Figure 2.11, stages I and V).

iii) When the stress increases with a constant rate (i.e. $d\sigma/dt > 0$ but $d^2\sigma/dt^2 = 0$) and whenever the stress change occurs within a time comparable with the relaxation time τ at a given temperature, no change of the dipole moment is observed because the distance of the mass centers of the system "core-cloud" remains constant (Figure 2.11, stage III).

Yoshida et al. (1997), performed a laboratory study in which Yoshida and colleagues investigated the DC potential response of granite samples during stick-slip event. During the two applied experiment types, three granite blocks, whose coinciding faces are ground well, are sheared on each other until stick slip event occurs or loaded until a level below the shear strength and suddenly unloaded. The electric potential data is gathered with the help of two silver electrodes (EL1, EL3) and shear strain data is recorded with 10 strain gauges with the set-up shown in Figure 2.12.

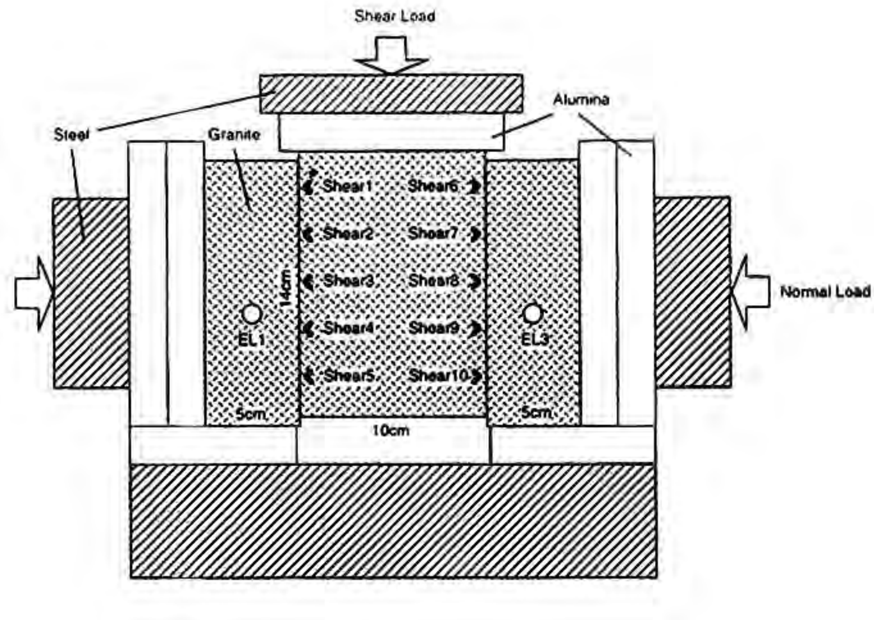

Figure 2.12 Experimental set-up used by Yoshida et al (1997)

Yoshida et al. (1997), reported the existence of both the preseismic and coseismic electric potential responses and at the same time proposed a model based on the piezoelectric effect. According to this theory; initially the polarization charges, that are proportional to the applied stress ($p_i^0 = c_{ijk}\sigma_{jk}$), are neutralized by the compensating bound charges which have moved to the surface of the quartz crystal (Figure 2.13, a). The rapid process of stick-slip causes a sudden drop of stress $\Delta\sigma_{jk}$ and the net polarization in the quartz crystal dropped to $p_i = c_{ijk}(\sigma_{jk}^0 - \Delta\sigma_{jk})$ (Figure 2.13, b). If the stress drop occurs rapid enough when compared with the relaxation time (τ), the net or effective polarization ($\hat{P} = p_i - p_i^0$) can be recorded as electric signal from the outside of the rock. In the third stage, the bound charges will move to cancel the effective polarization charges (Figure 2.13, c).

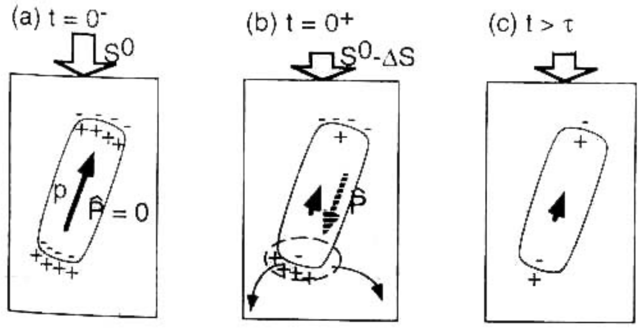

Figure 2.13 Polarization of quartz with applied load (Yoshida et al., 1997)

The combined polarization response of any piezoelectric rock can be given with the following formula (Yoshida et al., 1997):

$$d\hat{P}_i / dt = -c_{ijk} d\sigma_{jk} \Big/ dt - \hat{P}_i \Big/ \tau \qquad (2.15)$$

The generated time dependent piezoelectric potential of a rock mass v_0, can be expressed as follows (Yoshida et al., 1997):

$$V(t) = \frac{-\tau}{4\pi\varepsilon} \sum_m \frac{v_0^{(m)} r_i^{(m)} c_{ijk}^{(m)} \sigma_{jk}^{(m)}(t)}{\left| r^{(m)} \right|^3} \qquad (2.16)$$

The similar results obtained from stick-slip experiments and sudden release of stress experiments are, accepted as the proof of piezoelectric origin of produced potential by Yoshida et al., (1997).

Another valuable comment is about the preseismic potential variations during stick-slip event. According to Yoshida et al., (1997), the growth of the rupture nucleation process is closely related with the preseismic potential occurrence. When the rupture nucleation is observed on the left block the preseismic potential is observed in the EL1, the reverse is also true for right hand block without exception (Figure 2.12). The graphics given in Figure

2.14, indicates a growth nucleation from shear strain data along right surface and related preseismic electric potential.

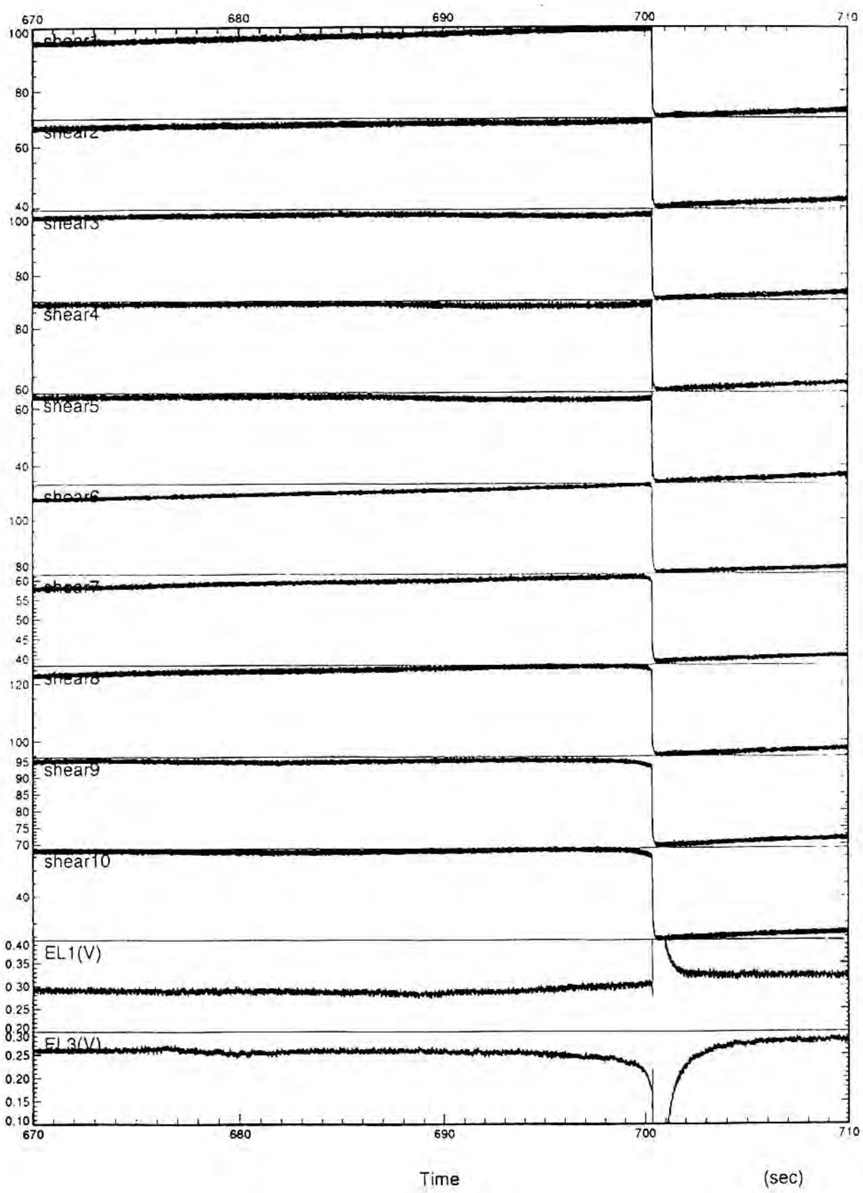

Figure 2.14 Progress of rupture nucleation from strain data on shear 6, 7, 8, 9, 10 and preseismic signal on EL3 (Yoshida et al. 1997)

Freund (2002), suggested a similar theory with Hadjicontis and Mavromatou (1994), which is based on the existence of more mobile charge carriers, namely “positive holes”. Actually positive holes are defect electrons, which are produced by the existence of oxygen atoms, with a rare oxidation state “O^{-}”. Before activation positive holes occur as positive hole pairs (PHP) as chemically equivalent to peroxy links, ($O_3X/^{oo}\backslash XO_3$). The chemical reaction series of mineral structure with water, that ends up with evolution of PHPs is given by Freund (2002), as follows:

$$(H_2O)_{dissolved} + (O_3X/^{o}\backslash XO_3)_{structure} \Leftrightarrow (O_3X/^{oH}{}_{Ho}\backslash XO_3)_{structure}$$

$$(O_3X/^{oH}{}_{Ho}\backslash XO_3)_{structure} \Leftrightarrow (H_2)_{structure} + (O_3X/^{oo}\backslash XO_3)_{structure}$$

Then the O^{-}-O^{-} bond can be easily broken, releasing a positive hole. Freund (2002) also explains the propagation of positive holes through an oxide or silicate matrix in terms of “electron hopping”. If one O^{2-} in the sea of O^{2-} changes to O^{-}, it creates a situation whereby electrons from neighboring O^{2-} can easily hop into the O^{-} site.

Aydan, has also many contributions to the study of electrical response of geomaterials / rock samples (Aydan et al., 2001, 2003). In an experiment, (Aydan et al., 2003), Aydan and his co-workers conducted rock fracturing (uniaxial compression) and sliding experiments, on non-piezoelectric rock and crystal samples, namely; pyrite, calcite, aragonite, fluorite, gypsum, rocksalt, soapstone, marl, limestone and tuff. Rock fracturing tests were conducted in Rock Mechanics Laboratories of Tokai University Toyota National College of Technology, Hacettepe University and Middle East Technical University.

The electric responses are recorded as AC or DC, since the electric responses of rocks may be different for both cases (Aydan et al., 2003). The acoustic emissions of rocks are also recorded, in order to monitor the relationship between the so-called seismic electric signals (SES) and fracture occurrence and propagation (Aydan et al., 2003).

As the outcomes of this study, Aydan et al. (2003), proposed a model about the electrification mechanism of either piezoelectric or non-piezoelectric geomaterials. Considering this model, theoretical calculations of electric responses of both the piezoelectric and the non-piezoelectric materials are given in the Figure 2.16 (Aydan et al., 2003). According to this model, the potential development could also be caused by the momentum associated with the state of stress and straining imposed on the geomaterials. The magnitude of induced electric potential both depends upon the piezoelectric characteristics of minerals or grains and the moment caused by the separation of electrons of minerals as a result of deformation and inter-crystal or inter-granular separation.

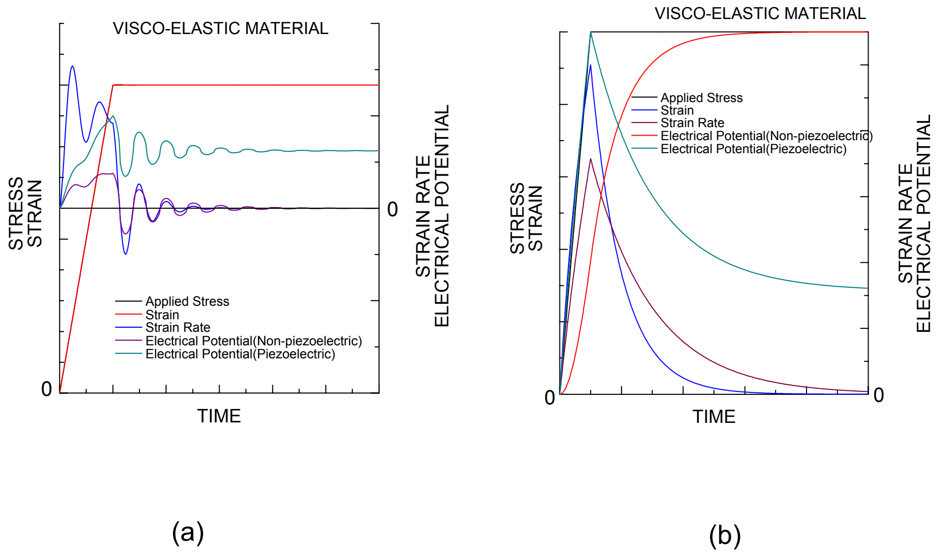

Figure 2.15 Computed responses of various parameters during a uniaxial loading, (a) with considering inertia, (b) without inertia (Aydan et al., 2003)

CHAPTER 3

EXPERIMENTAL SET-UP AND EQUIPMENT

The equipment used in the experiments are; MTS brand and MTS 815 model loading system for applying the load on the specimens, Agilent 34970A data logger with HP 34901A multiplexer for recording the potential changes and IOtech brand Daqbook/2000X and DBK80 combination for monitoring and recording the load.

3.1 MTS 815 Servohydraulic Testing System

The MTS 815 servohydraulic loading system, which is located in the Rock Mechanics Laboratory of Mining Engineering Department, METU, is utilized for uniaxial loading of the specimens, during the experiments. The MTS 815 testing machine is composed of four main components (MTS System Catalogue, 1992):

- Load Frame
- MicroConsole
- MicroProfiler
- Hydraulic Power Supply

3.1.1 Load Frame

Load frame is a highly rigid, free standing frame, which consists of an actuator located in the base chassis and an upper frame bolted to the lower chassis. The combined frame has a high loading capacity, without the need of an external rigidity system or support. The crosshead that is useful for handling different specimen sizes and shapes are located on the upper plate (Figure 3.1).

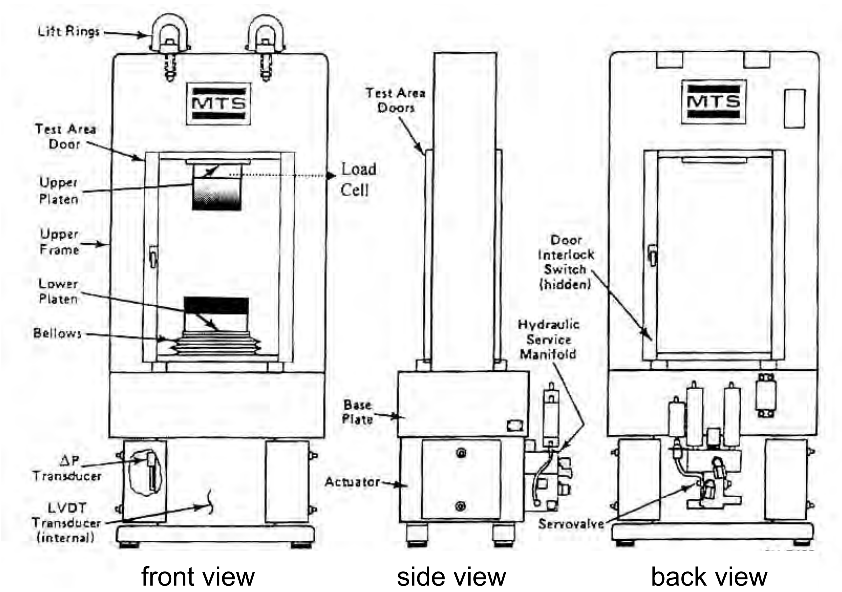

Figure 3.1 Schematic diagram of MTS 815 Load Frame
(MTS System Catalogue, 1992)

The load frame has an inbuilt load cell with a capacity of 2800 kN, but the working principle of this load cell is unsuitable for precise measurements especially with lower ranges. An external load cell with a capacity of ±500 kN and an accuracy of ±0.25 kN is attached and used for measuring the applied load throughout the experiments.

3.1.2 MicroConsole

Model 458/20C MicroConsole is responsible from providing the readout and station control functions (Figure 3.2). The unit also serves as a chassis for the 458 series plug-in modules. The unit also provides multifunction digital display, cycle counter, program and record control, hydraulic pressure control, interlocks and internal power supply to support up to six plug-in modules. The MicroConsole has ±0.01 % full-scale resolution and ±0.05 % full scale accuracy.

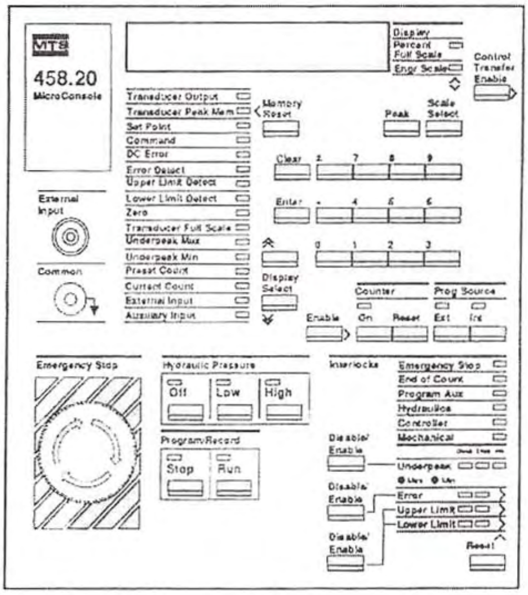

Figure 3.2 MicroConsole user panel (MTS System Catalogue, 1992)

3.1.3 MicroProfiler

MicroProfiler is a microprocessor based waveform generator. Programmed segments by MicroProfiler, can be linked together to create waveforms, including ramp, haversine, and hold time segments. Segments can also be combined in the forms of blocks (Figure 3.3).

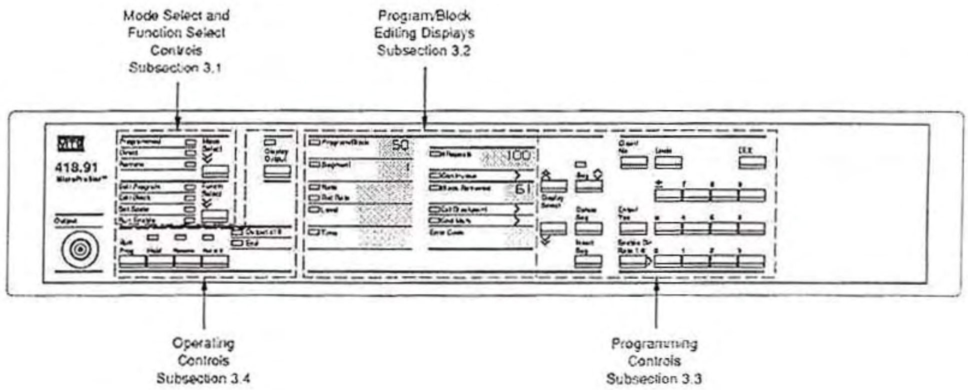

Figure 3.3 MicroProfiler Front panel (MTS System Catalogue, 1992)

Three modes of operation are available for MicroProfiler. The **programmed** mode is used for creating segments and grouping them together to form desired waveform programs. The **direct** mode is used for manually operating the system by selecting one of the pre-created 9 programs. The **remote** mode allows an external computer (i.e. Personal PC) to operate the MicroProfiler through a RS-232 serial interface.

3.1.4 Hydraulic Power Supply

The model 506.01E Hydraulic Power Supply (HPS) uses a fixed volume pump to provide a source of hydraulic power for hydraulic systems. The power supply is specifically designed for systems with servo-valves. The HPS can be either operated manually or from a remote control device (458/20C MicroConsole). The temperature control of HPS is automatically maintained by a fluid-water heat exchanger.

3.2 Data Recording System

3.2.1 Data Logger

Agilent 34970A is a multipurpose data acquisition / switch unit that can be used with combinations of 8 different available modules. In the experiments the HP34901A multiplexer module is used for the measurement of AC or DC potential of the samples. The resolution of the data read is 6½ digits (22 bit) and accuracy of the measurement is 0.004% for DC potential and 0.06% for AC potential measurement (Figure 3.4).

Figure 3.4 Agilent 34970A data logger (Agilent 34970A users guide, 1999)

3.2.2 Data Acquisition System

Daqbook/2000X is a 16 bit, 200 kHz multifunction data acquisition system with 3 slots for expansion. The DBK 80 is a low-noise, high speed, unity-gain multiplexer card with 16 channels of differential voltage input. The DBK80's gain combines with Daqbook/2000X to accept full scale inputs from ±156 mV to ±10V. DBK80 also has an on-board precision voltage source with +5 V or +10 V options, which can be used to bias strain gauges, thermistors or other transducers that require biasing (DBK Option Card & Modules Users Manual, 2003).

CHAPTER 4

EXPERIMENTAL PROCEDURE AND MATERIAL

Electric potential variations of different quartz bearing rock samples are monitored during uniaxial loading. Procedure and sample preparation work is explained in the following sections.

4.1 Experimental Procedure

Electric potential (EP) variations during uniaxial loading of three rock types are monitored. 4 different experiment types are conducted on quartz-sandstone, granite and granodiorite samples. The experiments are conducted in a displacement controlled manner with three different loading rates, LR1, LR2, and LR3. The utilized loading rates are, 0.005 mm/s, 0.01 mm/s and 0.05 mm/s, respectively. An example graph for LR1, LR2 and LR3 experiments is given in Figure 4.1.

In LR1 rate, the EP values are measured both in AC mode and in DC mode. The aim of measuring the EP both in AC and DC modes is to understand which mode gives better EP response. The load is applied through stiff testing system MTS 815, in the direct mode and the measured data are recorded in two desktop computers. In three of the experiment methods (LR1, LR2 and LR3), the samples are loaded continuously with the given loading rates until failure, as in the uniaxial compressive strength experiments. In the fourth experiment method (STEP), the samples are loaded with displacement rate 0.005 mm/s, in a stepwise manner with three load levels, and after the third step, load is continuously increased until failure. An example of STEP experiment graph is given in Figure 4.2. The number of samples tested for each method is 5 for each rock type. Schematic representation of set-up used in the experiments is given in the Figure 4.3.

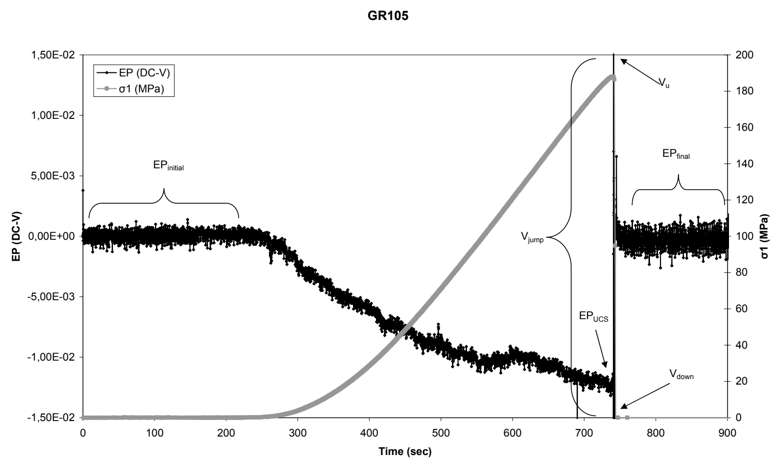

Figure 4.1 Example graph for LR1, LR2 and LR3 experiments

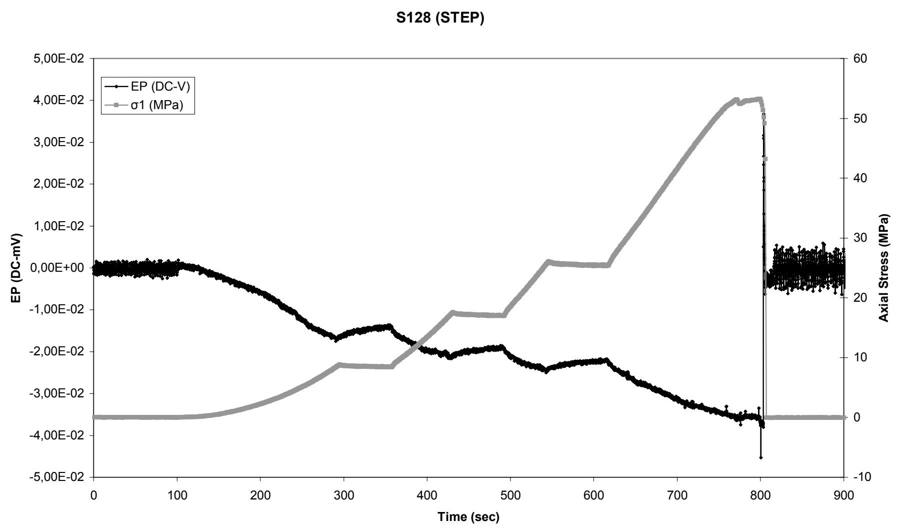

Figure 4.2 Example STEP loading experiment graph

The loading platens are grounded and samples are isolated from loading platens by PVC isolators, in order to eliminate the possible noise effects due to the electric operated hydraulic pump motor. The measuring electrodes were circular copper electrodes with 0.20 mm thickness.

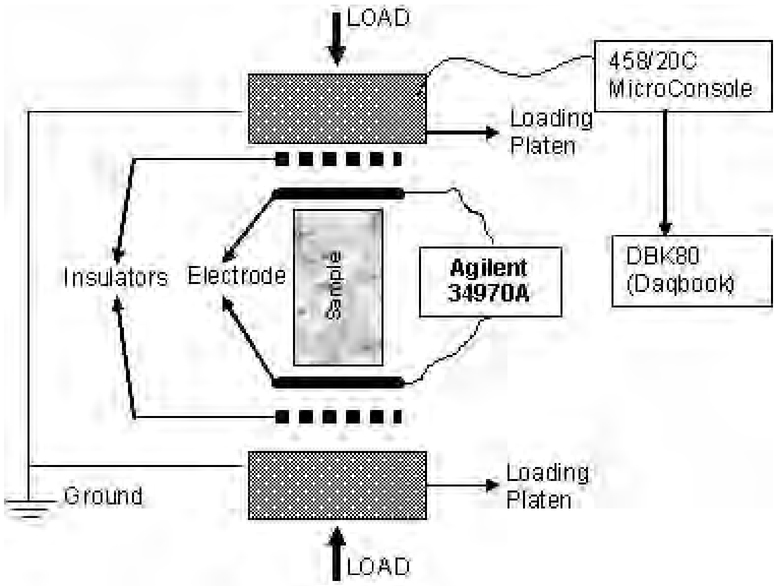

Figure 4.3 Schematic diagram of experimental set-up

4.2 Experimental Material

Three rock types are tested in the experiments. Tested rock types are quartz-sandstone from Kurucaşile – Bartın, and granite and granodiorite from Kaman – Kırşehir (Figure 4.4). Rock types to be used in the experiments are intentionally selected as quartz bearing rocks, in accordance with the subject of this thesis. The large block specimens, which are brought to the Rock Mechanics Laboratory of Mining Engineering Department, are cut as NX sized cylindrical samples with a length to diameter ratio (L/D) of 2-2.5, according to the standard of International Society for Rock Mechanics (ISRM, 1979). The loading surfaces of the cylindrical samples are ground smooth in order to obtain a uniform loading area on the sample.

The prepared samples are coded by a letter (two letters for granite and granodiorite samples) indicating the type of rock, a number indicating the loading rate and a two digit number for distinguishing the samples of same rock type (S106, GR217, GD323,… etc.). For the STEP experiments, the word STEP is added to the end of the explained coding system (GD128STEP,… etc.).

Figure 4.4 Tested rock types, left to right; quartz-sandstone granite and granodiorite

The Mechanical properties of the specimens such as, Dynamic Young's Modulus (E_d) , Poisson's Ratio (ν), P-wave velocity (V_p), S-wave velocity (V_s), are determined for 3 samples from each rock type, in the Geophysics Laboratory of Research Laboratories for Railways, Airports and Harbours (DHL) (Table 4.1). Physical properties of the samples, length (L), weight (W), diameter (D) and unit weight (ϕ) are also measured and calculated before the loading experiments. Mechanical properties of the specimens are given in Table 4.1.

Macroscopic description samples and thin sections prepared in the Geological Engineering Department of Middle East Technical University are used for macroscopic and microscopic inspection of the rock samples. According to test results obtained from DHL and inspection conducted in Geological Engineering Department of Middle East Technical University, the descriptions of the rock samples are as follows:

Table 4.1 Mechanical properties of tested rocks

Rock type	Sample Number	V_p (m/s)	V_s (m/s)	Poisson's Ratio	G_d (GPa)	E_d (GPa)	Unit Weight (gf/cm^3)
Granite	1	2,955	1,857	0.173	9.05	21.23	2.57
	2	3,115	1,883	0.212	9.30	22.55	2.57
	3	3,166	1,942	0.198	9.89	23.70	2.57
Average ± St. Dev.		**3,079 ±0.110**	**1,894 ±0.044**	**0.194 ±0.000**	**9.41 ±0.43**	**22.49 ±1.24**	**2.57 ±0.00**
Granodiorite	1	5,085	2,656	0.312	18.79	49.31	2.61
	2	4,960	2,520	0.326	16.92	44.86	2.61
	3	5,086	2,731	0.297	19.87	51.55	2.61
Average ± St. Dev.		**5,044 ±0.072**	**2,636 ±0.107**	**0.312 ±0.000**	**18.52 ±1.49**	**48.57 ±3.41**	**2.61 ±0.00**
Quartz-Sandstone	1	2,223	1,424	0.152	4.77	11.00	2.31
	2	2,106	1,385	0.119	4.70	10.52	2.40
	3	2,355	1,575	0.095	5.98	13.10	2.36
	4	2,190	1,363	0.184	4.44	10.51	2.34
	5	2,119	1,382	0.130	4.50	10.16	2.31
	6	2,207	1,471	0.100	5.40	11.89	2.45
Average ± St. Dev.		**2,200 ±0.090**	**1.433 ±0.079**	**0.130 ±0.000**	**4.97 ±0.60**	**11.20 ±1.11**	**2.36 ±0.00**

4.2.1 Granite

The average UCS of granite samples is determined as 167,57 MPa, average Dynamic Young's Modulus (E_d) is 22.5 GPa and unit weight (ϕ) is 2.60 gf/cm^3.

The rock is medium grained and includes more-less equigranular grains of K-feldspar, quartz and plagioclaise. The mafic mineral is dark brown biotite. Chlorite only occurs as alteration mineral surrounding biotite flakes. Quartz occurs as mosaic like crystals and includes tiny prismatic rutile. Zircon and apetite occurs as accessory minerals. The quartz content of the rock reaches up to 35 %.

4.2.2 Granodiorite

The average UCS of granodiorite samples is determined as 161.82 MPa, average Dynamic Young's Modulus (E_d) is 48.6 GPa and unit weight (ϕ) is 2.62 gf/cm^3.

The rock is holocrystalline and includes medium to large grains of K-feldspar, plagioclaise and quartz. The quartz content is %25. The mafic minerals are greenish-brown biotite, dark green hornblends, sphene, tourmaline and opaque minerals. Sericite, chlorite and calcite occurs as secondary minerals. The K-feldspars are perthitic and include prismatic plagioclaise crystals. The plagioclaises display polysynthetic twinning and are moderately altered. Quartz shows undulose (slightly deformed quartz crystals).

4.2.3 Quartz-sandstone

The average UCS of quartz-sandstone samples is determined as 49.6 MPa, average Dynamic Young's Modulus (E_d) is 11.2 GPa and unit weight (ϕ) is 2.40 g/cm^3.

Macroscopically, the rock is a fine grained quartz-sandstone. Under the microscope, it includes more-less rounded and well sorted grains up to 1 mm in diameter. The quartz grains are variably deformed and loosely cemented. The quartz content reaches up to 90 %. Other contents are; tourmaline, white mica (muscovite), zircon, rock fragments and opaque minerals.

CHAPTER 5

RESULTS AND DISCUSSION

The uniaxial load and the EP data recorded during the experiments are extensively processed with Microsoft Excel for further analysis. The load data is converted to axial stress (σ_1) first, and then time versus stress (σ_1) and EP graphs are drawn, which are used for analysis of the results. As shown on the sample graph (Figure 5.1), the horizontal axis denotes the time, the vertical axis on the left indicates EP values and the one on the right indicates the axial stress values. The graphs drawn for all the experiments are given in the APPENDIX-A, B and C. According to the piezoelectric theory given in Chapter 2, mainly a linear relationship between the stress level and the EP is expected in the analysis.

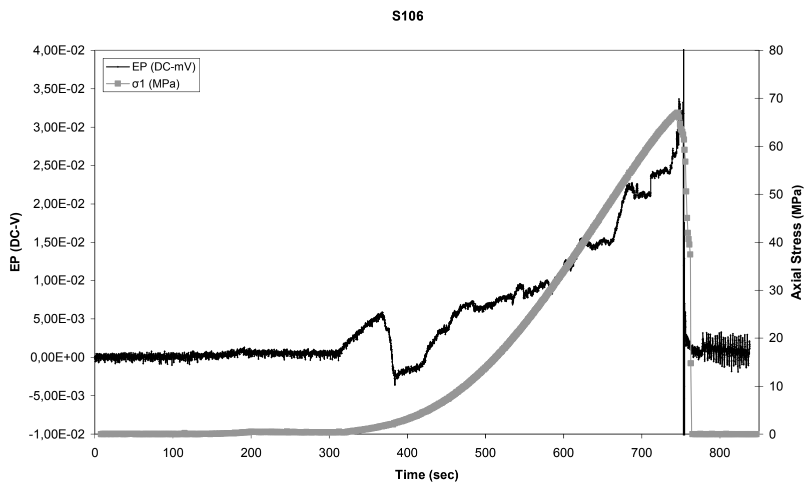

Figure 5.1 EP and Axial Stress versus time graph for sample No: S106

5.1 Analysis of the Results

For the analysis of the results, some criteria are developed to evaluate the specific EP changes in relation to stress and deformational behavior. Also the possible relationships between EP changes and some physical properties of the samples are sought. The developed criteria are:

- The spike-like up jump and down jump EP changes observed at failure (V_{up}, V_{down})
- The magnitude of the spike-like coseismic electrical signal at failure, (V_{jump})
- Logarithm of ΔV value, ($\log(V_{jump})$)
- The initial electric potential value before loading, ($EP_{initial}$)
- The final electric potential value after the load is released, (EP_{final})
- The electric potential value, achieved at failure stress, (EP_{UCS})
- For the STEP loading experiments, the average stress and EP values for load levels, ($\sigma 1_{step1}$, $\sigma 1_{step2}$, EP_{step1}, EP_{step2} etc.)

The physical properties of samples, such as unit weight are also searched for possible effects on EP generation mechanism. The prepared data tables for LR1, LR2 LR3 and STEP experiments on granite, granodiorite and quartz-sandstone samples are given in Table 5.1, Table 5.2, and Table 5.3, respectively. The data given in these tables are used for the analysis of the results.

From the given tables the average UCS of granite, granodiorite and quartz-sandstone are determined as 167.57 MPa, 161.82 MPa and 49.60 MPa. The average unit weights of the rocks are 2.60 gf/cm^3, 2.62 gf/cm^3 and 2.40 gf/cm^3, in the same order. The average Dynamic Young's Modulus values of rocks are determined as; granite 22.5 GPa, granodiorite 48.6 GPa and quartz-sandstone 11.2 GPa from the Table 4.1.

Table 5.1 EP measurement results of LR1, LR2 and LR3 and STEP experiments on Granite samples

Exp. Type	Experiment Number	EP	Sample Number	Unit Weight (gf/cm^3)	UCS (MPa)	V_{up} (mV)	V_{down} (mV)	V_{jump} (mV)	log (ΔV) (mV)	($EP_{initial}$-EP_{final}) (mV)	Abs($EP_{initial}$-EP_{final}) (mV)	Abs(EP_{UCS}) (mV)
LR1	GR105	DC	1	2,60	188,05	28,214	-88,890	117,104	-931,427	0,393	0,393	0,034
LR1	GR106	DC	2	2,60	110,43	10,612	-1,012	11,624	-1934,644	-0,971	0,971	8,556
LR1	GR107	DC	3	2,60	134,05	11,234	3,079	8,155	-2088,555	0,131	0,131	9,960
LR1	GR108	DC	4	2,60	109,78	0,147	-5,308	5,455	-2263,201	-0,584	0,584	0,082
LR1	GR116	DC	5	2,60	178,04	13,931	-61,072	75,003	-1124,921	1,604	1,604	5,232
LR1 AVERAGE				**2,60**	**144,07**	**12,828**	**-30,641**	**43,468**	**-1668,550**	**0,115**	**0,737**	**4,773**
LR2	GR217	DC	6	2,59	159,04	59,794	1,113	58,681	-1231,505	-1,097	1,097	2,480
LR2	GR220	DC	7	2,60	151,14	21,359	-78,370	99,729	-1001,180	2,026	2,026	15,079
LR2	GR222	DC	8	2,61	170,92	114,223	-33,092	147,315	-831,753	-0,867	0,867	18,104
LR2	GR223	DC	9	2,60	198,24	87,044	-41,916	128,960	-889,546	0,006	0,006	1,161
LR2	GR227	DC	10	2,60	165,78	56,886	-73,467	130,353	-884,879	-0,485	0,485	7,555
LR2 AVERAGE				**2,60**	**169,03**	**67,861**	**-45,146**	**113,007**	**-967,772**	**-0,083**	**0,896**	**8,876**
LR3	GR324	DC	11	2,61	189,07	-106,659	-13,178	93,481	-1029,274	3,065	3,065	30,520
LR3	GR325	DC	12	2,60	167,32	72,450	-78,578	151,028	-820,944	1,397	1,397	30,729
LR3	GR326	DC	13	2,62	184,97	65,938	-44,782	110,719	-955,777	-1,494	1,494	14,380
LR3	GR328	DC	14	2,61	158,16	-49,011	-164,203	115,192	-938,578	0,995	0,995	30,820
LR3	GR329	DC	15	2,61	198,49	112,276	-145,335	257,611	-589,035	-2,599	2,599	5,062
LR3 AVERAGE				**2,61**	**179,60**	**18,999**	**-89,215**	**145,606**	**-866,721**	**0,273**	**1,910**	**22,302**
STEP	GR135STEP	DC	16	2,58	186,80	198,215	-49,123	247,338	-606,709	-0,210	0,210	8,410
STEP	GR136STEP	DC	17	2,57	195,57	23,191	-103,045	126,236	-898,817	-1,567	1,567	4,903
STEP	GR137STEP	DC	18	2,57	199,78	46,805	-13,764	60,569	-1217,751	-0,608	0,608	1,295
STEP	GR138STEP	DC	19	2,58	136,30	44,302	-13,966	58,268	-1234,571	0,047	0,047	9,488
STEP	GR139STEP	DC	20	2,62	169,43	45,553	-13,865	59,418	-1226,080	-0,281	0,327	5,391
STEP AVERAGE				**2,58**	**177,58**	**71,613**	**-38,753**	**110,366**	**-1036,786**	**-0,524**	**0,552**	**5,897**

Table 5.2 EP measurement results of LR1, LR2, LR3 and STEP experiments on Granodiorite samples

Exp. Type	Experiment Number	EP	Sample Number	Unit Weight (gf/cm^3)	UCS (MPa)	V_{up} (mV)	V_{down} (mV)	V_{jump} (mV)	log (ΔV) (mV)	($EP_{initial}$-EP_{final}) (mV)	Abs($EP_{initial}$-EP_{final}) (mV)	Abs(EP_{UCS}) (mV)
LR1	GD104	DC	1	2,61	193,81	101,461	-23,462	124,923	-903,358	-1,168	1,168	24,987
LR1	GD105	DC	2	2,63	148,41	10,521	-14,553	25,074	-1600,785	-5,631	5,631	14,553
LR1	GD106	DC	3	2,61	192,47	6,682	-86,502	93,183	-1030,661	-6,092	6,092	0,773
LR1	GD107	DC	4	2,61	153,91	45,062	-24,284	69,346	-1158,977	-5,636	5,636	2,955
LR1	GD109	DC	5	2,61	150,53	2,338	-10,171	12,510	-1902,753	2,833	2,833	3,309
LR1 AVERAGE				**2,62**	**167,83**	**33,213**	**-31,794**	**65,007**	**-1319,307**	**-3,139**	**4,272**	**9,315**
LR2	GD217	DC	6	2,62	191,18	73,314	-36,417	109,730	-959,673	-0,355	0,355	19,693
LR2	GD218	DC	7	2,61	115,20	7,265	-3,298	10,563	-1976,215	1,535	1,535	7,265
LR2	GD219	DC	8	2,61	185,42	-1,846	-118,261	116,415	-933,992	-22,537	22,537	5,837
LR2	GD220	DC	9	2,61	172,06	0,329	-111,207	111,536	-952,585	0,266	0,266	21,185
LR2	GD221	DC	10	2,62	136,16	-3,232	-58,496	55,264	-1257,557	0,263	0,263	10,373
LR2 AVERAGE				**2,62**	**160,01**	**15,166**	**-65,536**	**80,702**	**-1216,005**	**-4,166**	**4,991**	**12,870**
LR3	GD322	DC	11	2,62	184,59	-6,326	-85,170	78,844	-1103,231	0,931	0,931	6,326
LR3	GD323	DC	12	2,63	177,22	70,799	3,591	67,209	-1172,575	-3,589	3,589	53,138
LR3	GD324	DC	13	2,61	156,61	2,546	-42,564	45,109	-1345,733	2,230	2,230	42,564
LR3	GD325	DC	14	2,64	165,78	27,091	-25,921	53,012	-1275,626	1,113	1,113	26,643
LR3	GD326	DC	15	2,62	138,09	15,452	-14,946	30,398	-1517,149	3,708	3,708	8,385
LR3 AVERAGE				**2,62**	**164,46**	**21,912**	**-33,002**	**54,914**	**-1282,863**	**0,879**	**2,314**	**27,411**
STEP	GD127STEP	DC	16	2,61	129,21	-2,987	-14,221	11,234	-1949,464	20,037	20,037	5,437
STEP	GD128STEP	DC	17	2,61	158,65	28,150	-7,840	35,990	-1443,814	-17,913	17,913	0,663
STEP	GD129STEP	DC	18	2,62	172,77	7,677	-28,090	35,767	-1446,513	-2,235	2,235	18,621
STEP	GD130STEP	DC	19	2,62	144,96	2,877	-11,853	14,730	-1831,792	1,180	1,180	8,805
STEP	GD131STEP	DC	20	2,61	169,39	2,419	-16,487	18,906	-1723,397	-25,804	25,804	2,419
STEP AVERAGE				**2,62**	**155,00**	**7,627**	**-15,698**	**23,326**	**-1678,996**	**-4,947**	**13,434**	**7,189**

Table 5.3 EP measurement results of LR1, LR2, LR3 and STEP experiments on Quartz-sandstone samples

Exp. Type	Experiment Number	EP	Sample Number	Unit Weight (gf/cm^3)	UCS (MPa)	V_{up} (mV)	V_{down} (mV)	V_{jump} (mV)	log (ΔV) (mV)	($EP_{initial}$-EP_{final}) (mV)	Abs($EP_{initial}$-EP_{final}) (mV)	Abs(EP_{UCS}) (mV)
LR1	S106	DC	1	2,41	66,95	48,000	-213,000	261,000	-583,359	-0,650	0,650	31,132
LR1	S107	DC	2	2,37	29,65	20,800	9,140	11,660	-1933,301	-3,681	3,681	13,810
LR1	S110	DC	3	2,48	19,36	-39,900	-47,900	8,000	-2096,910	3,151	3,151	31,759
LR1	S115	DC	4	2,41	52,48	-3,520	-135,000	131,480	-881,140	2,559	2,559	119,174
LR1	S116	DC	5	2,36	56,57	31,100	16,800	14,300	-1844,664	-0,156	0,156	24,849
LR1 AVERAGE				**2,40**	**45,00**	**11,296**	**-73,992**	**85,288**	**-1467,875**	**0,245**	**2,039**	**44,145**
LR2	S218	DC	6	2,35	47,76	32,600	23,100	9,500	-2022,276	0,407	0,407	25,030
LR2	S219	DC	7	2,48	29,06	-20,600	-26,900	6,300	-2200,659	0,646	0,646	18,789
LR2	S220	DC	8	2,44	78,91	11,600	-45,400	57,000	-1244,125	7,673	7,673	43,229
LR2	S221	DC	9	2,38	44,62	-21,700	-26,100	4,400	-2356,547	3,762	3,762	24,432
LR2	S222	DC	10	2,42	51,92	32,400	-4,599	36,999	-1431,813	3,647	3,647	31,213
LR2 AVERAGE				**2,41**	**50,45**	**6,860**	**-15,980**	**22,840**	**-1851,084**	**3,227**	**3,227**	**28,539**
LR3	S323	DC	11	2,43	58,06	44,100	-62,200	106,300	-973,467	0,139	0,139	31,039
LR3	S324	DC	12	2,48	39,84	100,000	15,400	84,600	-1072,630	0,732	0,732	23,952
LR3	S325	DC	13	2,42	38,29	-20,400	-25,700	5,300	-2275,724	0,425	0,425	19,638
LR3	S326	DC	14	2,34	47,28	57,800	-36,200	94,000	-1026,872	0,175	0,175	37,199
LR3	S327	DC	15	2,44	69,57	22,400	-99,800	122,200	-912,929	0,495	0,495	25,488
LR3 AVERAGE				**2,42**	**50,61**	**40,780**	**-41,700**	**82,480**	**-1252,324**	**0,393**	**0,393**	**27,463**
STEP	S128(STEP)	DC	16	2,34	52,64	36,800	38,000	1,200	-2920,819	0,186	0,186	38,002
STEP	S129(STEP)	DC	17	2,46	75,66	121,935	-76,845	198,780	-701,627	-0,126	0,126	12,902
STEP	S130(STEP)	DC	18	2,41	47,48	0,413	-11,162	11,575	-1936,477	-0,234	0,234	8,598
STEP	S131(STEP)	DC	19	2,29	40,96	-12,733	-19,471	6,739	-2171,437	0,935	0,935	14,378
STEP	S132(STEP)	DC	20	2,40	44,85	13,132	9,380	3,752	-2425,761	0,396	0,396	9,217
STEP AVERAGE				**2,38**	**52,32**	**31,909**	**-12,020**	**44,409**	**-2031,224**	**0,231**	**0,375**	**16,619**

5.1.1 Relation between Uniaxial Compressive Strength (UCS) and Electric Potential achieved at the instant of UCS (EP_{UCS})

Electric potential value (EP_{UCS}) just before the time of failure during uniaxial loading are compared with the UCS values. The EP_{UCS} values in different experiments occurred, either as a positive electric potential or negative electric potential. The absolute values of EP_{UCS} values are used in the analysis, since the polarity of produced EP is affected by the alignment of quartz crystals with respect to the loading axis.

As stated before, by the fundamental equations of piezoelectricity stated in Chapter 2, the existence of a linear relationship with direct proportionality between the developed (EP) criteria and stress level, is accepted as the proof of piezoelectric origin of generating EP.

There are three separate graphs drawn for analyzing the EP_{UCS} vs. UCS relation of three rock types. On each graph, the UCS and EP_{UCS} data of LR1, LR2, LR3 and STEP experiments, conducted on related rock type are depicted as individual data sets. The graph of granite experiments are given in Figure 5.2, the similar graphs for granodiorite and quartz-sandstone experiments are also presented in Figure 5.3 and Figure 5.4, respectively.

On the graphs given in Figure 5.2, Figure 5.3 and Figure 5.4, the related R^2 values of experiment groups are also indicated. From the Figure 5.2, it is clearly concluded that the LR1, LR2, LR3 and STEP experiments on granite samples, shows an inverse proportionality between UCS and Abs(EP_{UCS}) values. In other words the Abs(EP_{UCS}) values decreases with increasing UCS. This finding may be interpreted as follows:

i- Pure piezoelectric behavior controls EP change at low stress levels, ii- Effect of momentum or start of microcracking controls EP change at higher levels of stress

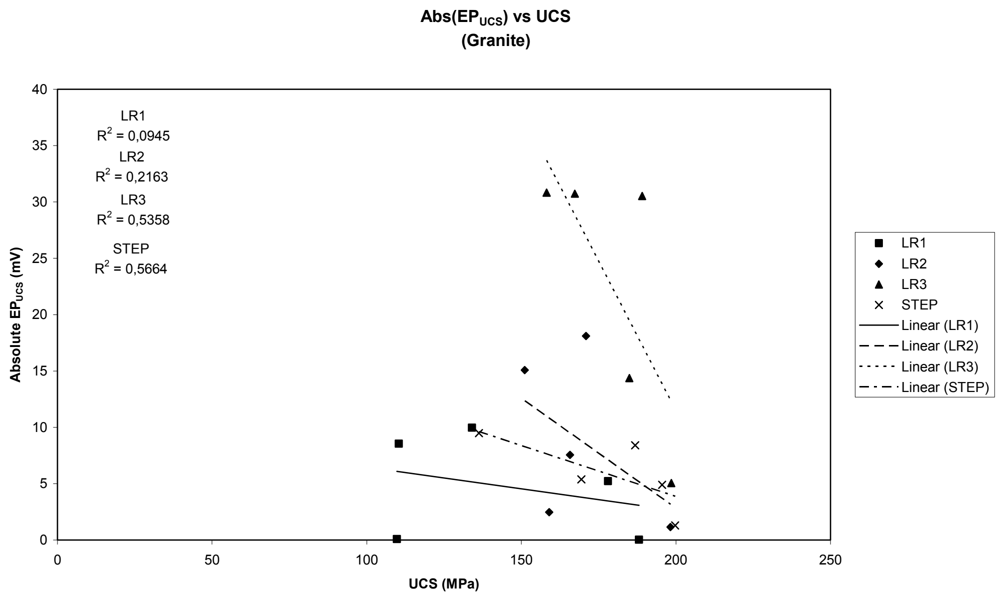

Figure 5.2 EP_{UCS} vs. UCS graph of LR1, LR2, LR3 and STEP experiments on granite

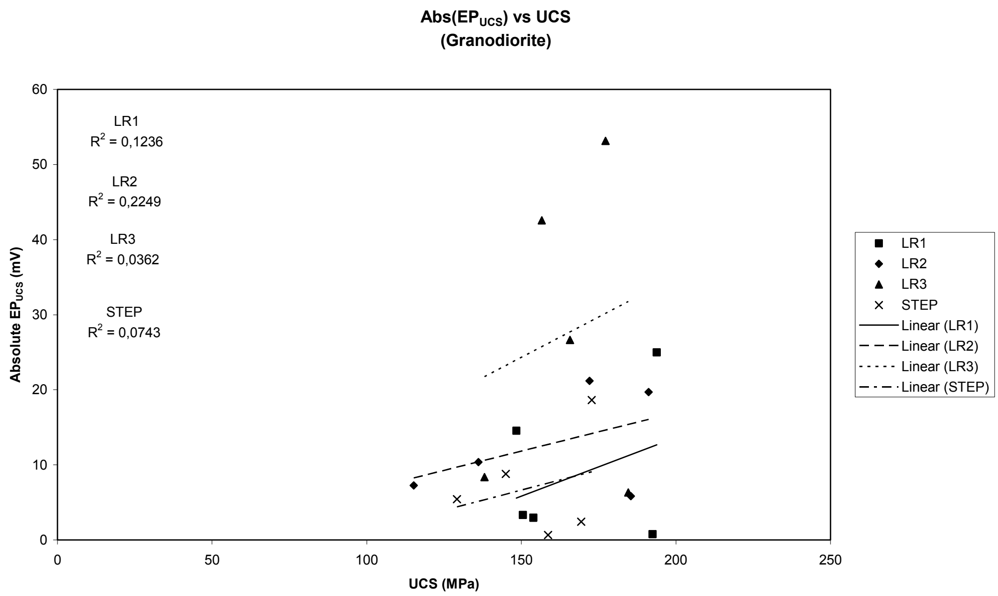

Figure 5.3 EP_{UCS} vs. UCS graph of LR1, LR2, LR3 and STEP experiments on granodiorite

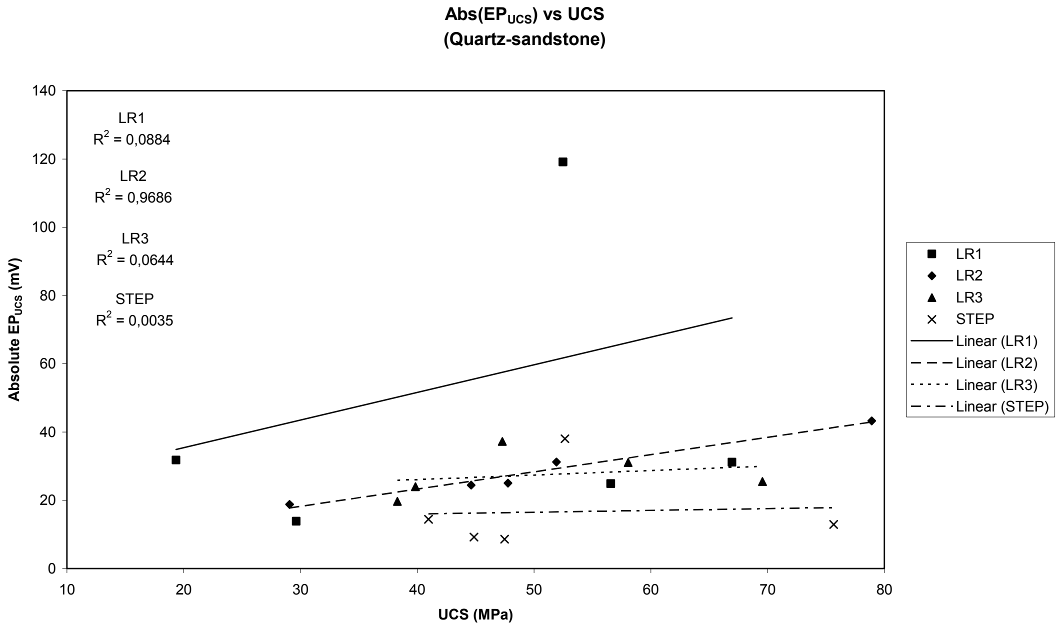

Figure 5.4 EP_{UCS} vs. UCS graph of LR1, LR2, LR3 and STEP experiments on quartz-sandstone

On the contrary, the experiments conducted on the other rock types, namely granodiorite and quartz-sandstone, Abs(EP_{UCS}) vs. UCS indicates a direct proportionality. In other words, absolute EP values increases with increasing UCS, i.e., with increasing stress level. However, the R^2 values of all experiments on three rock types indicate that, there is a poor linear relationship between the UCS and the EP_{UCS} values, as far as piezoelectricity is concerned.

Although the correlation coefficients are low, an obvious relation between the EP_{UCS} and UCS values are observed. It is clear that EP level (trend) of the samples changes with applied uniaxial stress, as indicated by the graphs drawn for granite, granodiorite and quartz-sandstone samples presented in Appendix-A, B and C, respectively. So a different mechanism other than piezoelectricity only should be affecting the magnitude of EP_{UCS} values.

The two possible explanations are, the momentum theory stated by Aydan et al. (2001, 2003) and the existence of charge clouds and dislocations stated by Hadjicontis and Mavromatou (1994).

5.1.2 Relation between Loading Rate (LR) and Electric Potential achieved at the instant of UCS (EP_{UCS})

As explained in the Section 4.1, the four different experiment types are conducted at three different continuous loading rates LR1 (0.005 mm/s), LR2 (0.01 mm/s), LR3 (0.05 mm/s) and STEP (0.005 mm/s) loading mode.

In order to search for the possible relations between the rate of loading and the EP_{UCS}, the EP_{UCS} values calculated for each experiment are drawn on a graph whose abscissa represents the loading rate. There are three graphs drawn for three rock types. These graphs include all LR1, LR2, LR3 and STEP experiments conducted on each rock type.

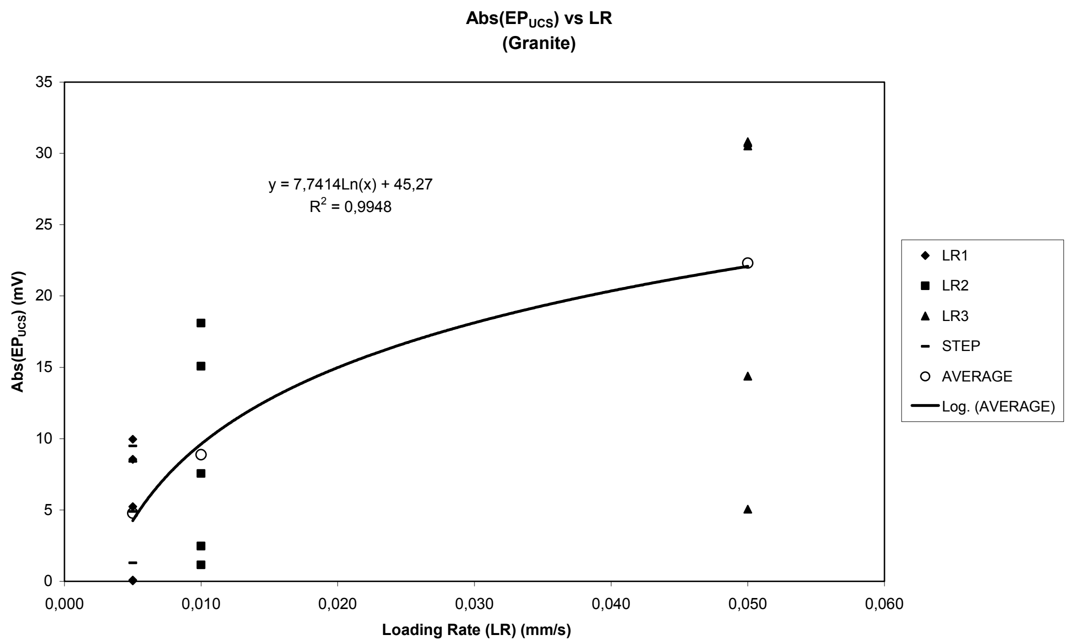

Figure 5.5 Abs(EP_{UCS}) vs. LR graph of granite experiments

On the graph given in Figure 5.5, the (EP_{UCS}) values for LR1 and STEP experiments appear on the same loading rate, since the utilized loading rate for the two experiment types are same (0.005 mm/s). Also a logarithmic best line is drawn in order to check the consistency of relationship between LR and the Abs(EP_{UCS}) values. The coefficient of determination for the best line of granite experiments is R^2=0.9948, which indicates that the logarithmic best line is strongly consistent with the data points. From Figure 5.5, it can be concluded that Abs(EP_{UCS}) value increases logarithmically with increasing loading rate for the granite samples. The similar graphs for granodiorite and quartz sandstone experiments are also drawn and given in Figure 5.6 and Figure 5.7, respectively.

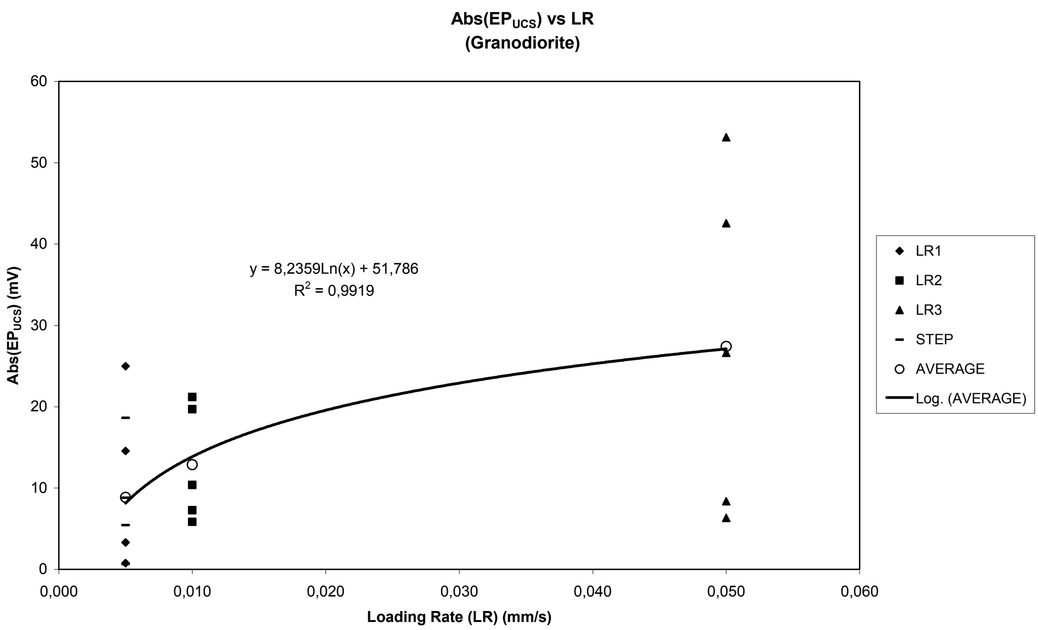

Figure 5.6 Abs(EP_{UCS}) vs. LR graph of granodiorite experiments

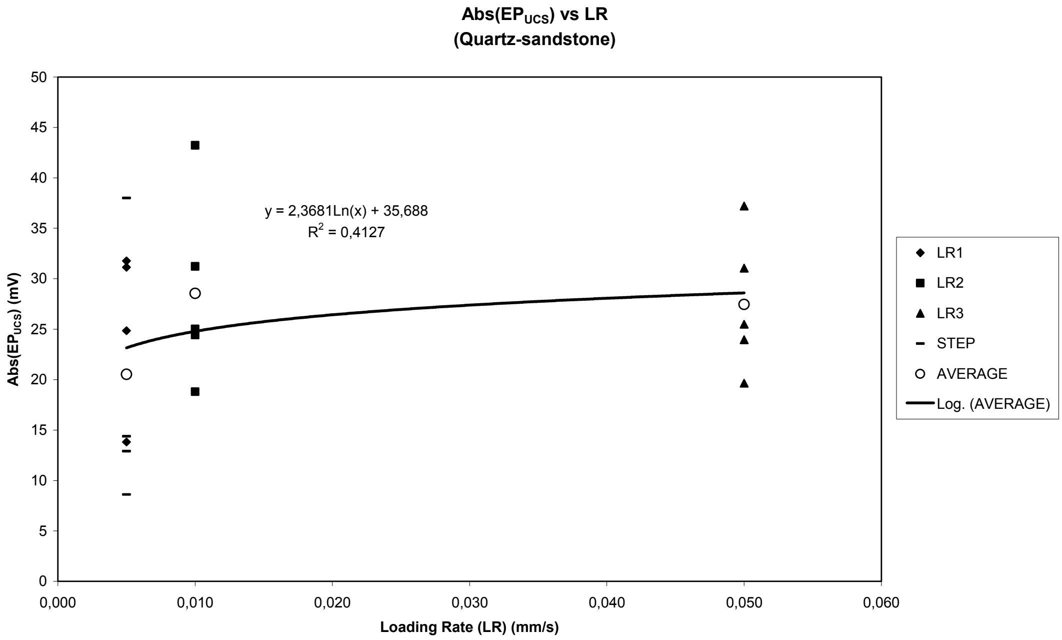

Figure 5.7 Abs(EP_{UCS}) vs. LR graph of quartz-sandstone experiments

The existence of a logarithmic correlation between the loading rate (LR) and Abs(EP_{UCS}) is also verified by the experiments conducted on granodiorite and quartz-sandstone samples. The value of logarithmic coefficient of determination for the granodiorite experiments is R^2=0.9919 and for the quartz-sandstone experiments R^2=0.4127. The difference between the high R^2 values of granite and granodiorite experiments and low R^2 value of quartz-sandstone experiments can be explained by basics of rock mechanics and the momentum theory stated by Aydan et al (2003).

From the rock mechanics point of view, the material behavior of a rock before the failure can be divided into two; the elastic part and the plastic part. As the stress increases, the behavior of the rock sample translates from the elastic response to the plastic response gradually. The increasing stress on a rock also causes the momentum imposed on the rock increase. The accumulating momentum energy on the rock is relaxed through the strain and the development of microcracks, which are formed during the stress increase. As the rocks approach towards the failure stress, the strain and microcrack growth increases, and the momentum energy imposed on the specimen is relaxed/released more rapidly. Therefore, as the sample approaches to the failure stress, the dominant source for the EP change becomes the momentum imposed on the sample by the applied stress. In other words, the EP values at close neighborhood of uniaxial compressive strength (EP_{UCS}), reflect the effect caused by the momentum rather than the piezoelectricity only.

The situation stated in the above paragraph, is also supported by the graphs given in Appendix-A, B and C and the average Dynamic Young's Modulus (E_d) values of the rocks.

In Figure 5.5 and Figure 5.6, it is clearly observed that as the loading rate (LR) increases the EP_{UCS} value increases also. As the loading rate increases the relaxation time for granite and granodiorite samples are shortened and strain and microcracks are developed within a much shorter time span. This results in more rapid release of momentum energy and higher EP_{UCS} values are measured at faster loading rates. This fact is also
60
supported by the high E_d values of granite and granodiorite samples. The granodiorite samples (48.6 GPa) result higher EP_{UCS} values than the granite samples (22.5 GPa) in the same loading rate. The granite and granodiorite samples can be said to show brittle behavior which means that the strain and microcrack development in the elastic range is too low and can be neglected.

In Figure 5.7, it is observed that the EP_{UCS} values of quartz-sandstone samples are not affected by LR as much as granite and granodiorite samples do. The low E_d value (11.2 GPa) of quartz-sandstone means that, rock is not a stiff rock and starts to create large amounts of strain even at the low stress levels. As a result, the EP generated by momentum energy is relaxed in a large time span as a more uniform EP effect. Also considering the graphs of quartz-sandstone experiments given in Appendix-C, the material behavior of quartz-sandstone can be named as elasto-plastic type. This idea is also supported by the loosely cemented fabric of quartz-sandstone, as described in the rock description in Section 4.2.1.

5.1.3 Relation between Uniaxial Compressive Strength (UCS) and Spike-like Coseismic Electric Signal (V_{jump})

The relations if any, between the uniaxial compressive strength (UCS) of the rock and the spike-like potential jump (V_{jump}) are searched for different loading rates and rock types. ΔV value for each sample is calculated by the formula; $V_{jump} = Abs\ (V_{up} - V_{down})$, and a graph is drawn for each rock type, on which 5 experiments of each loading rate are represented as an individual data set. The graphs prepared for granite, granodiorite and quartz-sandstone experiments are given in Figure 5.8, Figure 5.9 and Figure 5.10, respectively. In the V_{jump} vs. UCS plots of three rock types, all the experiment sets LR1, LR2, LR3 and STEP, resulted in a positive slope, meaning that the V_{jump} value increases with increasing UCS.

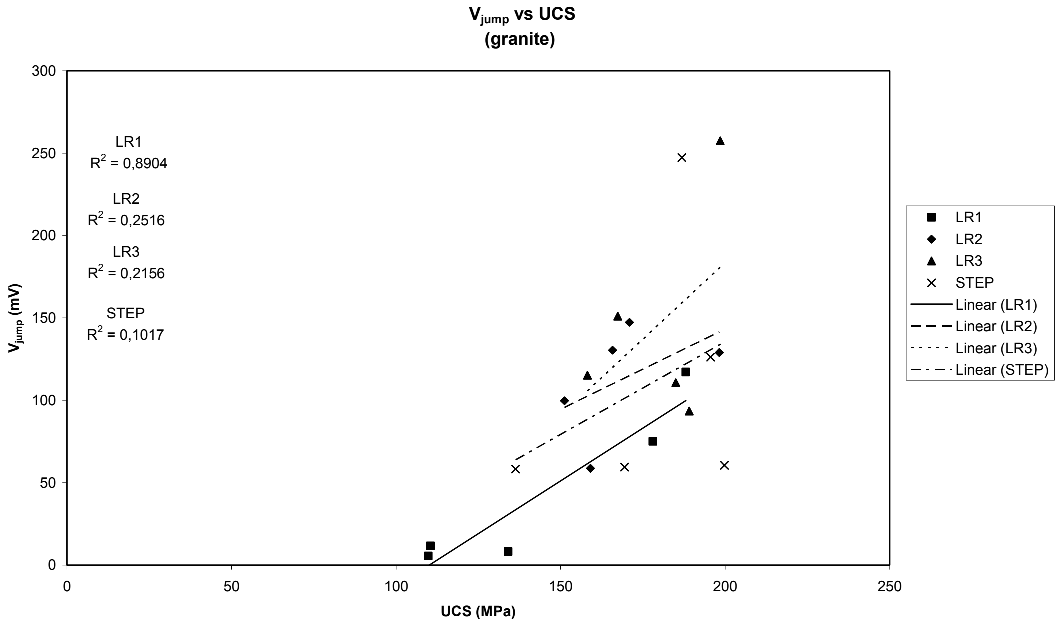

Figure 5.8 V_{jump} vs. UCS graph for LR1, LR2, LR3 and STEP experiments of granite

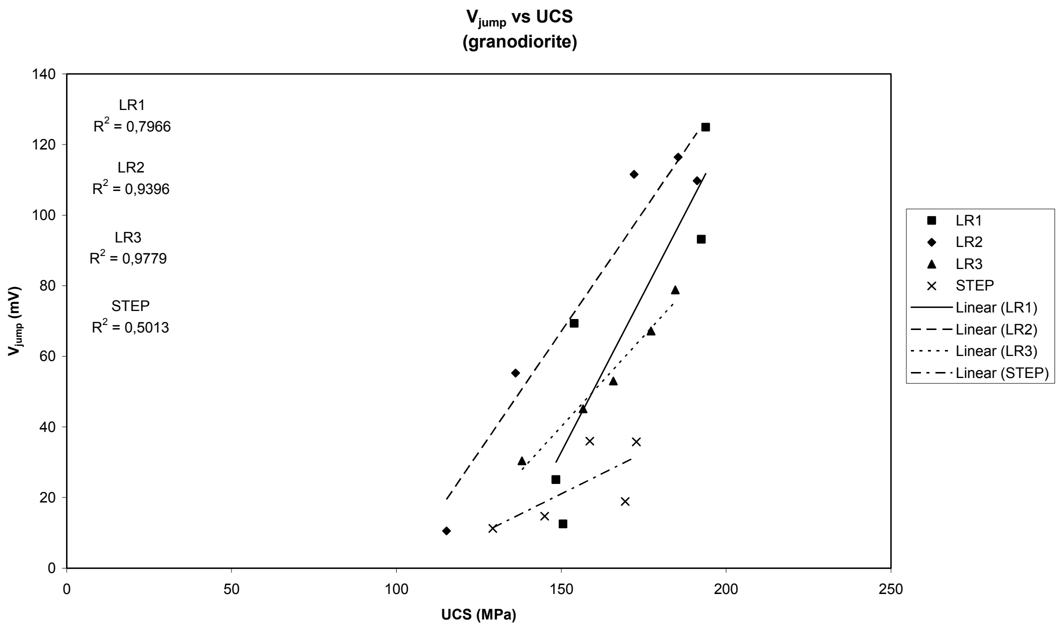

Figure 5.9 V_{jump} vs. UCS graph for LR1, LR2, LR3 and STEP experiments of granodiorite

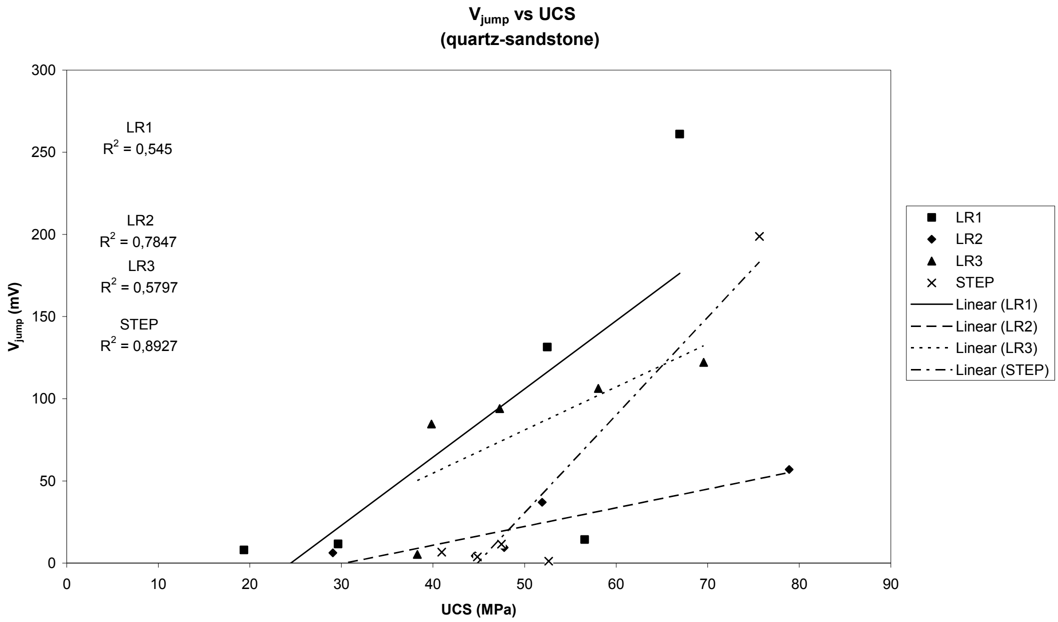

Figure 5.10 V_{jump} vs. UCS graph for LR1, LR2, LR3 and STEP experiments of quartz-sandstone

V_{jump} represents the magnitude of the released EP at the instant of failure, which is imposed on the sample either by piezoelectricity or momentum energy during loading. At the instant of failure, the most important final rupture occurs, by which the momentum energy accumulated on the sample is released. Also with the rapid drop of the stress, the EP generated by piezoelectric quartz crystals disappears very quickly. Therefore, the V_{jump} is generated as a combined effect of piezoelectricity and momentum energy.

In Figure 5.8, Figure 5.9 and Figure 5.10, it is observed that the V_{jump} value increases with increasing UCS value. This is a reasonable result if one thinks that, total EP released at the instant of failure is the sum of EPs generated by piezoelectric effect and momentum imposed. The R^2 values, which are given in Figure 5.8, Figure 5.9 and Figure 5.10, states that either the existence or the absence of a linear relationship is not clear. This fact shows once more that, EP change V_{jump}, occurs under the combined effect of piezoelectricity and the momentum imposed on the rock samples.

5.1.4 Relation between Uniaxial Compressive Strength (UCS) and Logarithm of Spike-like Coseismic Electric Signal ($\log(V_{jump})$)

As explained in the Section 2.2.1, Varotsos et al. (1984a, b), stated that there is a linear relationship between log (ΔV) and the magnitude (M) of the earthquake with an average slope of 0.3-0.4. Making use of this finding of Varotsos et al., search for a possible relation between $\log(V_{jump})$ and UCS is attempted. For drawing the graphs, the logarithm of V_{jump} values are calculated first and then these values are plotted on the normal scaled ordinate axis of graphs. The abscissas of graphs are used for plotting the corresponding UCS values of experiments. The $\log(V_{jump})$ vs. UCS graphs are drawn for three rock types. On these graphs, the LR1, LR2, LR3 and STEP experiments are depicted as individual data groups.

In Figure 5.11, Figure 5.12 and Figure 5.13, the $\log(V_{jump})$ vs. UCS graphs of granite, granodiorite and quartz-sandstone experiments are presented, respectively.

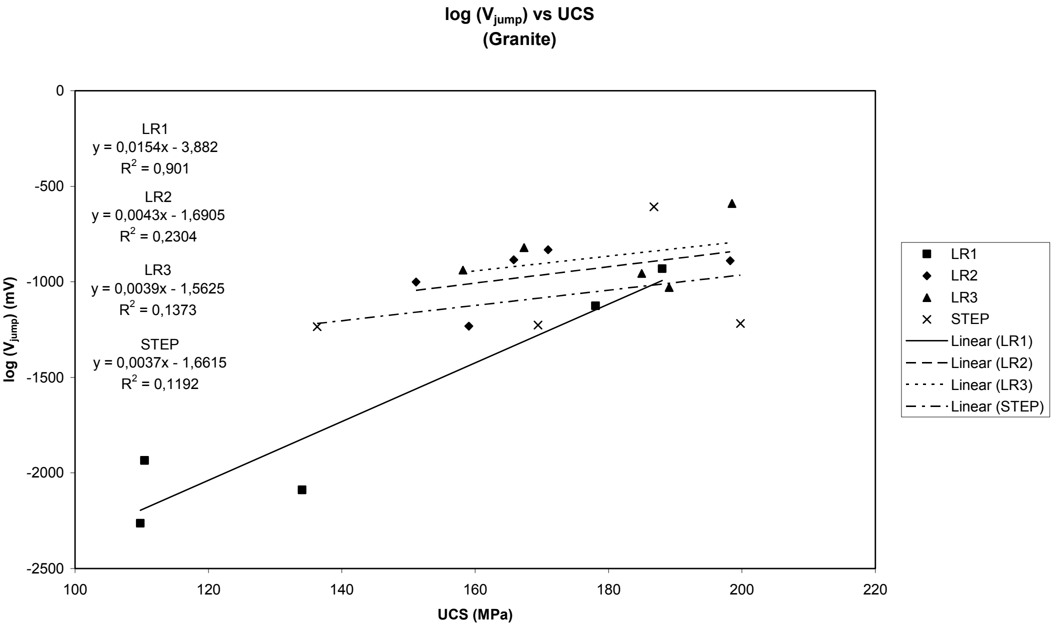

Figure 5.11 log(V_{jump}) vs. UCS graph for granite experiments

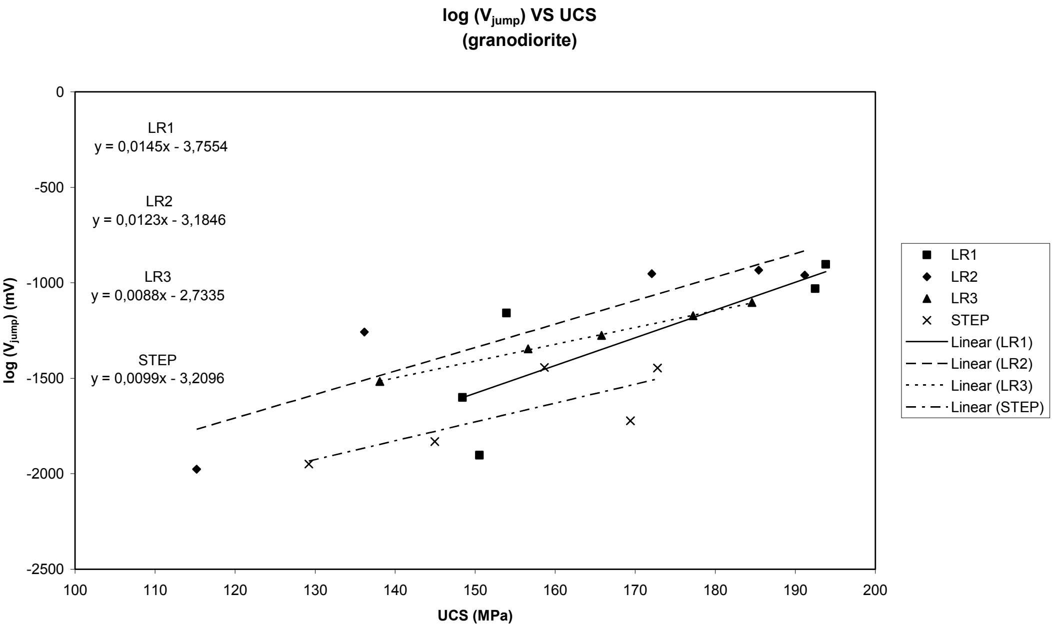

Figure 5.12 log(V_{jump}) vs. UCS graph for granodiorite experiments

On the graphs in Figure 5.11, Figure 5.12 and Figure 5.13, the respective linear best line equations are also given. From these equations respective slopes of lines for the LR1, LR2, LR3 and STEP experiments are determined, in order to compare with the slope range of 0.3-0.4, which is stated by Varotsos et al.

For the granite experiments, the slopes of the best line equations are determined as 0.0154 (LR1), 0.0043 (LR2), 0.0039 (LR3) and 0.004 (STEP). The slope values for LR1, LR2, LR3 and STEP experiments on granodiorite samples are, 0.0145, 0.0123, 0.088 and 0.0099, respectively. For the quartz-sandstone experiments, the slope values of 0.0273 for LR1, 0.022 for LR2, 0.0266 for LR3 and 0.0462 for STEP are calculated by best line equations.

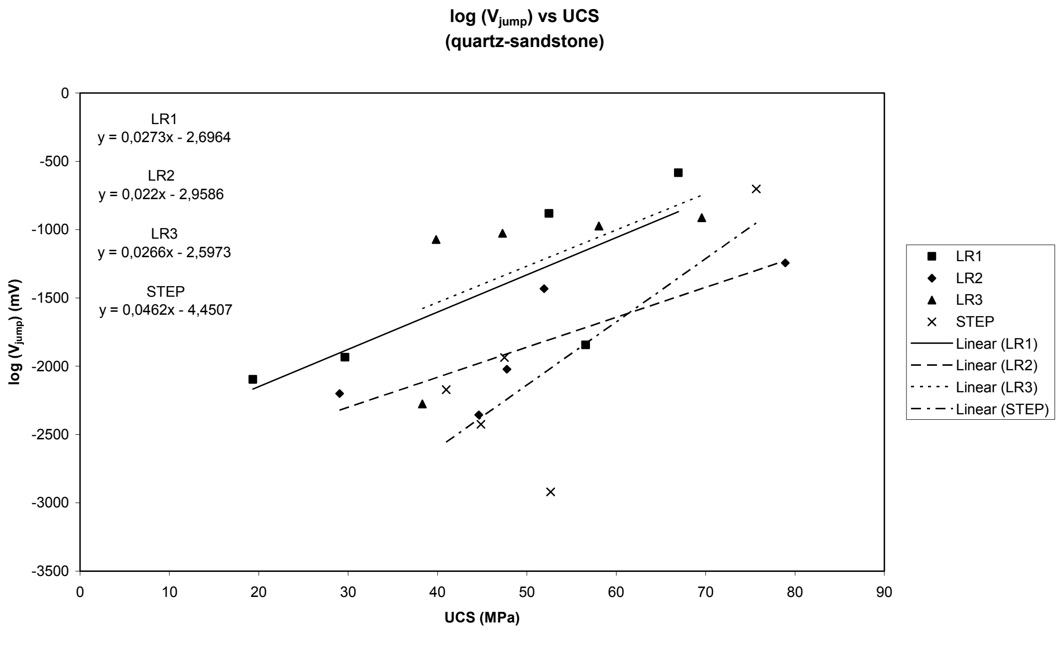

Figure 5.13 $\log(V_{jump})$ vs. UCS graph for quartz-sandstone experiments

The slope values for LR1, LR2, LR3 and STEP experiments seem to occur consistent with each other for the same rock type. In other words, the slope values are very close to each other for the same rock. The slope values for granite experiments vary around 0.004, with the exception of LR1 slope 0.0154. The slope values of granodiorite experiments are always around 0.011. The quartz-sandstone experiments give slope values, which are around 0.025, if the considerably different slope of STEP experiments (0.0462) is ignored.

Especially the slope values for LR2, LR3 and STEP experiments on granite are clearly consistent with the 1% of 0.3-0.4 range proposed by Varotsos et al. Considering the fact that, granitic rocks are the main constituents of continental crust (Tarbuck and Lutgens, 2003), this result sounds more logical. The 1% ratio can be treated as a scale factor, by considering the scales of observations conducted by Varotsos et al. (1984a, 1984b) and experiments conducted in this study. Varotsos et al. (1984a, 1984b) conducted their observations within kilometer scaled distances, whereas the rock samples used in this study were only centimeter scaled. In another words, the field studies conducted by Varotsos et al. can be accepted as macroscopic, whereas the scales of experiments conducted in this study are of microscopic.

From the idea stated in the above paragraph, slope values of best lines drawn for granodiorite and quartz-sandstone experiments are thought to be affected by certain scale factors also. In addition, considering the fact that, the slope values of LR1, LR2, LR3 and STEP experiments conducted on the same rock type are clearly close to each other, the slope values are thought to occur in a rock type specific manner.

If the existence of such a relation between UCS and $\log(V_{jump})$ is verified with further studies, a useful tool for observing the stress variations, for example in the underground mines, can be established. Continuous observation of EP changes in specific points of mines, and comparing these

EP values with the predetermined EP levels observed at rock failure, can be used as an early warning system.

5.1.5 STEP Loading Experiments

The STEP loading experiments are conducted with three purposes. First one is to understand and clarify the source of generating EP at different stages of loading. Second is to check the consistency of experiments conducted in this study and the theoretical EP response of piezoelectric rocks calculated by Aydan et al. (2003) (Figure 2.10). According to piezoelectric equations given in Chapter 2, when the load is kept constant at a specific level, the achieved EP should be preserved constant also. Third one is to better understand the relation of two EP generating mechanisms; piezoelectric polarization of quartz crystals and the momentum imposed on the rock by the applied stress.

In accordance with the experimental procedure, explained in Section 4.1, STEP experiments are conducted at the lowest loading rate 0.005 (LR1). After the load started to increase, the loading process is paused on three certain levels and stress is kept constant for a time period. During these constant stress periods the EP responses of the samples are observed and recorded values are compared with the theoretically calculated EP response stated by Aydan et al (2003).

As a general fact, the rock behavior is thought to remain in the elastic range, if the applied stress does not exceed the 50% to 67% of UCS of the rock, as far as the evidences from rock mechanics experiments are concerned. STEP experiments are conducted after the LR1, LR2 and LR3 experiments are completed. By completing the LR1, LR2 and LR3 experiments, the UCS values of three rock types are determined and the load levels to be applied in STEP experiments are calculated for each rock type separately. The experimental results of STEP experiments conducted on granite, granodiorite and quartz-sandstone samples are given in Table 5.4.

The load levels for quartz-sandstone experiments are chosen so that the corresponding magnitude of stress on sample is 17.5% of UCS for Step 1, 34.7% of UCS for Step 2 and 56.0% of UCS for Step 3 on average. Due to loosely cemented structure and low E_d of quartz-sandstone samples, stress levels are ensured to remain within the elastic limits even for Level 3.

For the granite and granodiorite experiments the applied Level 3 stresses are intentionally allowed to exceed the 67% of UCS values of respective rocks. Considering the high E_d values of granite and granodiorite, the samples are thought to compensate higher stress magnitudes without showing considerable plastic response.

Table 5.4 STEP experiment data of granite, granodiorite and quartz-sandstone

% Quartz Content	ROCK TYPE	EXPERIMENT NO	LOADING RATE	Step 1 Axial Stress (Mpa)	Step 1 Abs(EP) (mV)	Step 2 Axial Stress (Mpa)	Step 2 Abs(EP) (mV)	Step 3 Axial Stress (Mpa)	Step 3 Abs(EP) (mV)
35	Granite	GR135STEP	0,005	43,87	0,950	87,05	1,401	130,07	1,706
		GR136STEP	0,005	41,60	0,900	82,17	3,123	122,99	4,390
		GR137STEP	0,005	45,18	3,918	89,76	5,230	133,53	5,550
		GR138STEP	0,005	45,02	3,848	88,30	5,049	128,61	6,433
		GR139STEP	0,005	45,10	3,883	89,03	5,139	131,07	5,992
	Average			%UCS = 26,4		%UCS = 52,1		%UCS 77,1	
				44,15	**2,700**	**87,26**	**3,989**	**129,25**	**4,814**
25	Granodiorite	GD127STEP	0,005	43,23	7,615	85,20	5,747	115,73	0,512
		GD128STEP	0,005	42,29	10,396	84,61	8,222	125,92	0,032
		GD129STEP	0,005	42,22	16,943	84,29	15,706	125,52	18,228
		GD130STEP	0,005	42,45	15,900	99,03	13,261	143,30	2,533
		GD131STEP	0,005	72,06	11,461	92,30	2,934	129,36	4,011
	Average			%UCS = 29,9		%UCS = 55,1		%UCS 79,1	
				48,45	**5,063**	**89,09**	**9,174**	**127,97**	**12,463**
90	Quartz-sandstone	S128STEP	0,005	8,52	14,676	17,13	19,578	25,52	22,639
		S129STEP	0,005	8,44	10,902	16,88	15,404	25,78	15,400
		S130STEP	0,005	8,78	0,951	17,34	0,097	26,68	3,530
		S131STEP	0,005	8,89	10,621	17,43	13,153	26,69	14,853
		S132STEP	0,005	8,65	8,364	17,24	8,364	34,20	13,012
	Average			%UCS = 17,5		%UCS = 34,7		%UCS 56,0	
				8,66	**9,103**	**17,20**	**11,319**	**27,77**	**13,887**

From the data given in Table 5.4, Abs(EP) vs. Axial Stress graphs for each rock type are prepared. Experiment results of each sample are represented as an individual set on the graphs given in Figure 5.14, Figure 5.15 and Figure 5.16.

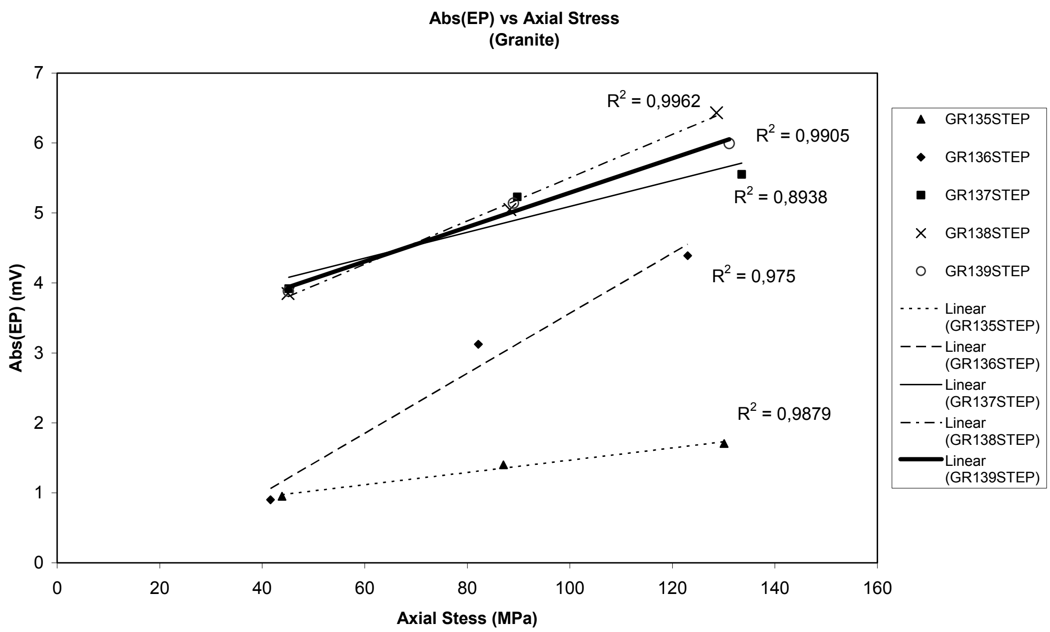

Figure 5.14 Abs(EP) vs. Axial Stress Levels graph of STEP experiments on granite

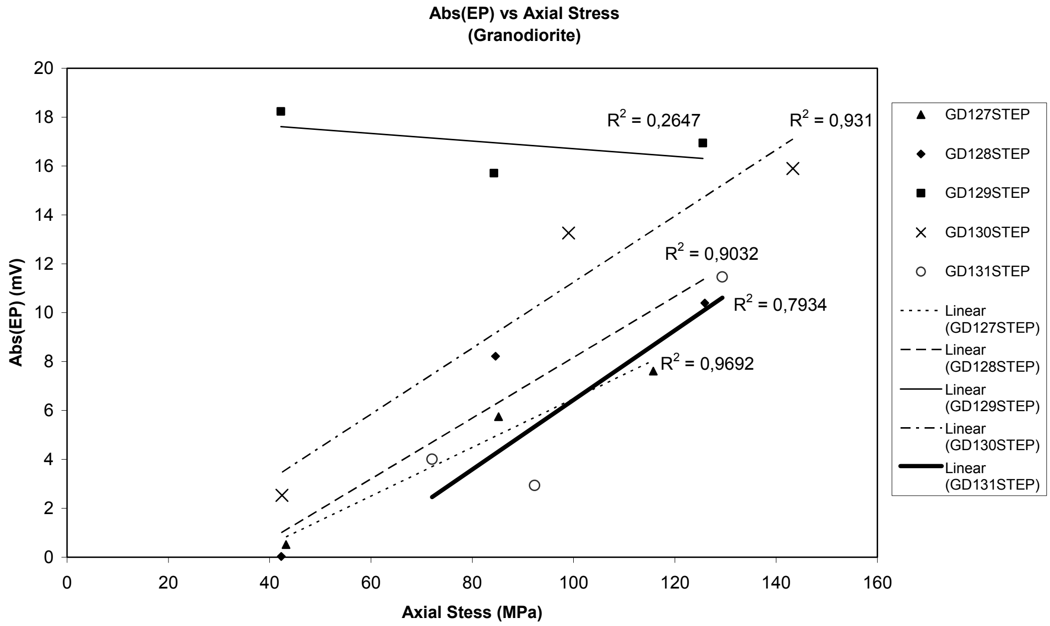

Figure 5.15 Abs(EP) vs. Axial Stress Levels graph of STEP experiments on granodiorite

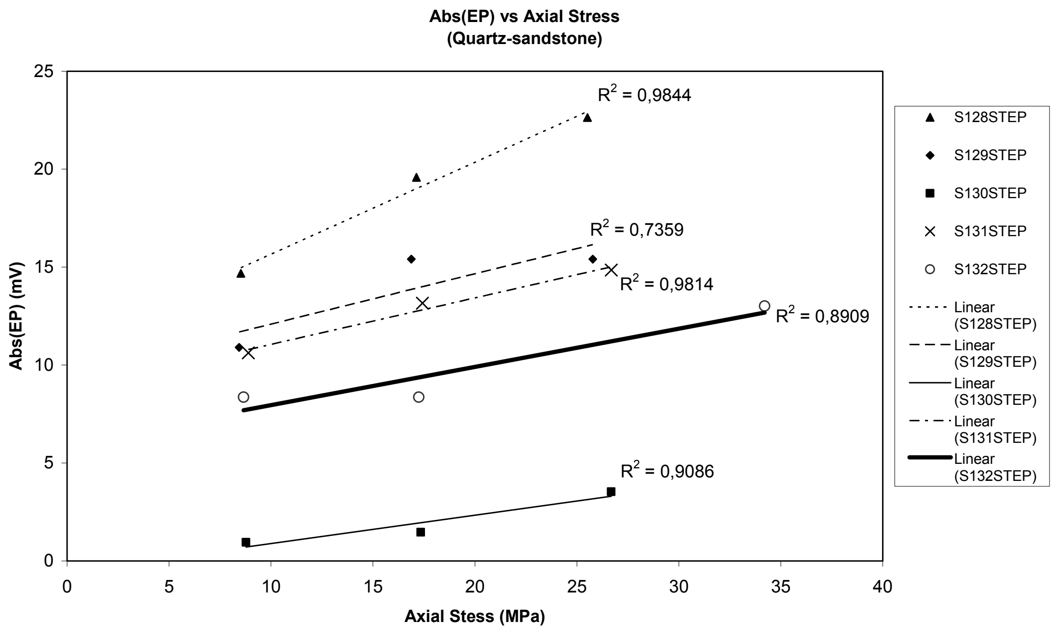

Figure 5.16 Abs(EP) vs. Axial Stress Levels graph of STEP experiments on quartz-sandstone

As stated before, the existence of a linear relationship between the applied stress and the EP is accepted as the proof of piezoelectric EP generation mechanism. The coefficient of determination (R^2) values, which are indicated on the graphs, state that there is a clear and strong linear relationship between the applied stress and the generating EP, for all three rock types. So it can be concluded that, the existence of piezoelectric EP generation mechanism for the quartz bearing rocks is verified.

The average stress level and corresponding average EP values, given in Table 5.4, are also drawn on separate graphs for quartz-sandstone, granite and granodiorite, which are given in Figure 5.17, Figure 5.18 and Figure 5.19 respectively. In Figure 5.17, it is observed that the average EP values for stress Levels 1, 2 and 3 are perfectly linear for quartz-sandstone experiments, which are ensured to remain within the elastic range. Whereas the average EP values for granite and granodiorite test results seem to deviate from linearity especially at the stress Level 3, which is known to exceed the elastic limit theoretically. As a result, it should also be emphasized that, existence of the linear relationship is valid, as far as the applied stress is kept within the elastic limits.

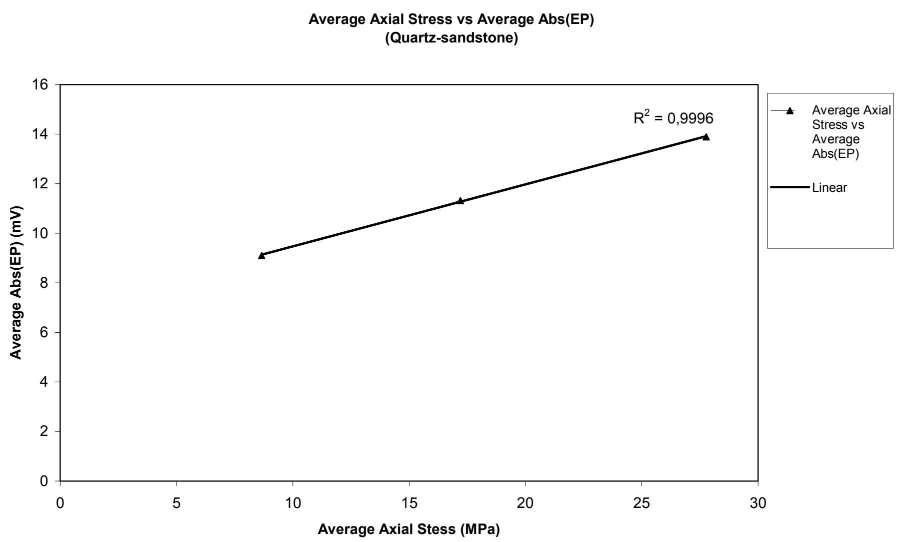

Figure 5.17 Average Abs(EP) vs. Average axial stress for quartz-sandstone

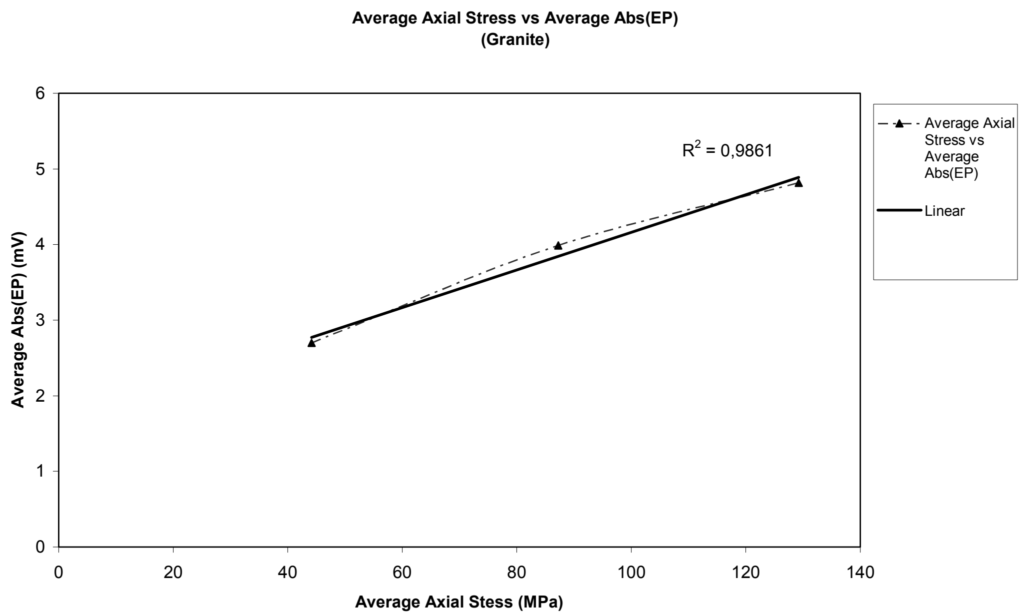

Figure 5.18 Average Abs(EP) vs. Average axial stress for granite

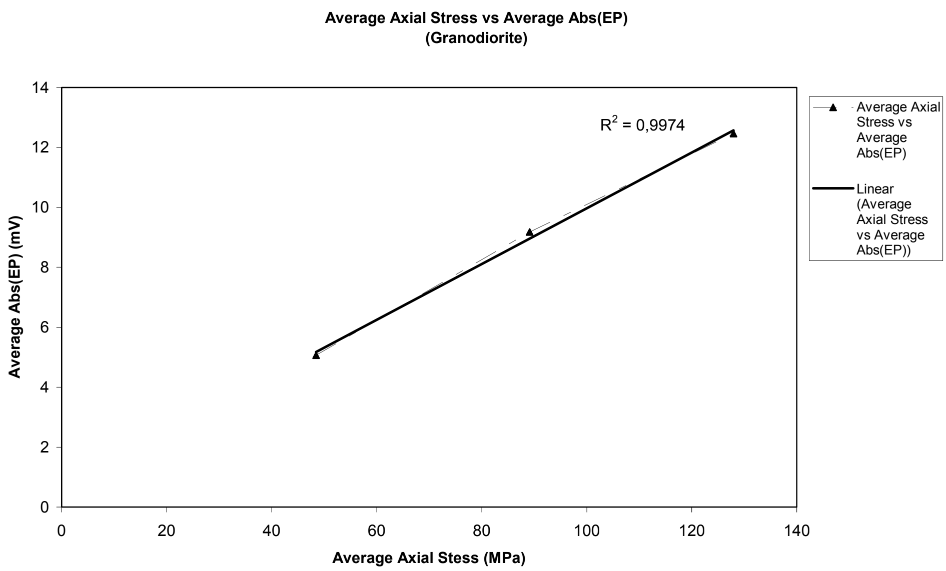

Figure 5.19 Average Abs(EP) vs. Average axial stress for granodiorite

Another important observation about the STEP experiments is that, the achieved EP level does not drop to zero with the pause of loading. On the contrary, the achieved EP level is preserved during the constant stress periods. This result supports the theoretically calculated response of piezoelectric rocks against the applied stress, which is stated by Aydan et al (2003).

However, according to the theory of Hadjicontis and Mavromatou (1994) given in Section 2.2.2, the EP level should have dropped to zero or to the initial EP level, with the pause of loading, even in mineral quartz (Figure 2.5). In other words, the charged edge dislocations theory claimed by Hadjicontis and Mavromatou (1994), contradicts with the results obtained in this study.

A second attempt for comparing the LR1, LR2, LR3 and STEP experiment results and the theory stated by Hadjicontis and Mavromatou (1994), is done by calculating the $d\sigma / dt$ responses of granite, granodiorite and quartz-sandstone experiments. According to Hadjicontis and Mavromatou (1994), the electric signals should follow, in form, the $d\sigma / dt$ response of the sample (Figure 2.5). A sample graph, showing the EP versus time response and the $d\sigma / dt$ versus time, is drawn and given in Figure 5.20. For the same experiment S128STEP, the EP versus time and axial stress versus time graphs are also drawn and presented in Figure 5.21.

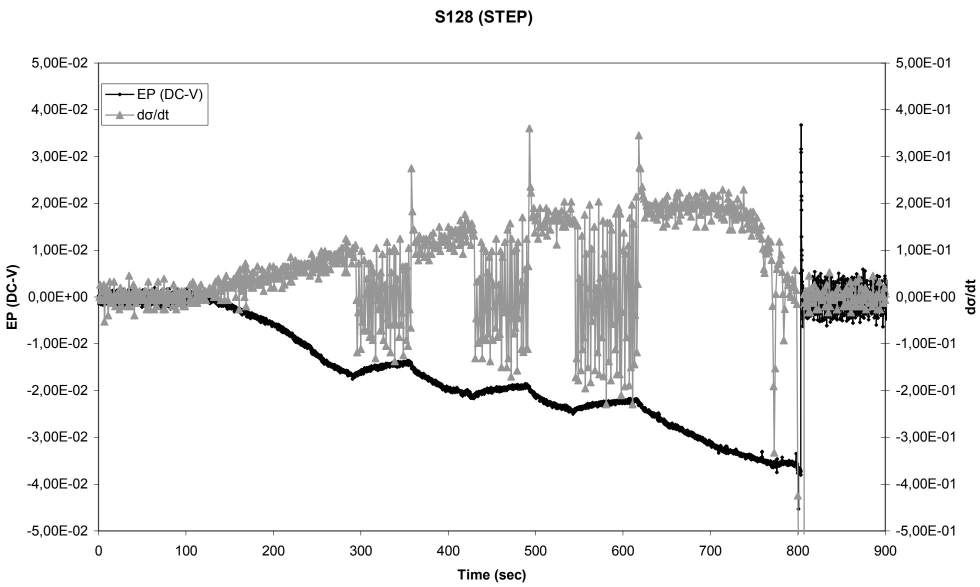

Figure 5.20 $d\sigma / dt$ and EP response graphs for experiment S128STEP

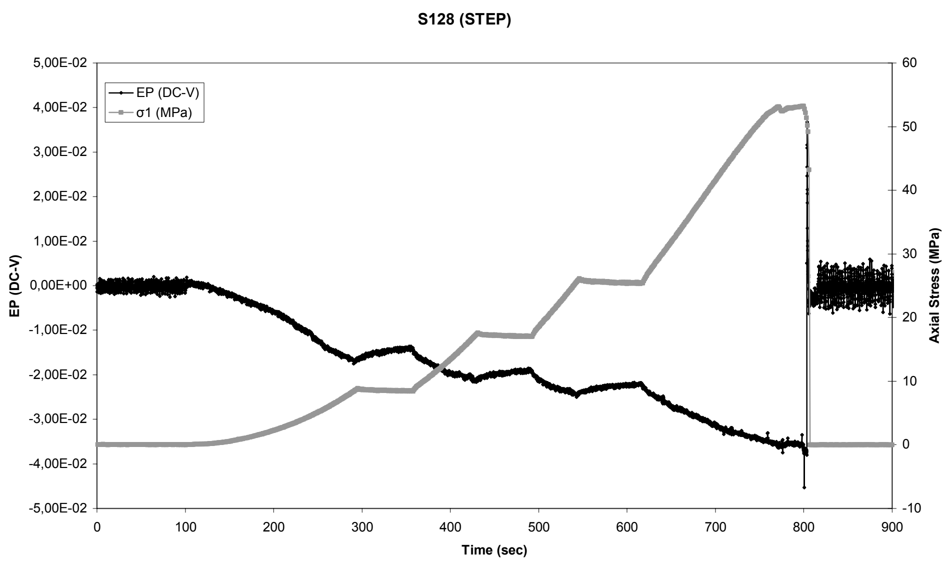

Figure 5.21 EP and Axial Stress versus time graph of experiment S128STEP

From Figure 5.20, it is obvious that $d\sigma / dt$ drops to zero level immediately with the pause of the loading, whereas the EP response preserves its level.

The results of this comparison also contradict with the claimed response of Hadjicontis and Mavromatou (1994).

5.1.6 The Initial Electric Potential Value ($EP_{initial}$) and the Final Electric Potential Value (EP_{final})

The initial and final EP values are calculated by taking the average of electric potential records belonging to the initial and final parts of the loading cycle, where there is no stress present on the sample. In most of the experiments, the $EP_{initial}$ values occurred at levels very close to the zero, whereas the EP_{final} values generally occurred as large and random oscillations.

The $EP_{initial}$ and EP_{final} values are calculated and compared for each experiment and it is observed that the EP_{final} values are affected by high noise and give no relationship with the $EP_{initial}$ values. In most of the experiments $EP_{initial}$ records reflected a steady state, whereas in the EP_{final} there is no steady state observed, the EP_{final} values resulted in abrupt and non-consistent responses. EP_{final} values are thought to be affected by the friction of broken rock surfaces. Table 5.5 gives the $EP_{initial}$ and EP_{final} values obtained from 5 experiments on granite samples for LR1 group of tests as an example.

Since the similar cases are observed in great majority of the experiments, no correlation between $EP_{initial}$ and EP_{final} values can be determined.

Table 5.5 $EP_{initial}$ and EP_{final} values from LR1 experiments on granite

Experiment Number	EP	$EP_{initial}$ (mV)	EP_{final} (mV)
GR105	DC	0,088	0,305
GR106	DC	0,972	0,001
GR107	DC	0,196	0,066
GR108	DC	0,132	0,452
GR116	DC	0,297	1,307

CHAPTER 6

CONCLUSIONS AND RECOMMENDATIONS

6.1 Conclusions

Electric potential (EP) responses of three quartz bearing rock types, under uniaxial loading are studied. The tested rock types are granite and granodiorite from Kaman-Kırşehir and quartz-sandstone from Kurucaşile-Bartın. Following conclusions are derived from the results of the conducted experiments.

1. The experimental results definitely show that the application of uniaxial stress creates a clear EP change on quartz bearing rocks.

2. The piezoelectric mineral bearing rocks give more consistent EP responses in DC mode when compared to AC mode (Figures in Appendix-D), under existing experimental conditions. The expected result, better response in DC mode, is more logical and consistent with the piezoelectric theory stated in Chapter 2.

3. It is observed that the measurements in AC mode pick up more noise.

4. In the STEP experiments, during the constant stress periods, the achieved EP level does not return to initial EP or zero level with the pause of loading. The EP level is maintained nearly constant which is a clear indication of piezoelectric behavior.

5. The spike-like EP signals occurs simultaneously with the rapid strain or microcrack growth instants.

6. In some experiments the observed EP changes occurred in the positive direction and in some other experiments the EP changes occurred in the negative direction. This difference between experiments is attributed to the directional properties of the quartz grains in the samples (Bishop, 1981). Therefore the absolute values of the electric potential changes, which are defined in this thesis, are used in the analysis and discussions.

7. During the elastic behavior in the early stages of the loading process, the EP change is dominated by piezoelectricity phenomena. Whereas during the plastic behavior and especially in the close neighborhood of UCS (failure), the EP change is dominated by the release of imposed momentum on the rock through unrecoverable strain or rapid microcrack growth.

8. From the rock mechanics point of view, quartz-sandstone samples show strain-softening type of behavior, whereas granite and granodiorite samples show brittle behavior. This fact is observed from the graphs given in Appendix-A, B and C. This situation resulted in extensive strain or rapid growth of microcrack, at the very close vicinity of failure for granite and granodiorite samples. On the other hand, the strain or microcrack formation occurs over a longer time span in quartz-sandstone samples, with respect to granite and granodiorite.

9. The material behaviors explained above in item 8, resulted in severe momentum effect on EP generation at the maximum stress level for granite and granodiorite. The effect of momentum on EP is observed as

a more uniform and mild effect occurring over a longer time period for quartz-sandstone (Figure 5.5, Figure 5.6 and Figure 5.7).

10. The induced EP depends both on the piezoelectric nature of the quartz crystals and the release of momentum imposed on the rock by mechanical changes such as strain, microcrack growth and initiation of failure.

11. In the STEP experiments for the same UCS level the achieved EP value is higher in quartz-sandstone samples when compared to granite and granodiorite samples. This is attributed to the high quartz content of quartz-sandstone.

12. The EP change after the uniaxial failure of samples show great fluctuations or oscillations which are thought to be created by friction of the broken surfaces. In other words, EP_{final} values are affected by excessive noise. As a result, comparison of the $EP_{initial}$ and the EP_{final} values did not result in any correlation.

6.2 Recommendations

From the experiment results and the figures given in Appendix-A, B and C, it is understood that the alignment of quartz crystals in the rock fabric with respect to loading axis, plays an important role in the form of generating EP. According to the alignment of quartz crystals the EP can be generated either with positive polarity or with negative polarity. In some experiments, no considerable change of EP with the application of stress is observed until failure of the rock. The unsuitable alignment of quartz crystals with respect to the loading axis is thought to cause this situation.

For the future studies, in the uniaxial loading experiments, using directional samples would be useful for eliminating some variances within experiments, such as the effect of quartz crystal alignment. Also carefully inspecting the microscopic structure and crystal alignment of directional rock samples can be useful for determining the expected response of rock samples.

From the outcomes of this thesis, it is also understood that the strain and microcrack formation plays an important role in the EP generation on rocks, with the applied stress. As a result, it is also recommended that, EP measurements should be accompanied with strain and acoustic emission measurements, for better understanding the effect of strain and microcrack formation, and hence the effect of momentum imposed on the sample.

The samples used in this study were NX sized cylindrical samples and the EP measurements were performed in only one direction, which was parallel to the loading direction. Performing a similar study on cubic or rectangular prism shaped, directional samples, and measuring the EP change in three orthogonal directions, is recommended for future studies, as well. By this method, it would be possible to resolve the EP response of rock samples into three dimensional components, and by utilizing the piezoelectric strain and stress coefficient matrices given in Chapter 2, the effect of applied stress can be better understood.

REFERENCES

Agilent 34970A Data Acquisition/Switch Unit User's Guide, 1999, Hewlett-Packard Company

Aydan, Ö., Minato, T., Fukue, M., 2001, An experimental study on the electric potential of geomaterials during deformation and its implications in Geomechanics, 38th US Rock Mechanics Symposium, Washington DC. June 2001

Aydan, Ö., Tokashiki, N., Ito, T., Akagi, T., Ulusay, R., Bilgin, H. A., 2003, "An Experimental Study on the Electric Potential of Non-piezoelectric Geo-materials During Fracturing and Sliding", Technology Roadmap for Rock Mechanics, South African Institute of Mining and Metallurgy, Proceedings of the 10th Congress of the ISRM, Sandton, September 8-12, 2003

Ballato, A., 1995, Piezoelectricity: old effect, new thrusts, Ultrasonics, Ferroelectrics and Frequency Control, IEEE Transactions on, Vol. 42, Issue: 5, Sept. 1995, pp. 916–926

Ballato, A., 1996, Piezoelectricity: History and New Thrusts, IEEE Ultrasonics Symposium, pp. 575-583

Bishop, J. R., 1981, Piezoelectric Effects in Quartz-Rich Rocks, Tectonophysics, Vol. 77, pp.297-321

Bottom, V. E.,1982, Introduction to Quartz Crystal Unit Design, Van Nostrand Reinhold Company, New York

Bravais, A., 1850, On the systems formed by points regularly distributed on a plane or in space, translated by Shaler, A. J., Crystallographic Society of America, 1949,

Cady, W. G., 1964. Piezoelectricity, Vol. 1-2, Dover Publications, Inc., New York

DBK Option Card & Modules Users Manual, 2003, IOtech Inc., USA

Fedotov, S. A., Dolbilkina, N. A., Morozov, V. N., Myachkin, V. I., Preobrazensky, V. V., Sobolev, G. A., 1970, “Investigation on Earthquake Prediction in Kamchatka”, Tectonophysics, Vol. 9, pp. 249-258

Fedotov, S. A., Gusev, A. A., Boldyrev, S. A., 1972, Progress of Earthquake prediction in Kamchatka, Tectonophysics, Vol.14, pp.279-286

Freund, F., 2002, “Charge generation and propogation in igneous rocks”, Journal of Geodynamics, Vol. 33, pp. 543-570

Geller, R. J., Jackson, D. D., Kagan, Y. Y., Mulargia, F., 1997, “Earthquakes Cannot Be Predicted”, Science (New Series), Vol. 275, No.5306, pp. 1616-1617

Giacovazzo,C.,1992, Fundamentals of Crystallography, Oxford Science Publications, New York

Hadjicontis, V., Mavromatou, C., 1994, “Transient Electric Signals Prior to Rock Failure under Uniaxial Compression”, Geophysical Research Letters, Vol.21, No.16, pp. 1687-1690

Ikeda, T., 1996, Fundamentals of Piezoelectricity, Oxford University Press., New York

Le Mouel, J.L., Morat, P, 1987, “Variation of the electrical resistivity of large rock samples with stress”, Geophysics, Vol. 52, No. 10, pp. 1424-1430

MTS System Catalogue, 1992

Rikitake, T., 1976. Earthquake Prediction, Elsevier Scientific Publishing Co., Amsterdam

Scholz, C. H., Sykes, L. R., Aggarwal, Y. P., 1973, “Earthquake Prediction: A Physical Basis”, Science, Vol. 181, No. 4102, pp. 803-810

Shields, J. P., 1966. Basics of Piezoelectricity, Howard W. Sams & Co. Inc., Indianapolis, Indiana

Sobolev, G. A., 1975, "Application of Electric Method to the Tentative Short-Term Forecast of Kamchatka Earthquakes", Pageoph, Vol.113, pp.233-235

Tarbuck, E. J., Lutgens, F. K., 2003. Earth Science, Prentice Hall, Pearson Education Inc, New Jersey

Trainer, M., 2003, Kelvin and Piezoelectricity, European Journal of Physics, Vol.24, pp.535-524.

Varotsos, P., Alexopoulos, K., 1984a, "Physical Properties of the Variations of the Electric Field of the Earth preceding Earthquakes I", Tectonophysics, Vol. 110, pp.73-98

Varotsos, P., Alexopoulos, K., 1984b, Physical Properties of the Variations of the Electric Field of the Earth preceding Earthquakes II. Determination of Epicenter and Magnitude, Tectonophysics, Vol. 110, pp.99-125

Varotsos, P., Lazaridou, M., 1991, Latest Aspects of Earthquake Prediction in Greece Based on Seismic Electric Signals, Tectonophysics, Vol. 188, pp. 321-347

Varotsos, P., Alexopoulos, K., Lazaridou, M., 1993, Latest Aspects of Earthquake Prediction in Greece Based on Seismic Electric Signals II, Tectonophysics, Vol. 224, pp. 1-37

Wyss, M., 2000, Why is earthquake prediction research not progressing faster?, Tectonophysics, Vol.338, pp. 217-223

Yılmaz, R., 2001, GEOE 527- Elements of Seismology, Lecture Notes, Geological Engineering Department, METU

Yoshida, S., Uyeshima, M., Nakatani, M., 1997, “Electric Potential Changes Associated with Slip Failure of Granite: Preseismic and Coseismic Signals”, Journal of Geophysical Research, Vol.102, No.B7, pp.14883-14897

APPENDIX-A

GRAPHS OF DC MEASUREMENTS ON GRANITE SAMPLES

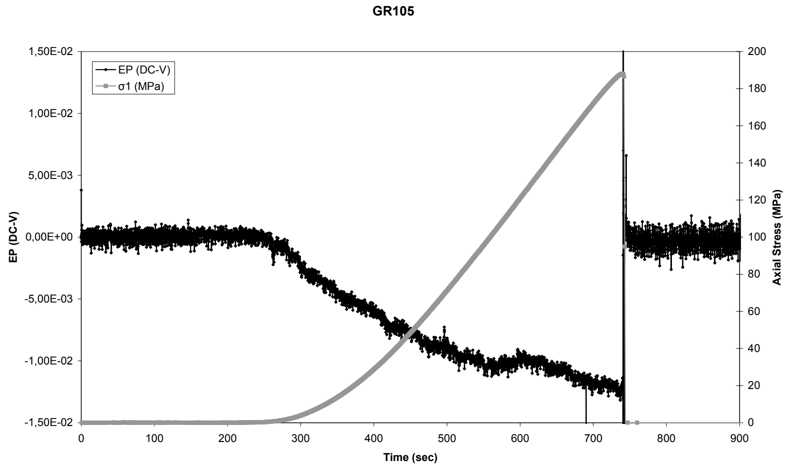

Figure A.1 Stress-time & EP-time graph for GR105 experiment

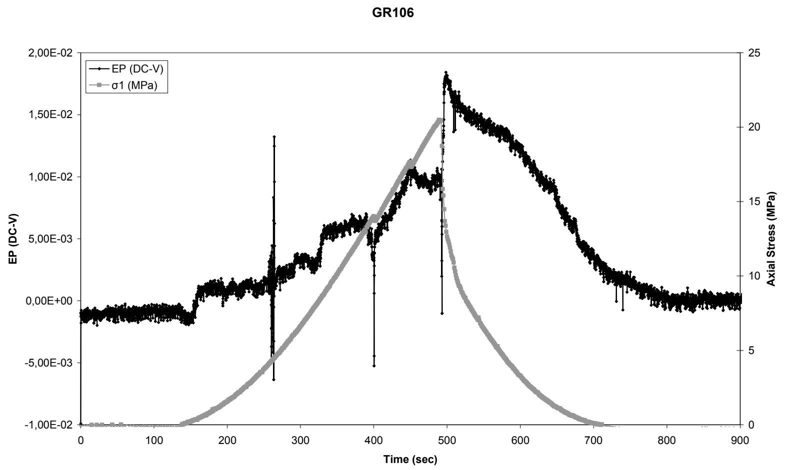

Figure A.2 Stress-time & EP-time graph for GR106 experiment

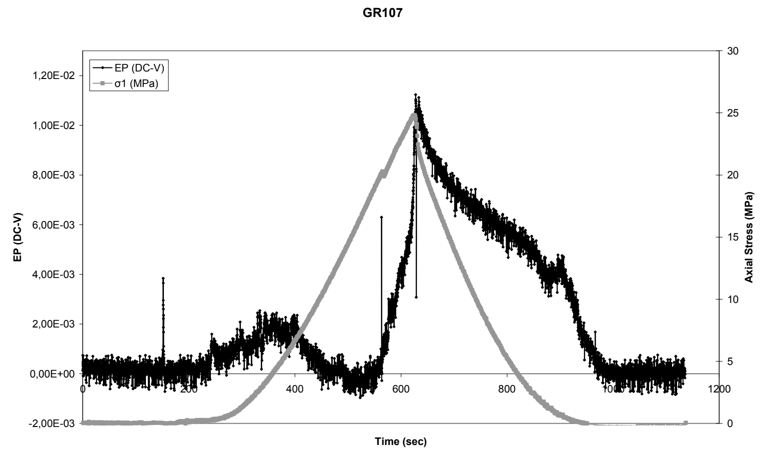

Figure A.3 Stress-time & EP-time graph for GR107 experiment

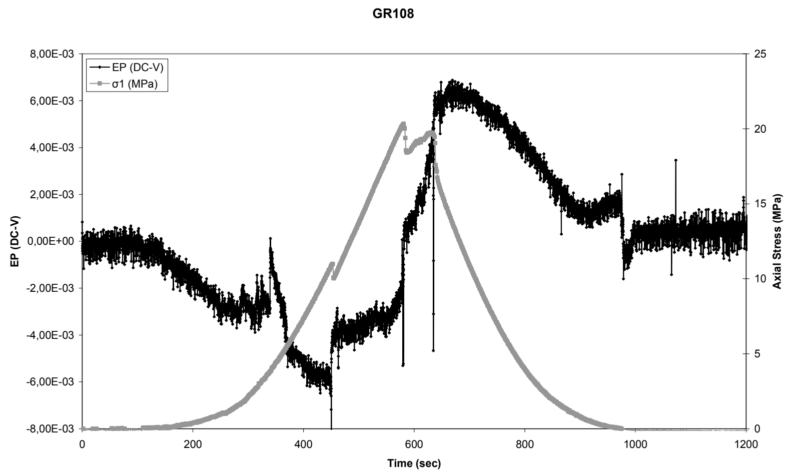

Figure A.4 Stress-time & EP-time graph for GR108 experiment

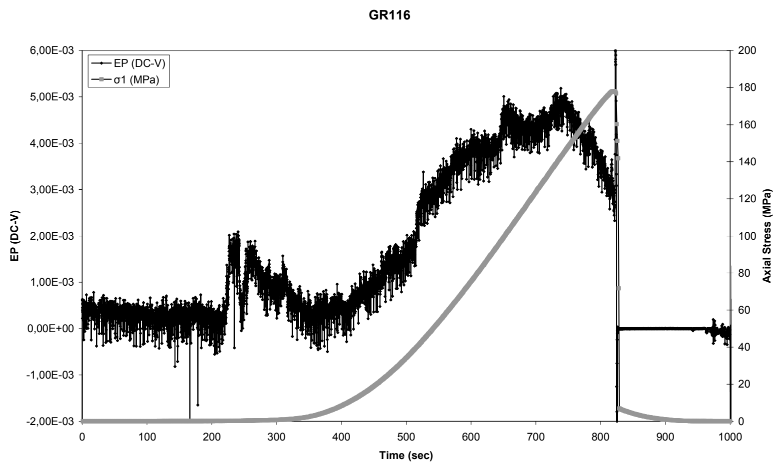

Figure A.5 Stress-time & EP-time graph for GR116 experiment

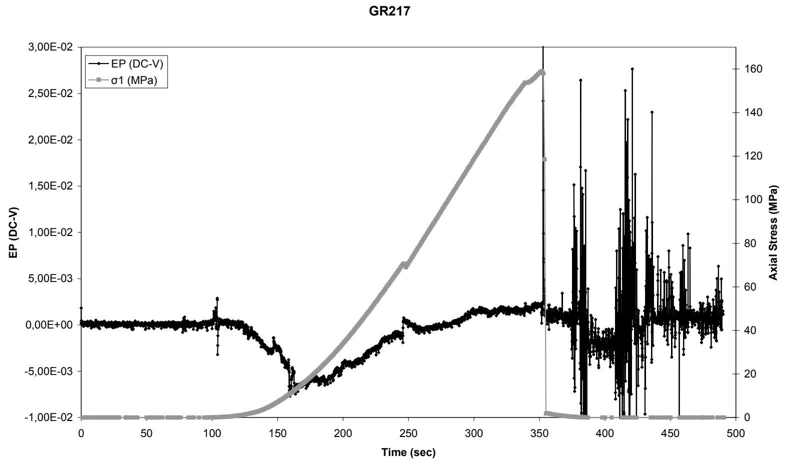

Figure A.6 Stress-time & EP-time graph for GR217 experiment

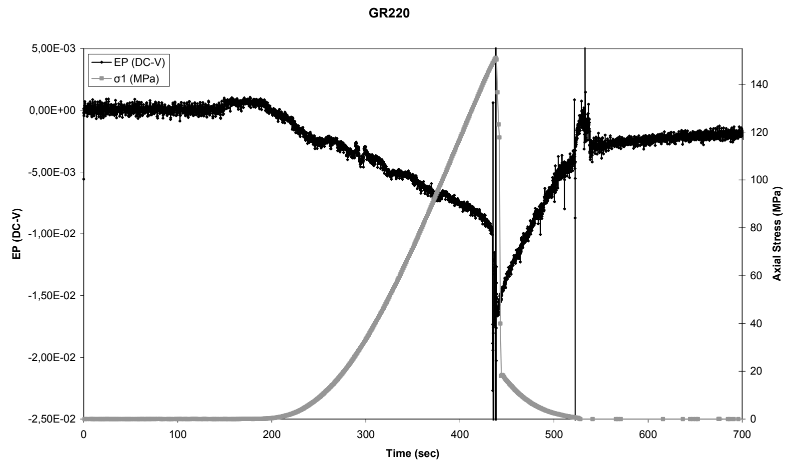

Figure A.7 Stress-time & EP-time graph for GR220 experiment

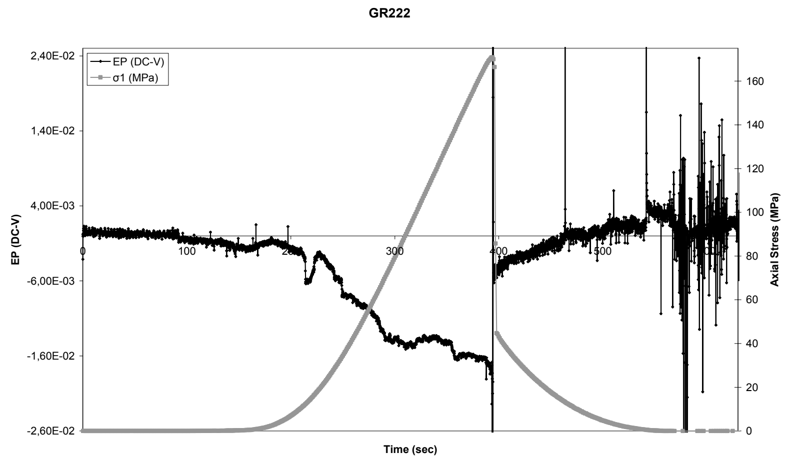

Figure A.8 Stress-time & EP-time graph for GR222 experiment

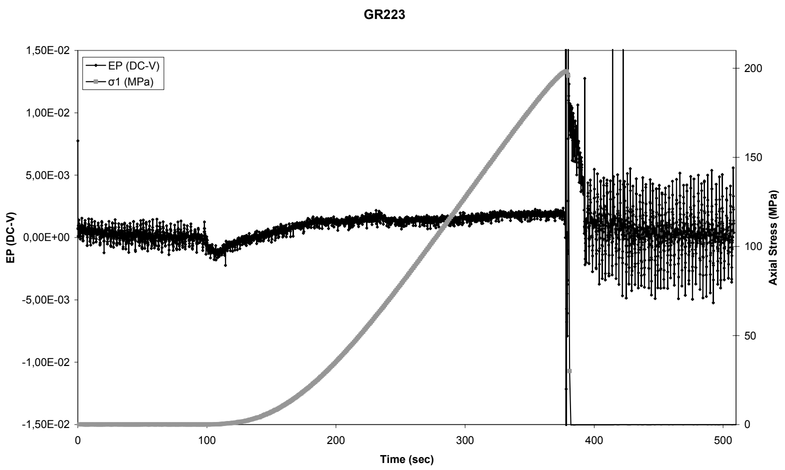

Figure A.9 Stress-time & EP-time graph for GR223 experiment

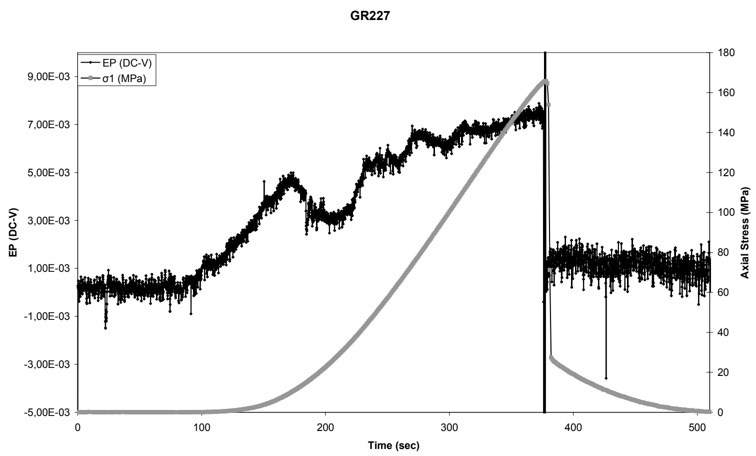

Figure A.10 Stress-time & EP-time graph for GR227 experiment

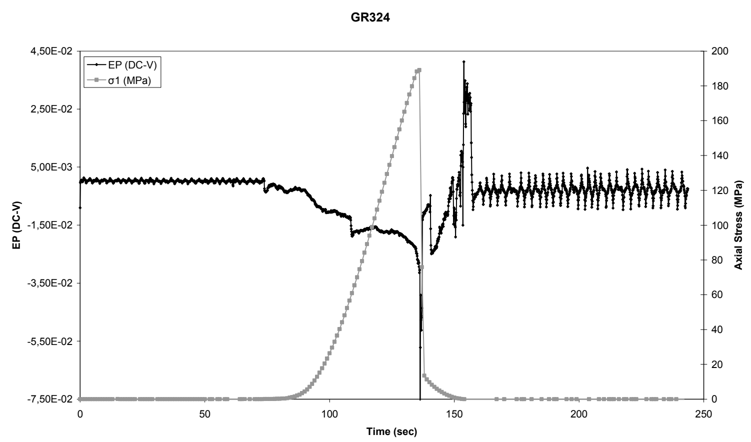

Figure A.11 Stress-time & EP-time graph for GR324 experiment

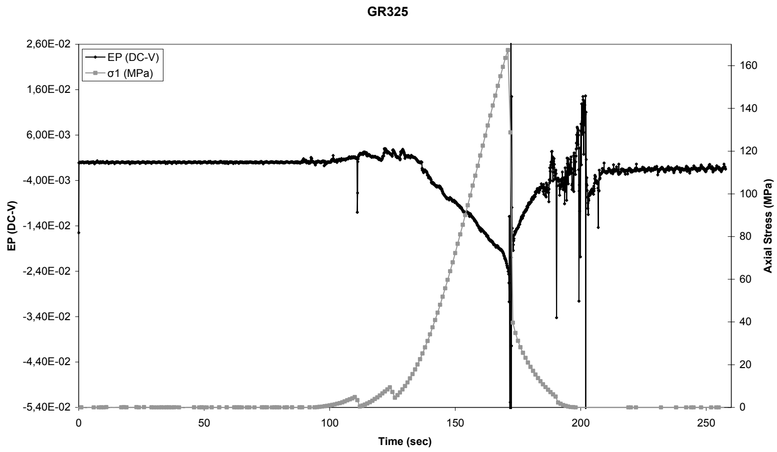

Figure A.12 Stress-time & EP-time graph for GR325 experiment

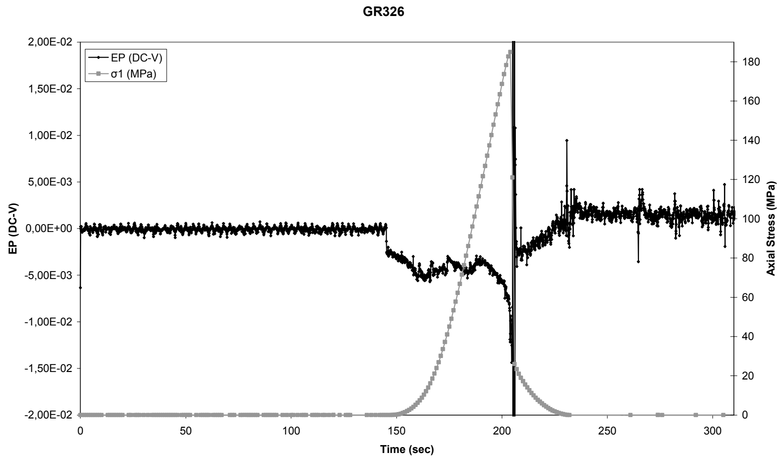

Figure A.13 Stress-time & EP-time graph for GR326 experiment

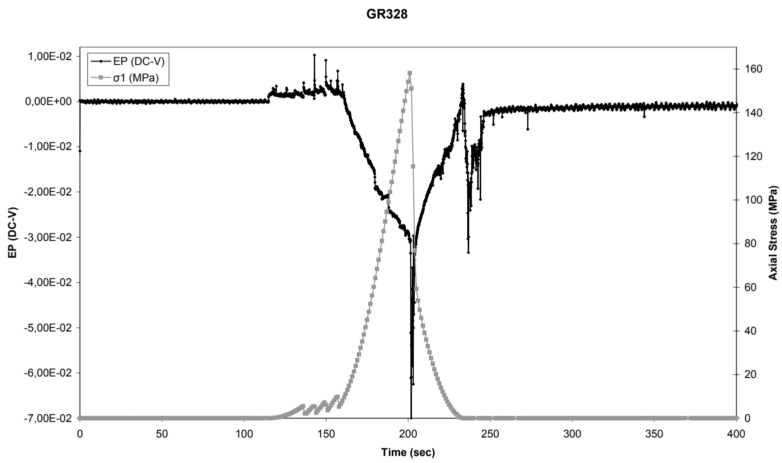

Figure A.14 Stress-time & EP-time graph for GR328 experiment

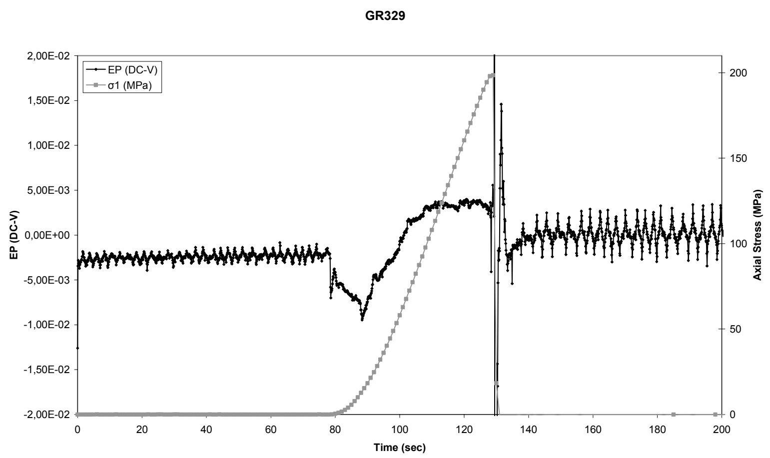

Figure A.15 Stress-time & EP-time graph for GR329 experiment

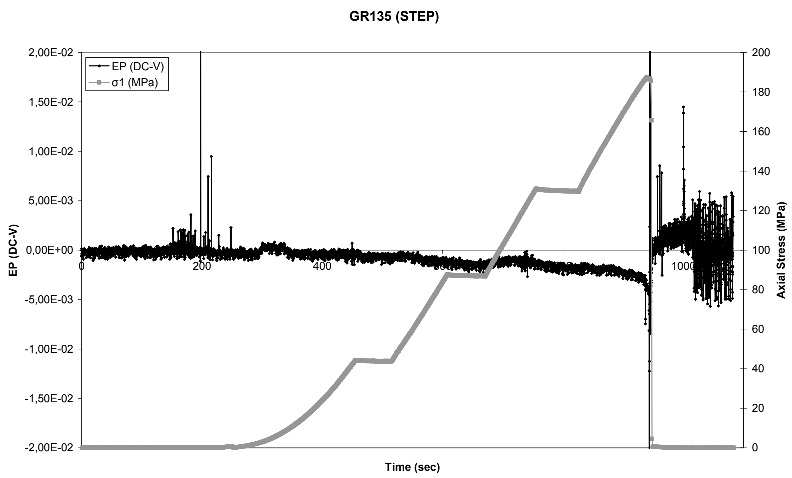

Figure A.16 Stress-time & EP-time graph for GR135(STEP) experiment

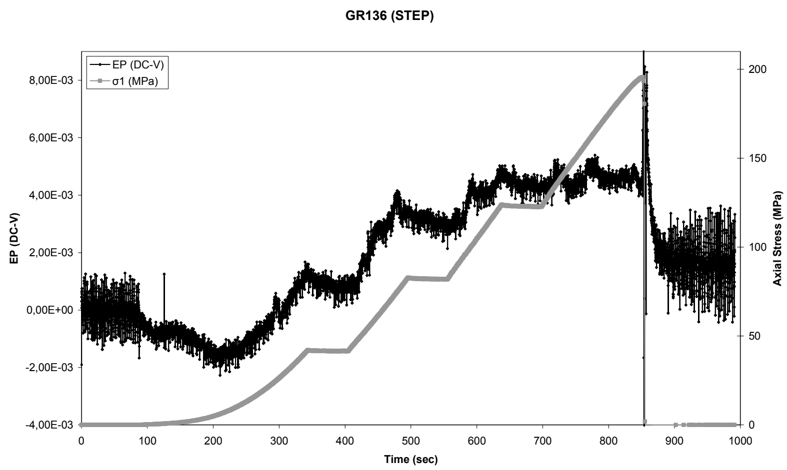

Figure A.17 Stress-time & EP-time graph for GR136(STEP) experiment

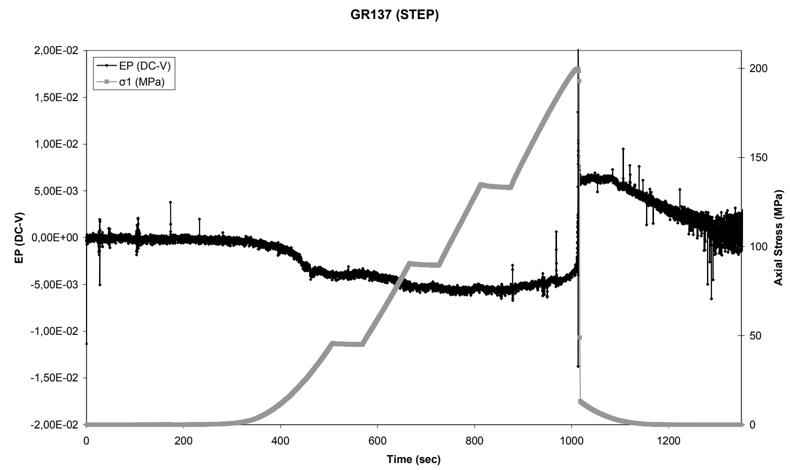

Figure A.18 Stress-time & EP-time graph for GR137(STEP) experiment

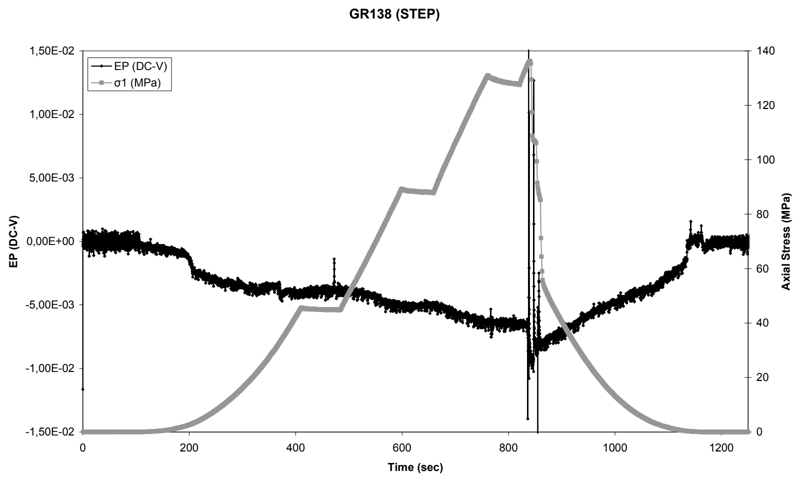

Figure A.19 Stress-time & EP-time graph for GR138(STEP) experiment

APPENDIX-B

GRAPHS OF DC MEASUREMENTS ON GRANODIORITE SAMPLES

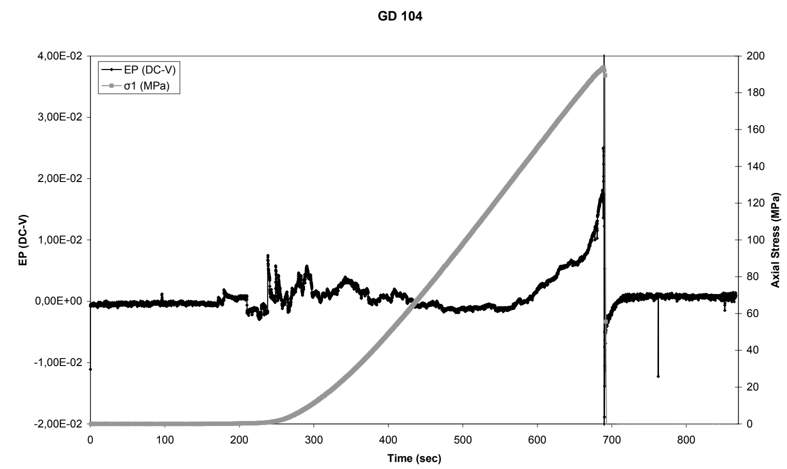

Figure B.1 Stress-time & EP-time graph for GD104 experiment

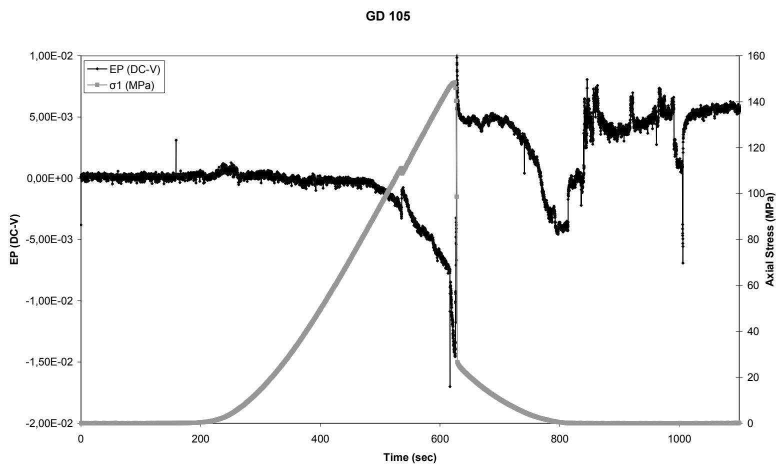

Figure B.2 Stress-time & EP-time graph for GD105 experiment

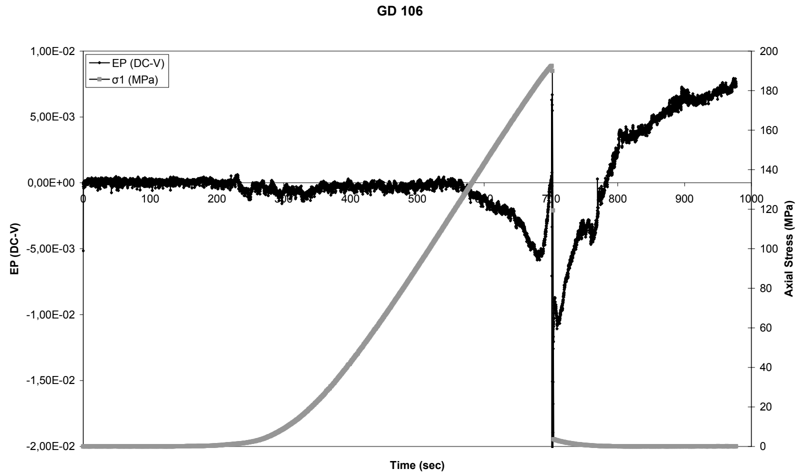

Figure B.3 Stress-time & EP-time graph for GD106 experiment

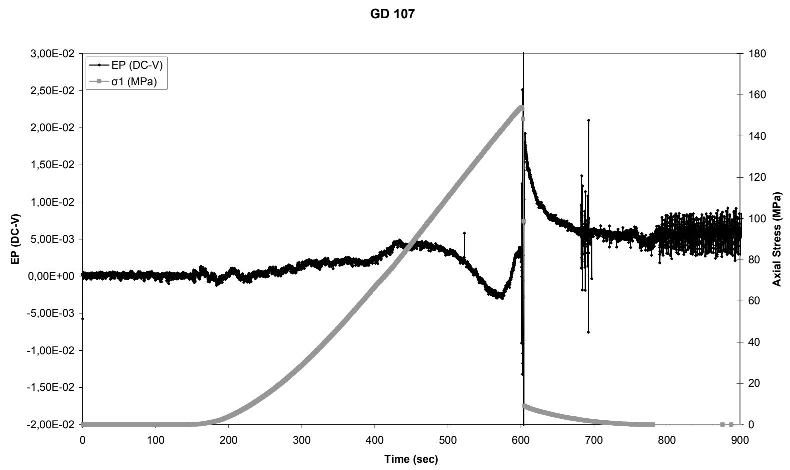

Figure B.4 Stress-time & EP-time graph for GD107 experiment

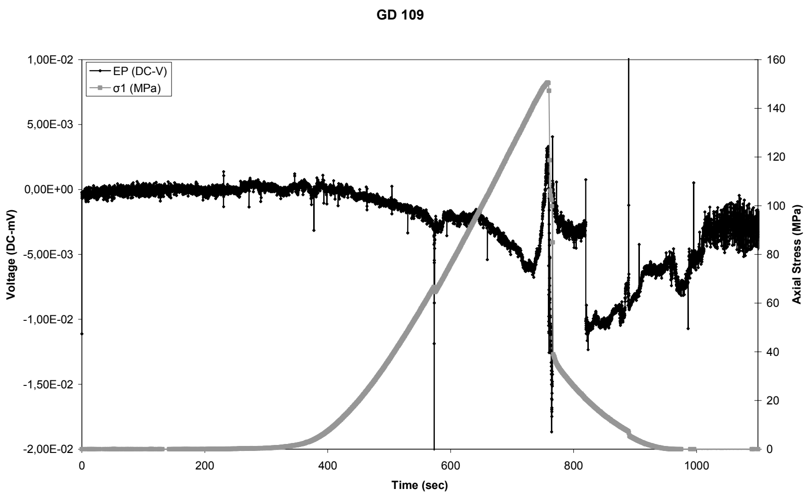

Figure B.5 Stress-time & EP-time graph for GD109 experiment

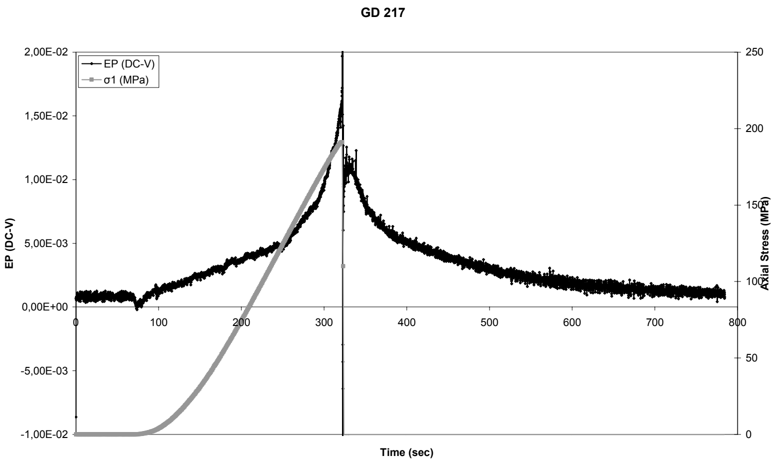

Figure B.6 Stress-time & EP-time graph for GD217 experiment

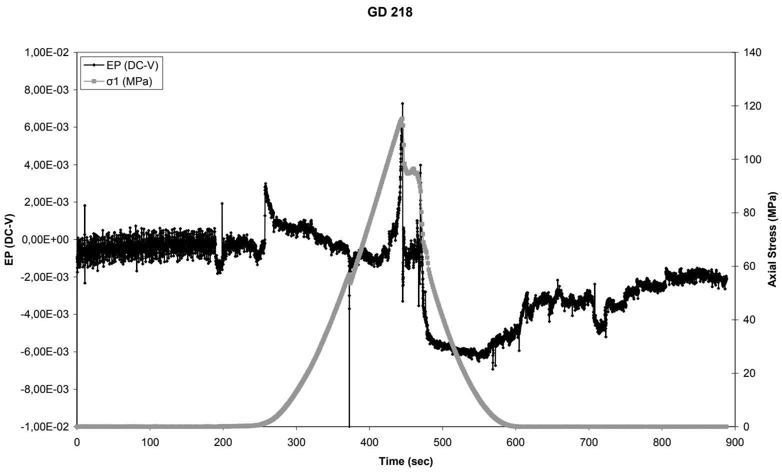

Figure B.7 Stress-time & EP-time graph for GD218 experiment

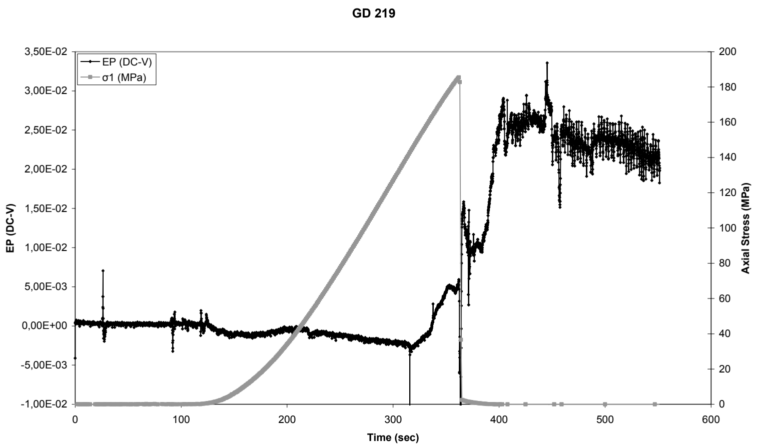

Figure B.8 Stress-time & EP-time graph for GD219 experiment

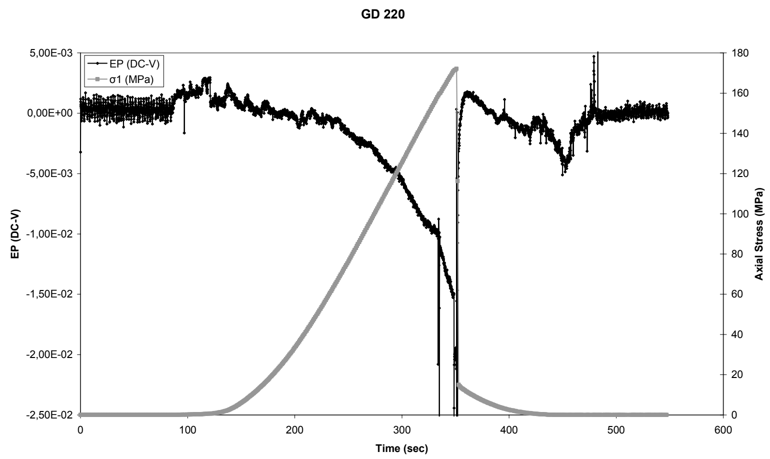

Figure B.9 Stress-time & EP-time graph for GD220 experiment

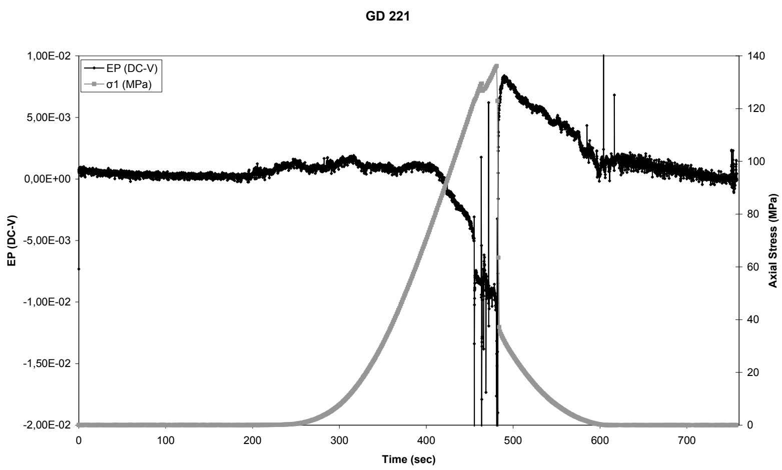

Figure B.10 Stress-time & EP-time graph for GD221 experiment

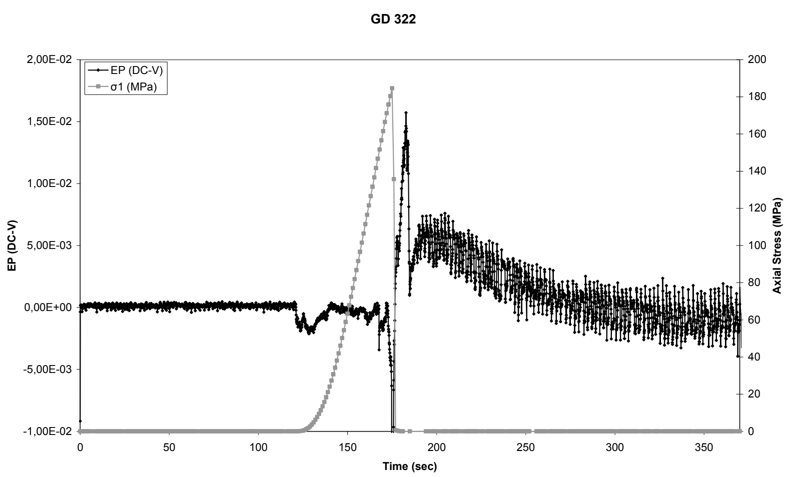

Figure B.11 Stress-time & EP-time graph for GD322 experiment

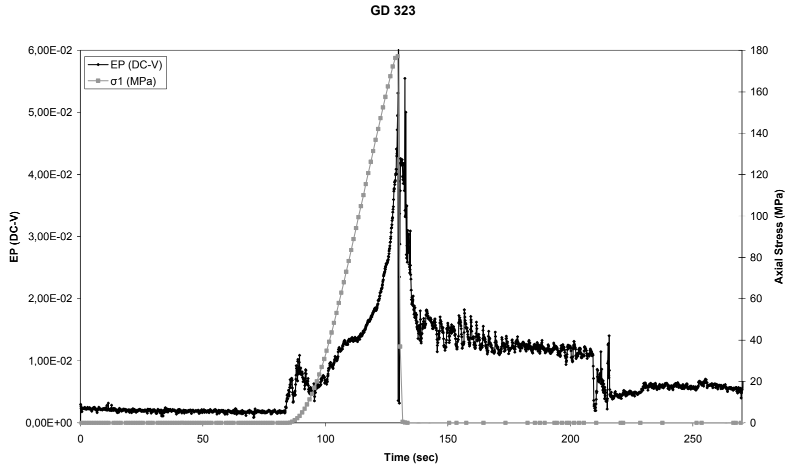

Figure B.12 Stress-time & EP-time graph for GD323 experiment

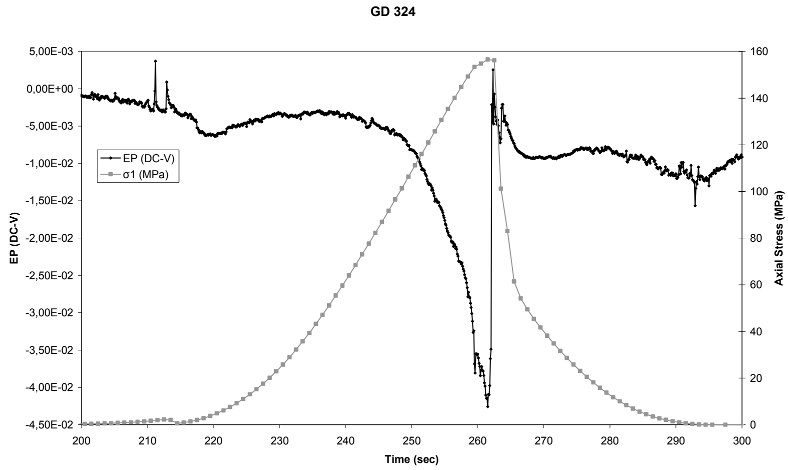

Figure B.13 Stress-time & EP-time graph for GD324 experiment

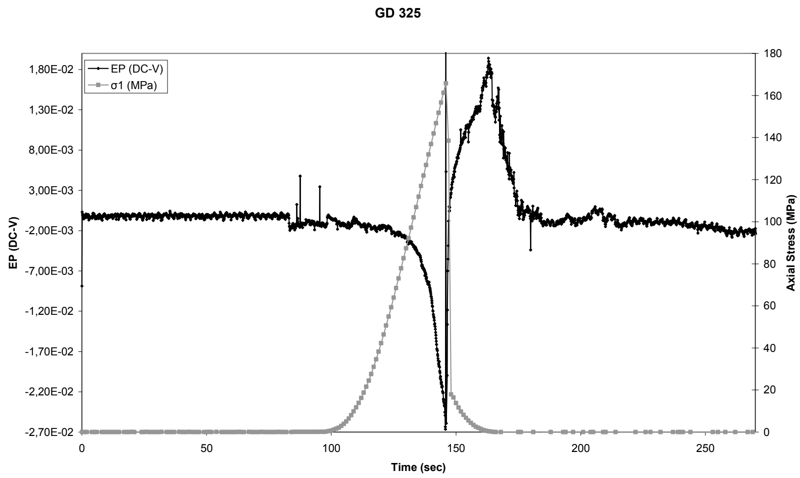

Figure B.14 Stress-time & EP-time graph for GD325 experiment

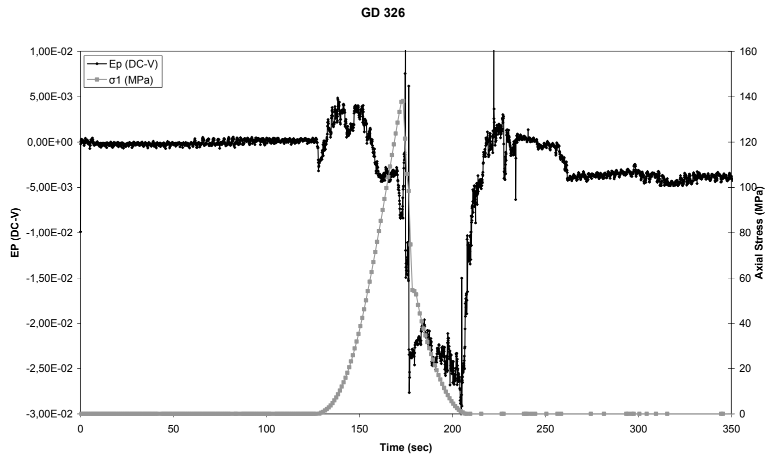

Figure B.15 Stress-time & EP-time graph for GD326 experiment

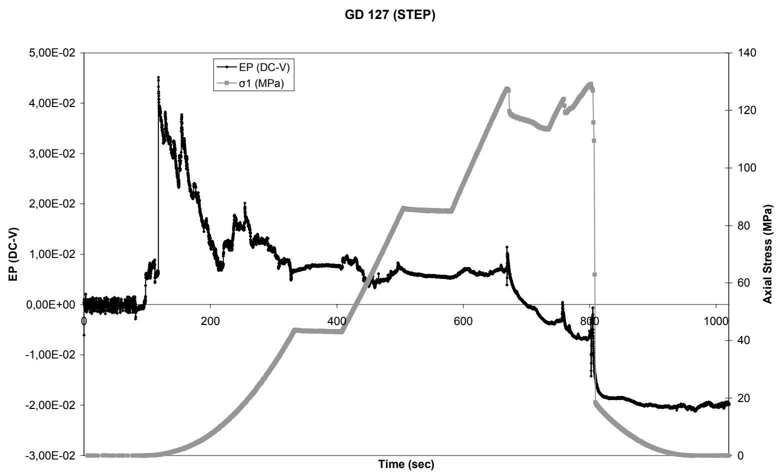

Figure B.16 Stress-time & EP-time graph for GD127(STEP) experiment

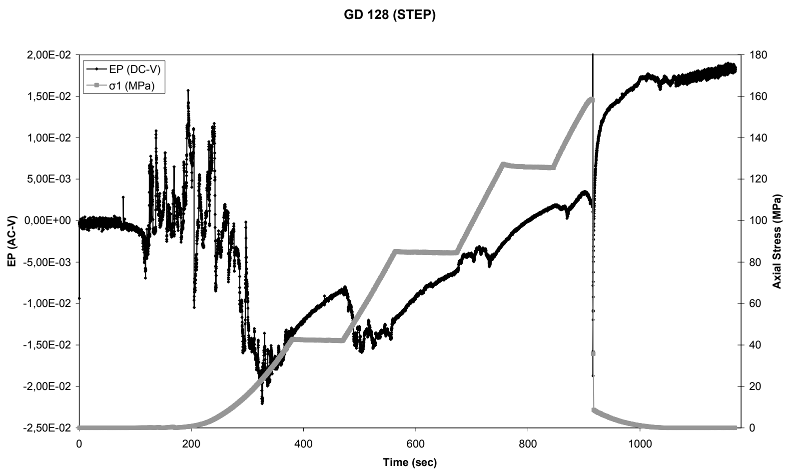

Figure B.17 Stress-time & EP-time graph for GD128(STEP) experiment

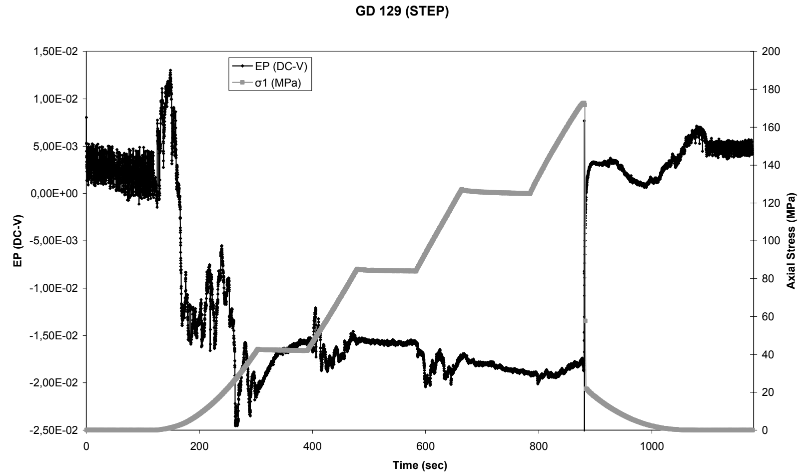

Figure B.18 Stress-time & EP-time graph for GD129(STEP) experiment

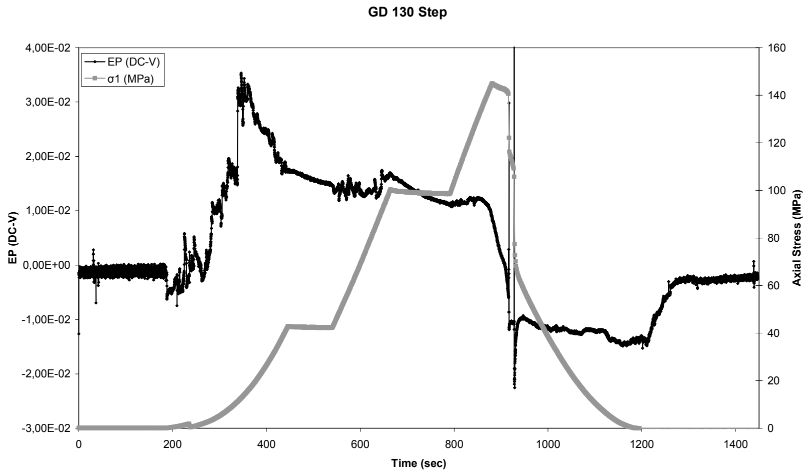

Figure B.19 Stress-time & EP-time graph for GD130(STEP) experiment

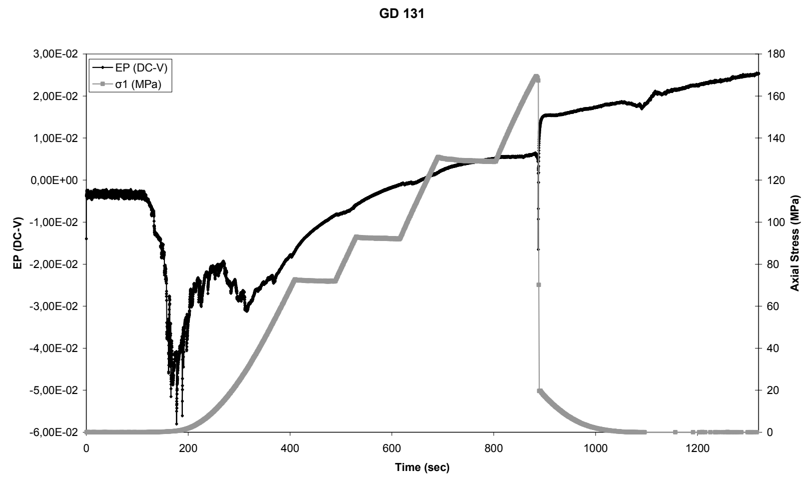

Figure B.20 Stress-time & EP-time graph for GD131(STEP) experiment

APPENDIX-C

GRAPHS OF DC MEASUREMENTS ON QUARTZ-SANDSTONE SAMPLES

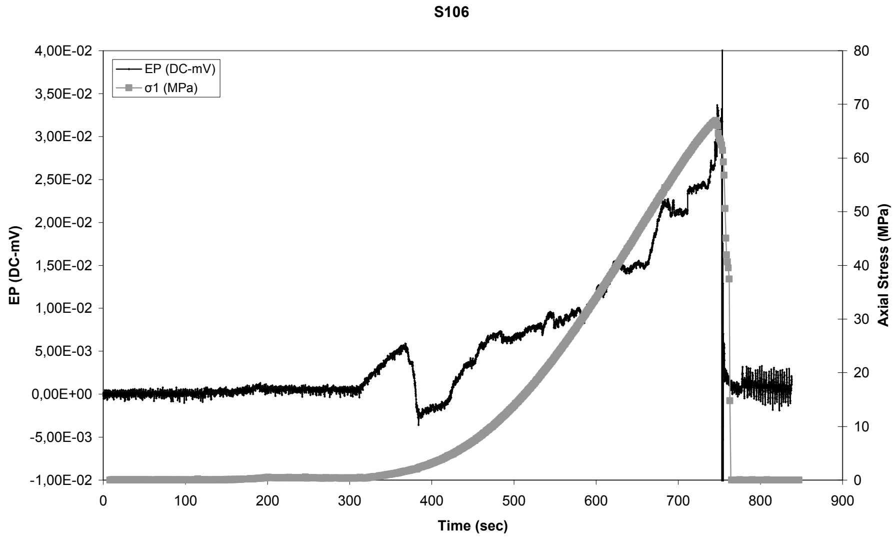

Figure C.1 Stress-time & EP-time graph for S106 experiment

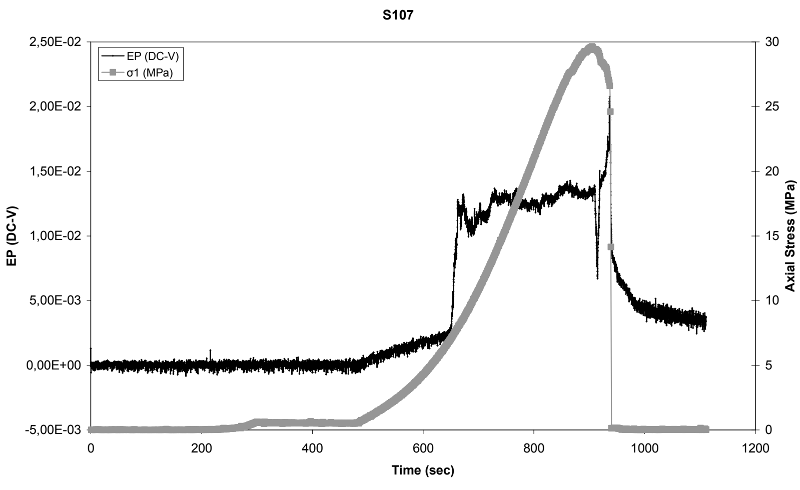

Figure C.2 Stress-time & EP-time graph for S107 experiment

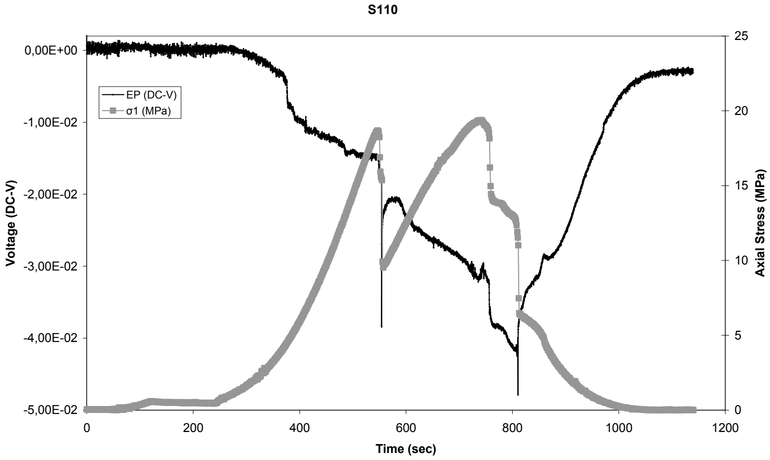

Figure C.3 Stress-time & EP-time graph for S110 experiment

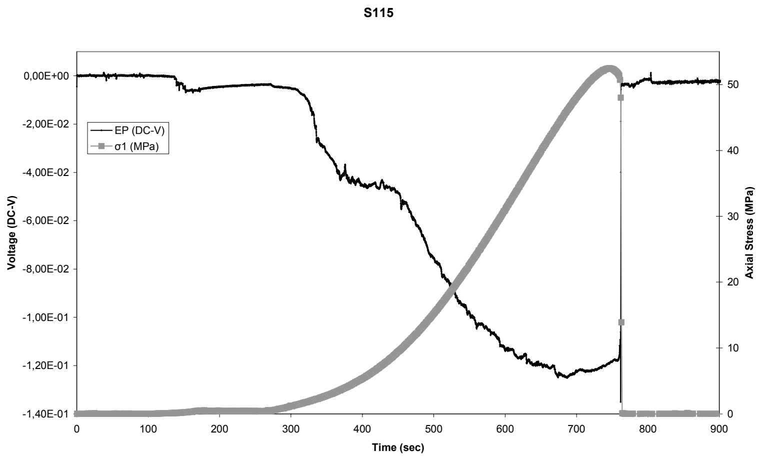

Figure C.4 Stress-time & EP-time graph for S115 experiment

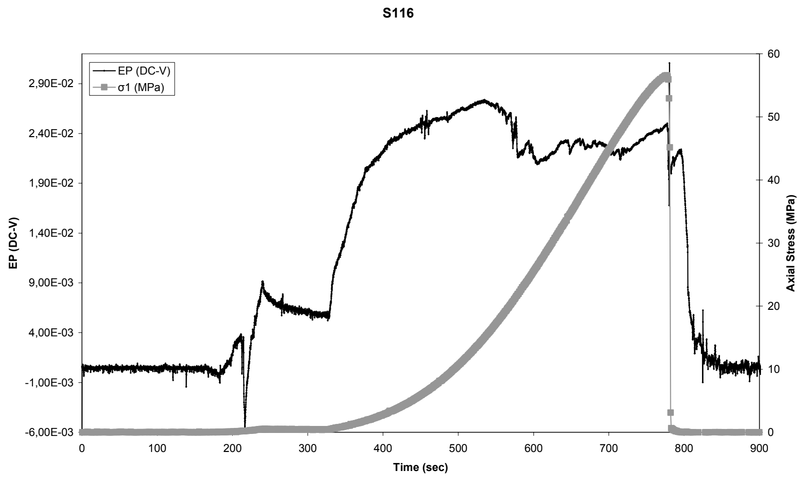

Figure C.5 Stress-time & EP-time graph for S116 experiment

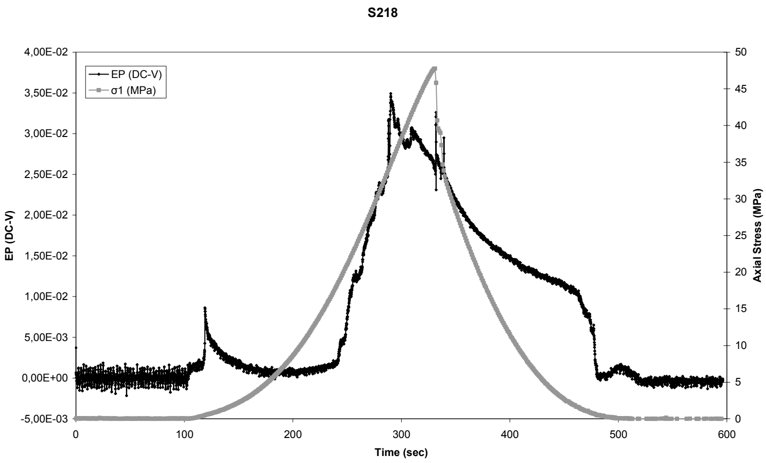

Figure C.6 Stress-time & EP-time graph for S218 experiment

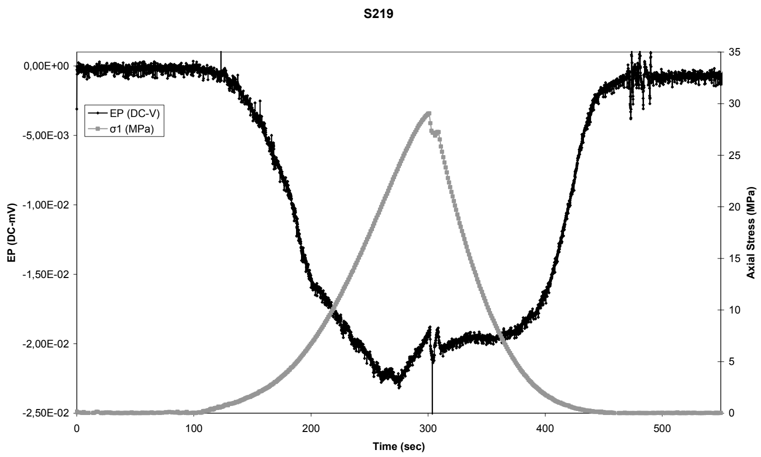

Figure C.7 Stress-time & EP-time graph for S219 experiment

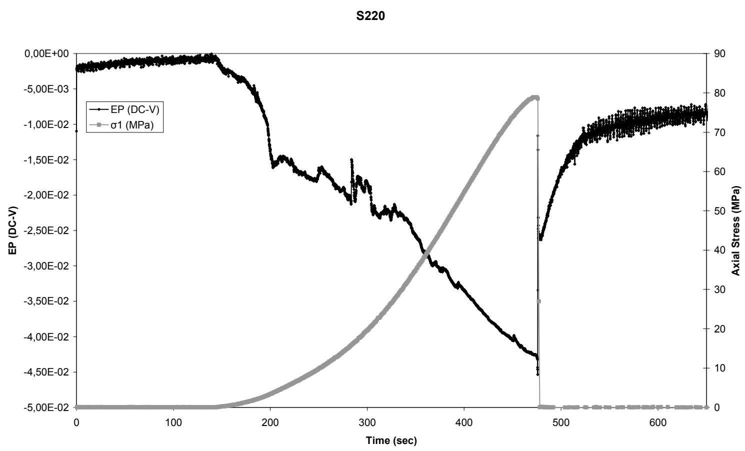

Figure C.8 Stress-time & EP-time graph for S220 experiment

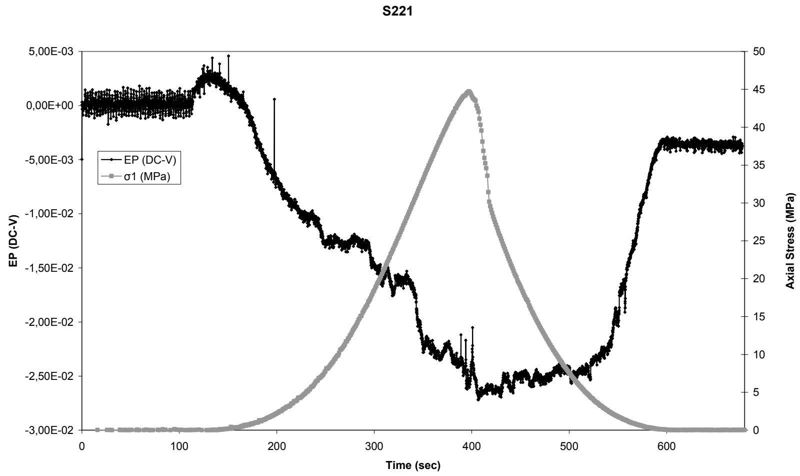

Figure C.9 Stress-time & EP-time graph for S221 experiment

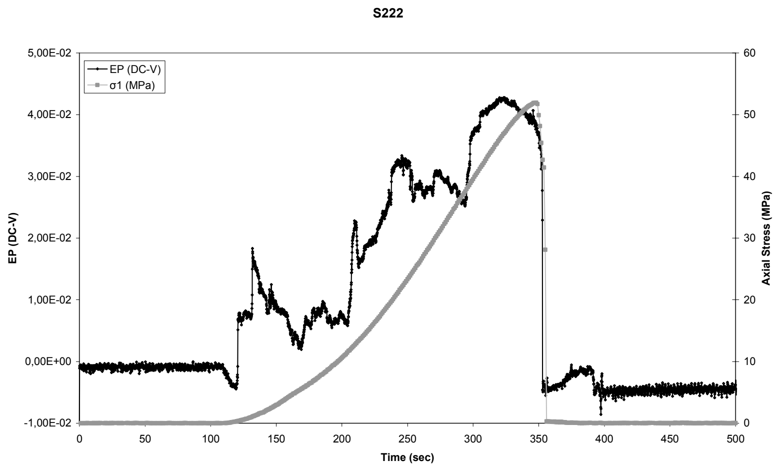

Figure C.10 Stress-time & EP-time graph for S222 experiment

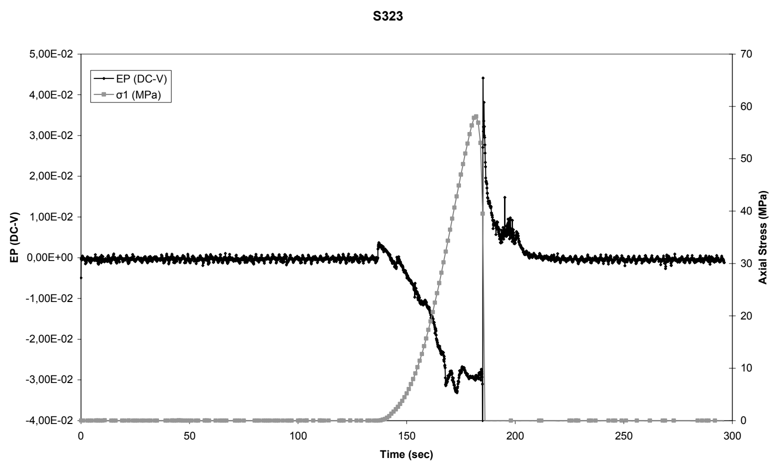

Figure C.11 Stress-time & EP-time graph for S323 experiment

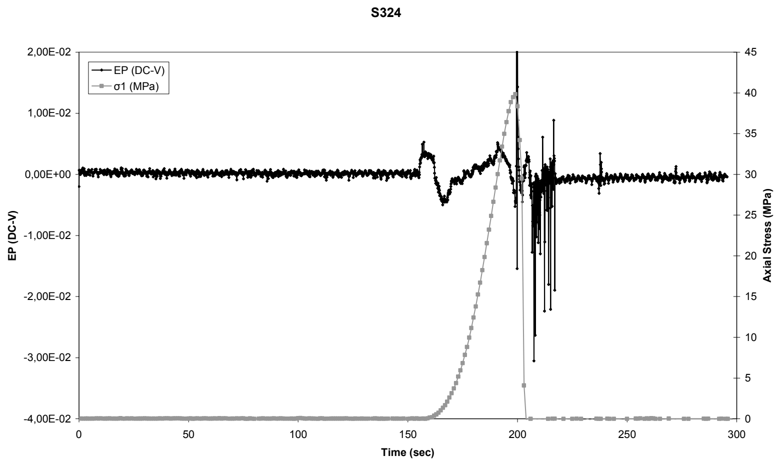

Figure C.12 Stress-time & EP-time graph for S324 experiment

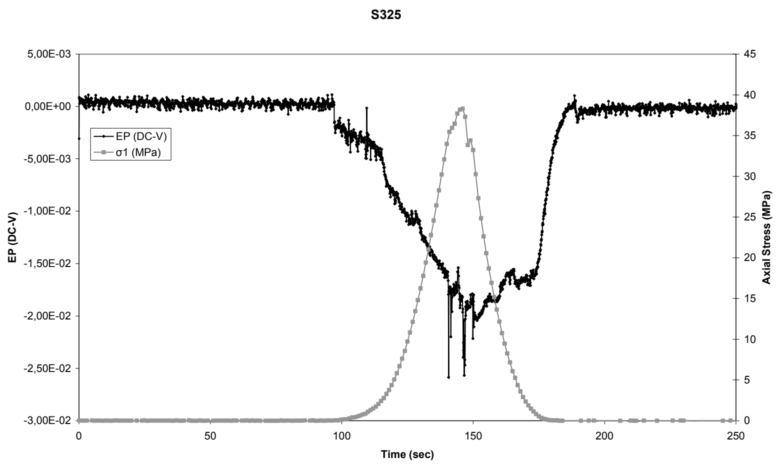

Figure C.13 Stress-time & EP-time graph for S325 experiment

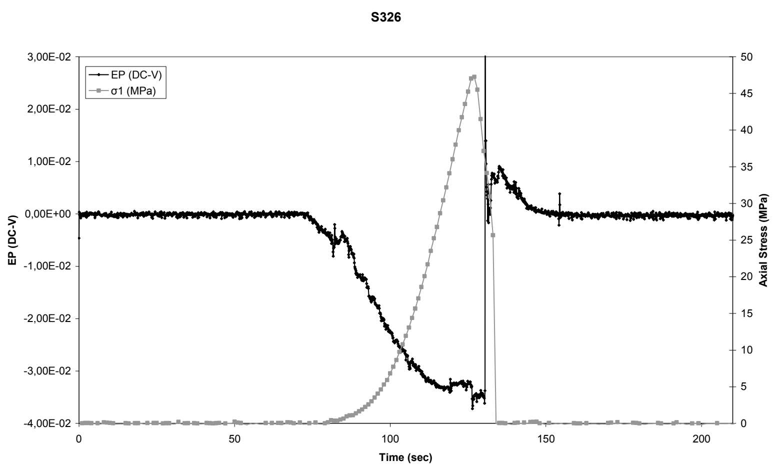

Figure C.14 Stress-time & EP-time graph for S326 experiment

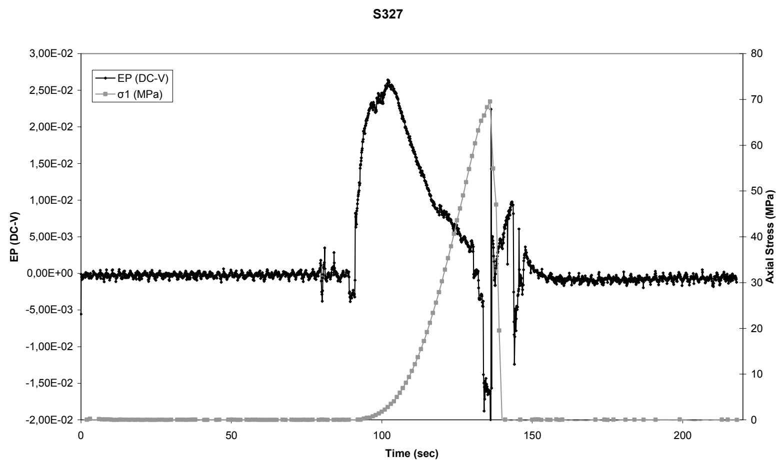

Figure C.15 Stress-time & EP-time graph for S327 experiment

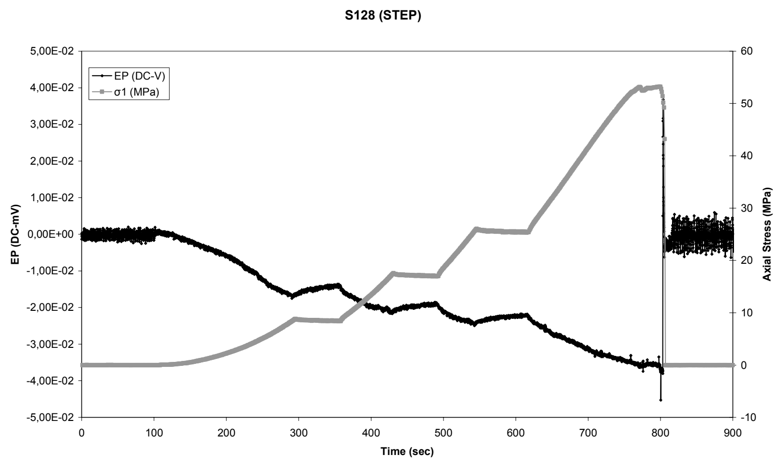

Figure C.16 Stress-time & EP-time graph for S128(STEP) experiment

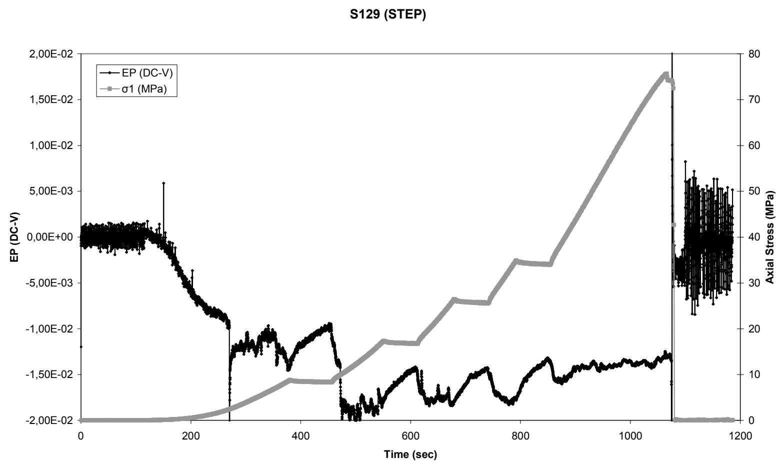

Figure C.17 Stress-time & EP-time graph for S129(STEP) experiment

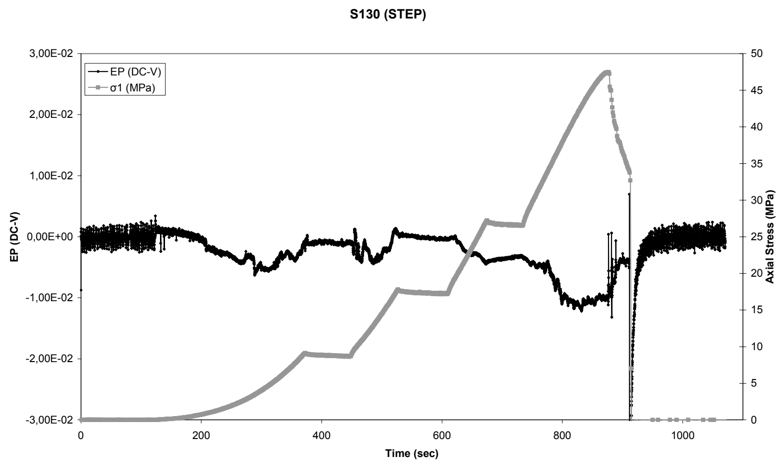

Figure C.18 Stress-time & EP-time graph for S130(STEP) experiment

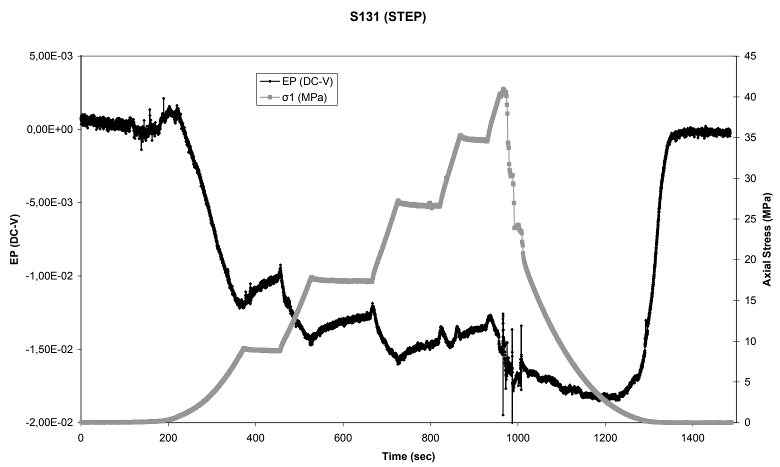

Figure C.19 Stress-time & EP-time graph for S131(STEP) experiment

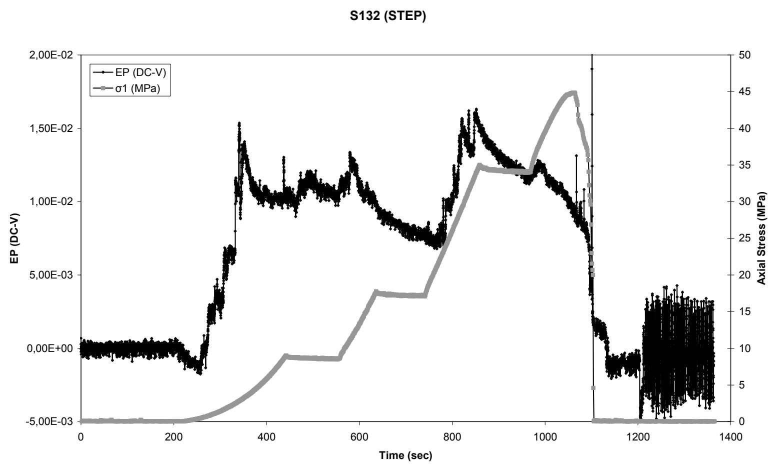

Figure C.20 Stress-time & EP-time graph for S132(STEP) experiment

APPENDIX-D

GRAPHS OF AC MEASUREMENTS ON GRANITE, GRANODIORITE AND QUARTZ-SANDSTONE SAMPLES

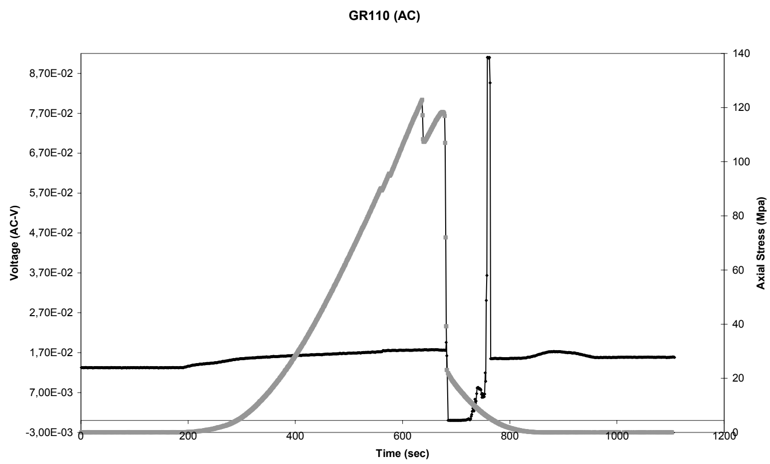

Figure D.1 Stress-time & EP-time graph for GR110 (AC) experiment

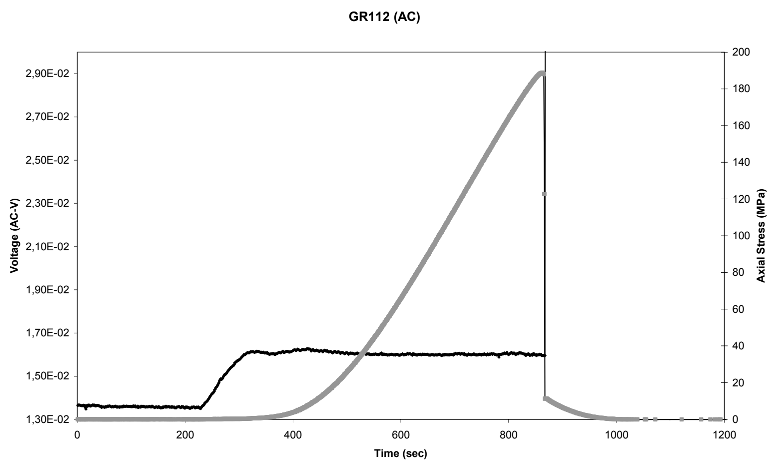

Figure D.2 Stress-time & EP-time graph for GR112 (AC) experiment

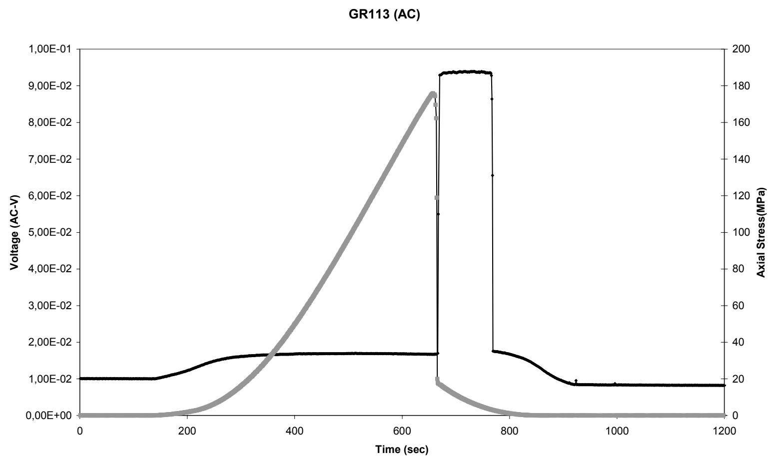

Figure D.3 Stress-time & EP-time graph for GR113 (AC) experiment

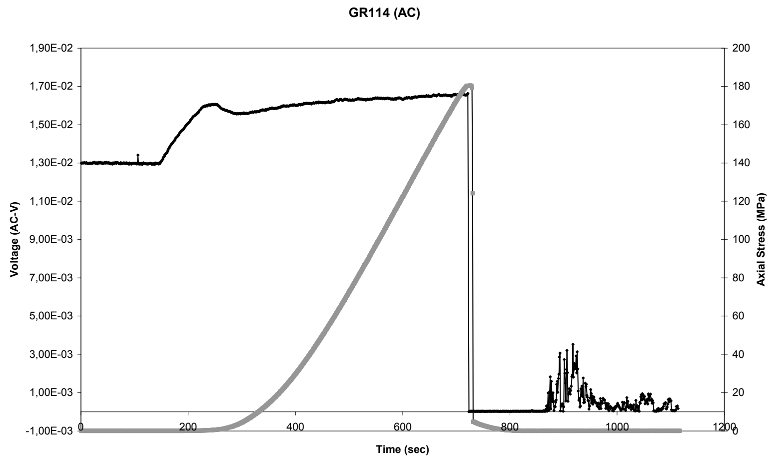

Figure D.4 Stress-time & EP-time graph for GR114 (AC) experiment

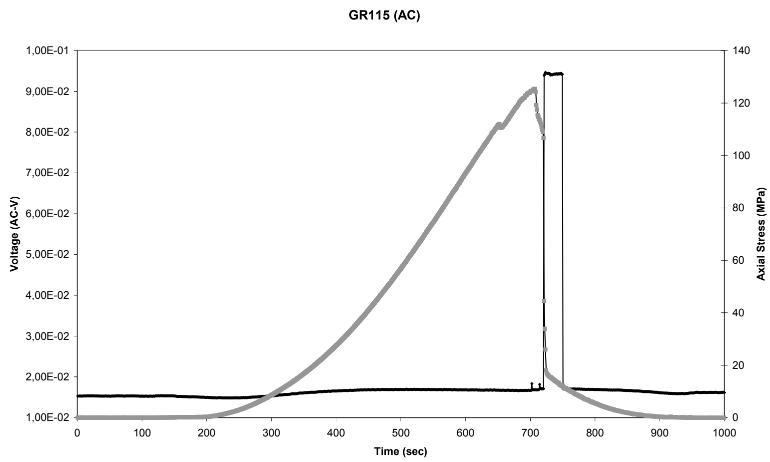

Figure D.5 Stress-time & EP-time graph for GR115 (AC) experiment

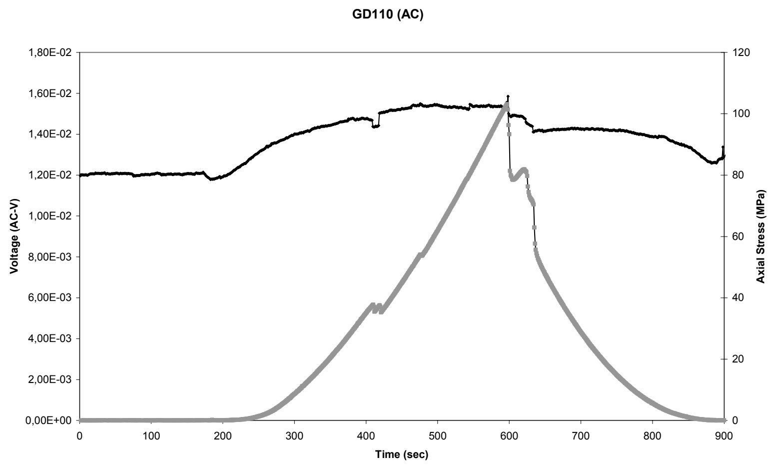

Figure D.6 Stress-time & EP-time graph for GD110 (AC) experiment

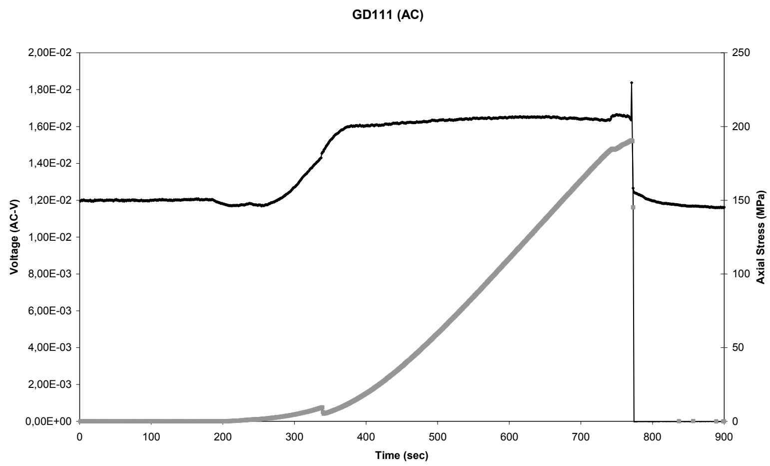

Figure D.7 Stress-time & EP-time graph for GD111 (AC) experiment

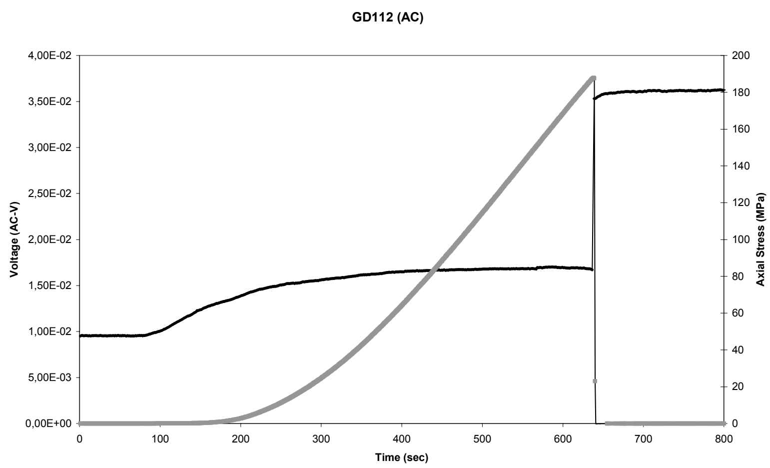

Figure D.8 Stress-time & EP-time graph for GD112 (AC) experiment

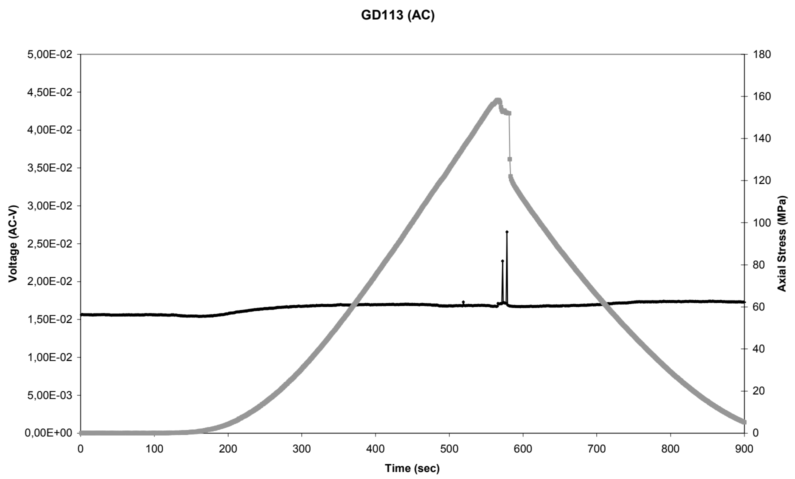

Figure D.9 Stress-time & EP-time graph for GD113 (AC) experiment

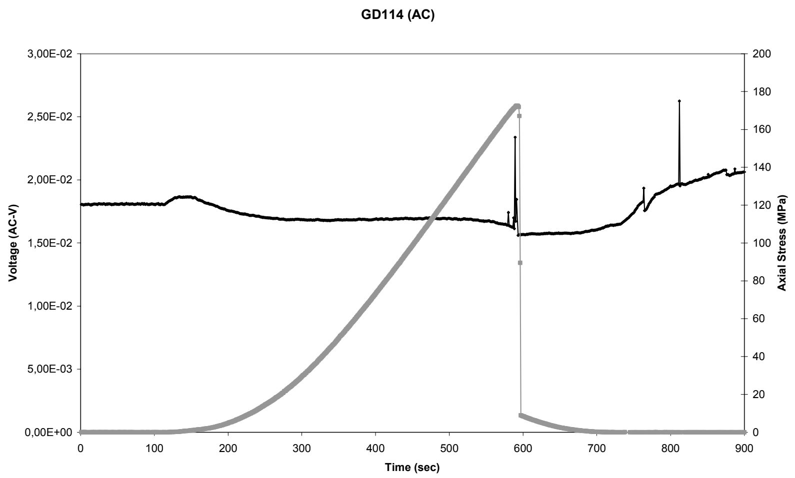

Figure D.10 Stress-time & EP-time graph for GD114 (AC) experiment

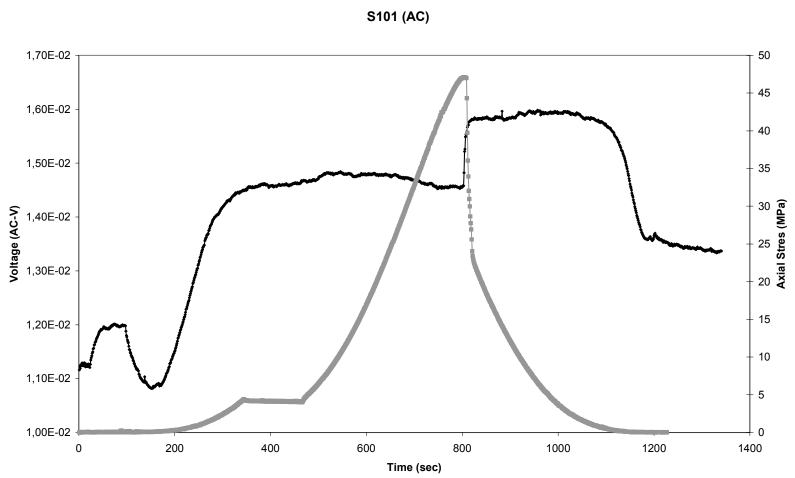

Figure D.11 Stress-time & EP-time graph for S101 (AC) experiment

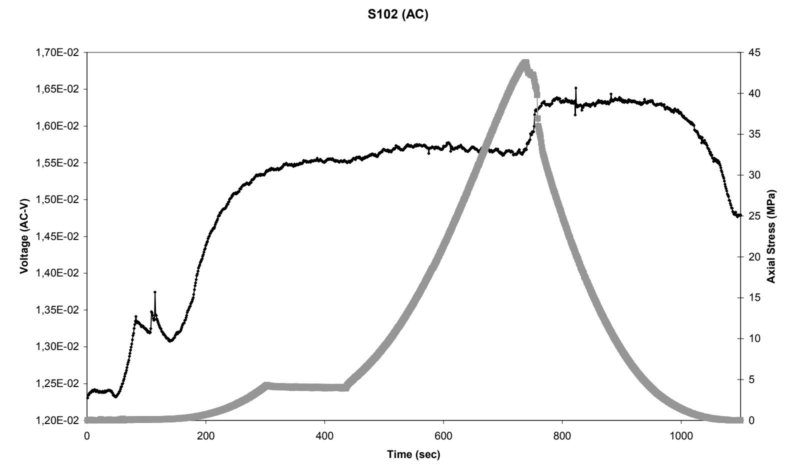

Figure D.12 Stress-time & EP-time graph for S102 (AC) experiment

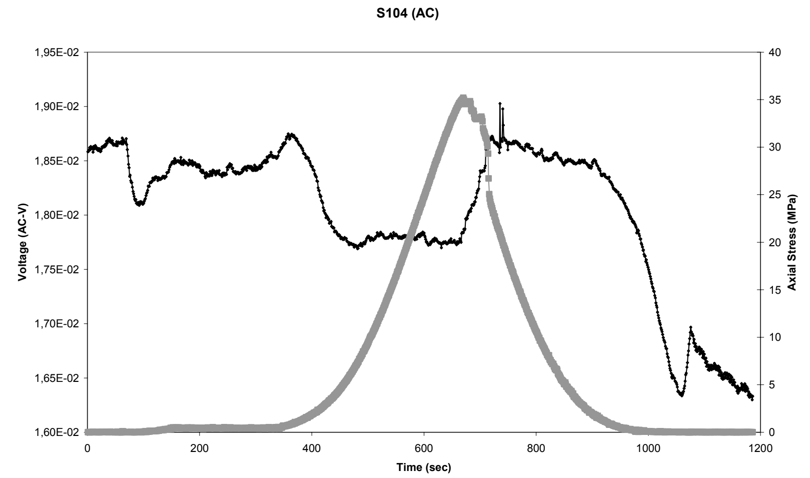

Figure D.13 Stress-time & EP-time graph for S104 (AC) experiment

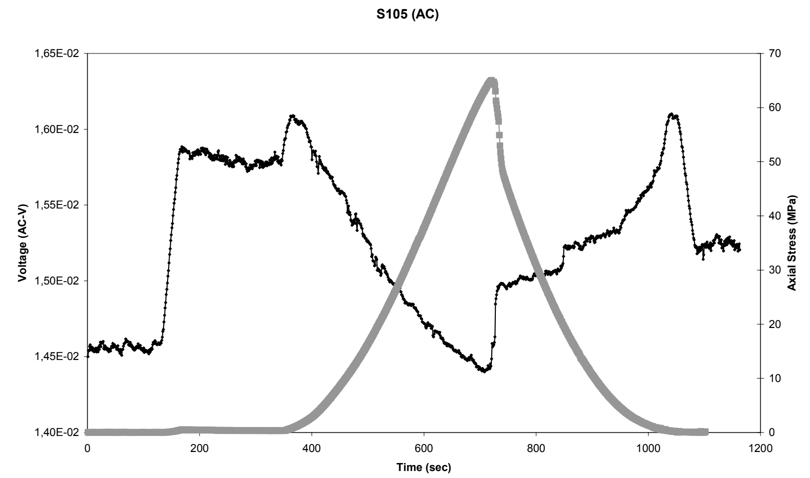

Figure D.14 Stress-time & EP-time graph for S105 (AC) experiment

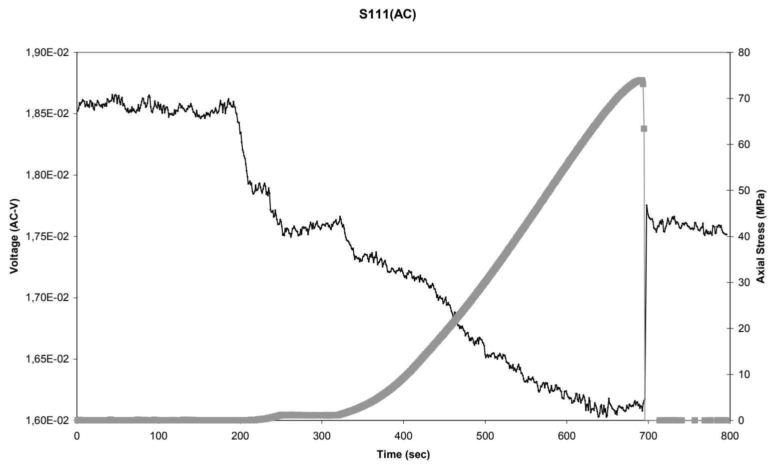

Figure D.15 Stress-time & EP-time graph for S111 (AC) experiment